Incremental Nonlinear Dynamic Inversion Control of Pneumatic Actuators

H. Das

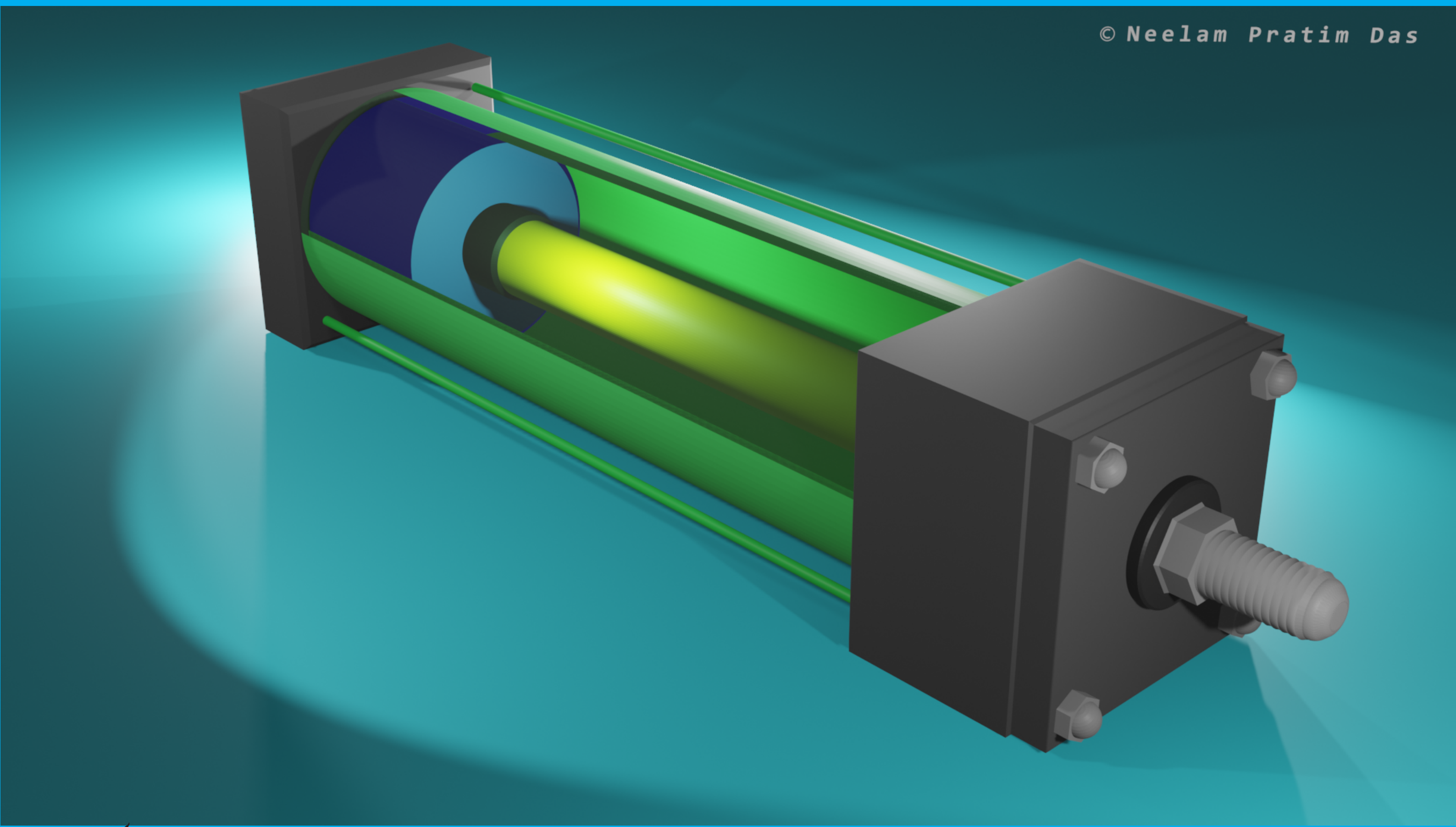

TU Delft

Incremental Nonlinear Dynamic Inversion Control of Pneumatic Actuators

by

H. Das

to obtain the degree of Master of Science
at the Delft University of Technology,
to be defended publicly on Thursday July 23, 2020 at 02:00 PM.

Student number:	4893123	
Project duration:	September 1 , 2019 – July 23, 2020	
Thesis committee:	Dr. ir. Rene van Paassen,	TU Delft, Chairman
	Dr. ir. D. Pool,	TU Delft, Daily Supervisor
	Dr. ir. E. van Kampen,	TU Delft, Daily Supervisor
	Dr. ir. E. Mooij,	TU Delft, External Member

Preface

This masters thesis marks the end of my two years of wonderful journey at the Technical University of Delft. I was always enthusiastic about aerospace engineering, specifically about control systems. Having previously worked with Nonlinear Dynamic Inversion controllers, I wanted to work on a similar project for my Masters thesis. Therefore, I mailed the respective faculty members working in this field, only to realize that all of them were busy and could not supervise any new masters student. I got very disappointed, but after waiting for two more months, I received a email from Qiping Chu with a possible thesis topic on Incremental Nonlinear Dynamic Inversion (INDI) control of a pneumatic actuator. At that time, I was not sure of what a pneumatic actuator is, but on hearing about INDI control, I could not control my emotions and immediately accepted the thesis project. That marked the beginning of a glorious research journey, which is soon coming to an end.

Firstly, I would like to thank Qiping Chu for giving me the opportunity to work on such a amazing research project, and its a privilege for me to make a little contribution in INDI, by implementing it for a new application. Secondly, I would like to thank my daily-supervisor Daan Pool who always cheered me up and motivated me to improve, with every meeting. I clearly remember that I was over-enthusiastic a few times and he taught me a very important lesson of not deviating from the main research goal and rather concentrate on things that are actually needed. Besides this, his extra-detailed reviews of my various first-drafts which also contains a few red-coloured copyrighted symbols have greatly improved my academic writing, besides making it more enjoyable. Thirdly, I want to thank my other daily-supervisor Erik-Jan van Kampen, who showed a lot of enthusiasm and interest for my thesis-project. I am very influenced by his research prospective, which incited a lot of creative thinking in me, and also improved my approach to a given research problem, by making it more smart and efficient. Finally, after having a total of thirty highly-productive and enjoyable progress-meetings with my daily-supervisors, and also after having this wonder experience of designing a controller for a pneumatic system, I have become more confident and capable in tackling a given nonlinear system, by designing an appropriate controller for it.

I would also like to thank my wonderful friends at Delft, for giving me a lot of good memories, and also a few embarrassing ones, in the last two years. Lastly, I would like to thank my parents for their unconditional love, and always supporting me, in every possible way.

H. Das
Delft, July 2020

Contents

List of Figures

List of Tables

List of Symbols

P_A	Chamber A pressure
P_B	Chamber B pressure
M_L	Mass of external load
M_p	Mass of piston
A_A	Chamber A area
A_B	Chamber B area
P_a	Ambient atmospheric pressure
A_r	Area of piston
F_{sf}	Static friction coefficient
F_{df}	Dynamic friction coefficient
R	Ideal gas constant
T	Room temperature
k	Specific heat ratio
L	Total stroke length
$\dot{m}_{in,i}$	Mass inflow in chamber i
$\dot{m}_{out,i}$	Mass outflow from chamber i
C_f	Discharge constant
A_v	Area of orifice-opening
P_u	Upstream pressure
P_d	Downstream pressure
P_{cr}	Critical pressure
x_{xs}	Valve-spool displacement
τ	Valve time-constant
x	Piston position
$\dot{x}$	Piston velocity
L_t	Length of connecting-tube
c	Speed of sound
R_t	Resistance of connecting-tube

List of Abbreviations

NDI	Nonlinear Dynamic Inversion
INDI	Incremental Nonlinear Dynamic Inversion
SRS	SIMONA Research Simulator
SIMONA	SImulation, MOtion and NAvigation Institute
PID	Proportional Integral Derivative
RMSE	Root Mean Square Error

1
Introduction

The research context and the motivation behind this research project are given in Sec. 1.1. Next, some of the related research works are presented in Sec. 1.2 and the contributions of this research work are listed in Sec. 1.3. In Sec. 1.4.1, the research objective and the research questions are presented. Finally, the report outline is given in section 1.5.

1.1. Research context and motivation

An actuator is a part of a machine which can control and propel it, by the virtue of opening and closing a valve. Various actuator types are available in the market and can be classified based on their working principle as hydraulic, electric, pneumatic, thermal, twisted and coiled polymer (TCP), thermal and magnetic. The first use of hydraulic and pneumatic actuation system dates back to the first world-war. Hydraulic actuators harness the power of fluid to create either a linear, oscillatory or rotatory kind of motion. These actuators can generate considerable amount of force due to the incompressible property of fluids [40]. Some of the industrial applications require these actuators to be either a single-acting type, where the pressure is applied only on one side or a double-acting type, where the pressure acts on both the sides [6]. Pneumatic actuators on the other hand, utilize atmospheric air as it working medium, which is compressible [35]. Electric actuators are also one of the most widely used actuators in the market [14]. They work on the principle of conversion of electrical energy into mechanical energy. Most of the electric motors are fitted with various sensors to ensure a good closed-loop performance.

Pneumatic actuators have many advantages to offer, over their electric and hydraulic counterparts. For instance, the power generated by a pneumatic actuator is greater than an equivalent weight of hydraulic or electric actuator [70]. This is advantageous for many industries where enough space is not available for bigger equipment. As the pneumatic actuators use air as its working medium, there is no leakage of any harmful industrial fluid into the environment, unlike hydraulic equipment [70]. External leakage can further lead to wear and tear of the hydraulic equipment, thus reducing its operating life. Thus safe and clean actuation is possible in pneumatic actuators, by only utilizing atmospheric air supply. Depending on the external load and type of equipment, electric actuators might require a large flow of electric current to pass through their circuits which can be hazardous, if care is not taken. But this is not the case with pneumatic actuators, which are much safer to operate, due to its requirement of less supply current. Besides this, the viscosity of hydraulic fluids [68] is high, when compared to the negligible viscosity of air. In spite of having these advantages, pneumatic technology is not being harnessed efficiently in industries and for other applications, due to a few of its major shortcomings. One of the issues with these actuators is their highly nonlinear behaviour, due to the compressibility of air and the switching dynamics of air-flow through a pneumatic valve [73]. The other issue is the friction force which acts between the piston and cylinder [54] that makes it difficult to implement high-precision control in these actuators. The connecting tubes that lets the air to flow from the valve to cylinder are a source of time-delay and attenuation, due to which the bandwidth of the controlled system gets reduced, thus reducing its overall speed of operation.

1.2. Related work

Over the past thirty years, a number of controllers have been designed to utilize the pneumatic technology in the best possible way, as discussed here. Pole placement is one of the first developed controllers for a pneumatic actuator [52], but the limitations of the dynamic model and hardware forced the feedback gains to be high. Very high control gain creates extra burden for the actuators, which might also lead to its breakdown. Following the work done in [52], fixed-gain linear controllers are developed in [47] and [49]. Various adaptive control methods have also been explored to estimate the unknown model parameters and thus get a better control performance [62], [88]. Sliding-mode control has also been implemented for the control of pneumatic actuators such as in [89] and [71]. Techniques of backstepping controller design have also been applied for the control of pneumatic actuators [80], [69]. The comparison of some of these nonlinear controllers have been done with conventional linear controllers by considering their respective Root Mean Square Error (RMSE), which shows improvement over the conventional linear control techniques, and in some applications, the useful benefits of different controllers have been combined such as adaptive with backstepping controller [70]. Modern control theory such as artificial neural networks and genetic algorithm are developed recently, as compared to classical control and has since then been used for the control of pneumatic actuators [20], [18]. The performance and the accuracy of pneumatic actuators have increased over the past few years due to application of the above-mentioned control techniques and as such are replacing the electric and hydraulic actuator in Stewart platform-based flight simulators [48], [7]. However, most of the commercially available pneumatically-driven Stewart platform are of miniature scale, because of implementation issue in large pneumatic systems.

As mentioned previously, a model of pneumatic actuator is highly nonlinear and also difficult to obtain accurately. This obviates the widespread use of model-based control techniques for its application, as its performance might degrade on changing parameters such as external load and friction force. In some cases, model-based control techniques demand an iterative process [5] to identify an accurate model of the system, which also requires immense validation and verification at the end. The occurrence of chattering in sliding mode control [62] can cause wear and tear of actuator components, and thus require careful measures to preclude such a phenomenon. Besides this, some of the adaptive and modern control techniques usually require costly hardware equipment, capable of performing a number of computationally complex operations [51].

1.3. Contribution

Recent developments on incremental nonlinear dynamic inversion (INDI) control have led to its widespread use for aerospace control applications [77], [78]. INDI combines the advantages of incremental form with that of a model-based NDI controller, to result in a more robust controller that relies less on the system model and depends more on the accuracy of sensor feedback. The implementation of INDI does not involve any complicated processors, unlike the controllers based on model predictive control (MPC) and artificial neural network (ANN) [51]. INDI being a sensor-based technique relies on the accuracy of sensor feedback, which carries information about the unmodelled system dynamics in the controller [78]. The other important factor that is crucial for the efficient performance of INDI is the time synchronisation of various time-delays in both the plant model and sensors. These factors make the implementation of INDI on a pneumatic actuator difficult and there is no available research work which exploited INDI control for such applications. This necessitates additional research on the components of a pneumatic systems such as its two chambers, inactive volumes at the end of each chamber, connecting tubes and its time-delay, valve and piston dynamics. Thus, the major contribution of this research project is to investigate these pneumatic characteristics and implement INDI controller on a pneumatic system. The considered system will be a long-stroke pneumatic cylinder that is capable of actuating the SIMONA flight simulator of the Delft University, and thus it also serves as a motivation behind our first contribution. Besides this, a number of industrial-standard pneumatic cylinders utilize PID controllers [54], [6], mainly due to its simplified implementation approach, compared to other nonlinear controllers. However conventional linear controllers do not give efficient performance across all the operating conditions [52], without further modification. Therefore, a second contribution of this research project is to implement PID and investigate the benefits of incremental control approach over it, in context of pneumatic actuation. These control techniques will be compared in the presence of realistic sensor noise and conditions of varying external load.

1.4. Research formulation

A research framework has been formulated in order to accomplish this research project, such that the effectiveness of pneumatic actuators can be demonstrated for its use as a commercial flight simulator.

1.4.1. Research objective

The main research objective is formulated as follows:

Research Objective : *The research objective is to increase the position-tracking accuracy of a pneumatically driven system with respect to a conventional linear controller, by designing an incremental nonlinear dynamic inversion (INDI) controller which is simple to implement and relies less on the system dynamics.*

The pneumatic system dynamics considered for designing a controller should account for the actual physical phenomenons, so that the final controlled system can be used commercially in industries. Furthermore, the performance of the designed incremental controller will be compared with that of a Proportional-Integral-Derivative (PID) controller, which is chosen as the baseline controller for comparison with INDI. PID is chosen as the baseline for comparison, as a number of commercial industries relies on PID for controlling their pneumatic systems [54], [6]. Therefore, this comparison will try to highlight some of the possible advantages of INDI over PID controller, and thus stress the importance of incremental controller for industrial applications that utilize pneumatic actuation technology.

1.4.2. Research questions

The research objective is then used to frame a main research question, which is divided into a number of sub-questions. A satisfactory response to the central question will require proper and accurate answers to all its sub-questions. The main research question is formulated as follows:

Research Question : *How can an incremental control law (INDI) be designed for controlling a pneumatic actuator with highly nonlinear and uncertain dynamics, such that the position tracking accuracy of such a system increases with respect to a conventional linear controller ?*

The research sub-questions are given as follows:

1. How to describe the dynamics of a pneumatic system ?
    (a) What are the various components of a pneumatic system and what are its working principle?
    (b) How can the dynamics of each of these components be described using mathematical models?
    (c) How to choose the various parameters in these set of equations, such that it replicates an actual hardware and also suits our application?
2. How to implement incremental control for a pneumatic system ?
    (a) What measures are needed in order to implement INDI controller on a long-stroke pneumatic cylinder ?
    (b) How does the designed controller take into account the various physical phenomenons associated with an actual hardware ?
    (c) How can a conventional INDI controller be augmented for improving the tracking performance of a pneumatic system ?
3. How to check the robustness and any limitations of the designed controller ?
    (a) How to introduce uncertainty and noise in the system dynamics, while performing the simulations ?
    (b) When does the controlled system becomes unstable and starts to degrade its performance ? Can the stability of the controlled system be proved ?
    (c) What are its limitations, in terms of fidelity of a flight simulator ?
4. What measures are needed for comparing the performance of INDI with a baseline PID controller ?

(a) How to implement PID controller for a long-stroke pneumatic cylinder ?

(b) Which tasks should the controlled system perform, such that it gives a fair comparison of both the controllers ?

(c) What metrics are needed for comparing the tracking results of the two controllers ?

Some of the above-mentioned research questions are answered while performing the preliminary research. The rest of the unanswered questions will be analyzed during the masters thesis phase. The solutions to the answered questions and some more recommendations are provided at the end in chapter 5.

1.5. Report Outline

The report is split into three parts. The scientific article is presented in part I. Following it, part II contains the performed literature study and consists of three chapters. Chapter 2 describes the modelling of pneumatic system, which includes the dynamics of piston and rod, model of the cylinder chambers, valve-spool dynamics and the mass flow-rate through a connecting tube. It then discusses the dynamical modelling of a Stewart platform using Newton-Euler's equation. Finally this chapter reviews the state-of-the-art on pneumatic systems, which includes both the actuator and parallel robots. Various controllers which have been designed for different pneumatic systems are also presented here. Finally, chapter 3 evaluates the state-of-the-art on incremental control and discusses some of its applications, issues and improvements. Moreover, the concepts and formulation of both NDI and INDI are also discussed in this chapter.

Next, chapter 4 of part II contains the performed preliminary study, which involves designing a PID and INDI controller for a pneumatic actuator. An INDI controller is initially designed with only piston-position feedback, and then the other formulation of INDI uses both position and pressure feedback. Some of the real-world physical phenomenons are also taken into consideration such as the deviation of the mass-flow rate due to the dynamics of connecting tubes, actuator dynamics and friction forces. Finally, part III draws some conclusion and recommendations based on the performed research work and it also answers the research questions mentioned in this chapter.

I

Scientific Article

Incremental Nonlinear Dynamic Inversion Control of Long-Stroke Pneumatic Actuators

Hemjyoti Das

Abstract

Pneumatic cylinders provide an environment-friendly actuation means by minimizing the leakage of any harmful industrial fluids, as occurs for hydraulic actuators. Thus, pneumatic actuators require less maintenance, compared to hydraulic actuators. Moreover, for a similar weight of hydraulic actuator, the cost of a pneumatic actuation system is less. However, pneumatic actuation has not been utilized widely for industrial applications due to its highly-nonlinear nature. The compressibility property of air, friction forces in the cylinder and the switching dynamics of air flow-rate through the valve are some of the causes for this non-linearity. Therefore, these characteristics can often make the implementation of a model-dependent controller for a pneumatic system difficult. Incremental nonlinear dynamic inversion (INDI) is a control approach which uses less plant-model information, and is thus inherently robust to mismatches in the known plant-model, and also to external disturbances. INDI has recently gained popularity, especially in the aerospace-control research community, but it has never been implemented for controlling a pneumatic system, which necessitates additional research. Therefore, developing an incremental nonlinear controller for a pneumatic system is the main focus of this research article which is accomplished by utilizing a cascaded-control approach, where the inner-loop INDI tracks a given force and the outer-loop NDI is for controlling the piston-position. Moreover, realistic sensor noises have been added in the simulation and the robustness of incremental approach is demonstrated with respect to a baseline PID controller. Besides this, the external load attached to the cylinder-piston is increased by five times and also made variable, in order to show the effectiveness of the incremental control approach. Furthermore, a first-order filter is used for attenuating the sensor noise and the pneumatic valve is simulated using a first-order model. Finally, a series of recommendations is discussed at the end, for future works.

Index Terms

Pneumatic Actuator, Incremental Nonlinear Dynamic Inversion, INDI, Robust Control, Long-Stroke Pneumatic Cylinder, Cascaded-Control, Force-Control, Position-Control, NDI, PID

NOMENCLATURE

P_A	Chamber A pressure
P_B	Chamber B pressure
M_L	Mass of external load
M_p	Mass of piston
A_A	Chamber A area
A_B	Chamber B area
P_a	Ambient atmospheric pressure
A_r	Area of piston
F_{sf}	Static friction coefficient
F_{df}	Dynamic friction coefficient
R	Ideal gas constant
T	Room temperature
k	Specific heat ratio
$\dot{m}_{in,i}$	Mass inflow in chamber i
L	Total stroke length
$\dot{m}_{out,i}$	Mass outflow from chamber i
C_f	Discharge constant
A_v	Area of orifice-opening
P_u	Upstream pressure
P_d	Downstream pressure
P_{cr}	Critical pressure
x_s	Valve-spool displacement
τ	Valve time-constant
x	Piston position
$\dot{x}$	Piston velocity
L_t	Length of connecting-tube
c	Speed of sound
R_t	Resistance of connecting-tube

Abbreviations

NDI	Nonlinear Dynamic Inversion
INDI	Incremental Nonlinear Dynamic Inversion
SRS	SIMONA Research Simulator
SIMONA	SImulation, MOtion and NAvigation Institute
PID	Proportional Integral Derivative
RMSE	Root Mean Square Error

I. INTRODUCTION

An actuator is a very important component of many machines. It helps a machine achieve the desired motion, by converting different forms of energy into a mechanical movement. Hydraulic [1], electric [2] and pneumatic [3] actuators are some of the common means of actuation, for controlling a machine. The SIMONA Research Simulator (SRS) [4] at Delft University of

Hemjyoti Das is a graduate student at the Control and Simulation Group at the Faculty of Aerospace Engineering at Delft University of Technology Kluyverweg 1, 2629HS Delft, the Netherlands

Technology currently uses six hydraulic actuators for generating high-fidelity motion cues. The power of a hydraulic actuator is more than a electric actuator of similar-weight, and also provides high stiffness [5]. Moreover, the performance of hydraulic actuators under conditions of high external load is very satisfactory [6]. However, pneumatic actuators offer many advantages, over their hydraulic counterparts. The working medium of a pneumatic actuator is compressed-air [6], whereas hydraulic cylinders use a mineral oil based-fluid. These hydraulic fluids leak into the environment and can become a major source of pollution [7]. This external-leakage might further lead to internal-leakage and also wearing of the cylinder components [8]. These shortcoming of an hydraulic actuator can be overcome by replacing it with a much safer pneumatic actuation. Thus, pneumatic actuators require much less maintenance, compared to hydraulic actuators and therefore, it can be economically beneficial for a number of industries.

Moreover, the operating condition for most long-stroke hydraulic cylinders is around 100 bar [9], whereas most industrial pneumatic cylinders are certified for a maximum supply pressure of 5 bar [10]. In spite of having the above-mentioned advantages, pneumatic technology is not being harnessed efficiently in industries and for other applications, due to few of its major shortcomings. One of the major issues with these actuators is their highly nonlinear behaviour, due to the compressibility property of air [6]. Moreover, the flow of air can be further classified as either supersonic or subsonic, depending on the ratio of upstream and downstream pressure [11]. So the dynamics of air-flow keep switching, depending on the cylinder's chamber pressure. This becomes a issue with model-based controller, in order to generate precise tracking response. The other major nonlinearity in pneumatic system dynamics is their friction, which includes viscous and Coulomb friction forces [10]. The dynamic-friction forces depend on the direction of piston-velocity and therefore it results in constant switching near the zero piston-velocity. Finally, the tubes connecting the pneumatic valve to the cylinder are a source of attenuation and time-delay in the mass-flow rate of air. The time-taken by the input-wave to reach from valve to the end of the tube is directly proportional to the length of tube [11].

Over the past forty years, a wide range of control techniques have been implemented to utilize pneumatic technology in the best possible way. Pole-placement is one of the first developed controllers for a pneumatic actuator [12], but the limitations of the dynamic model and hardware forced the feedback-gains to be high. High control-gain creates an extra burden for the actuators, which can also sometimes lead to their breakdown. Various adaptive control methods have also been explored to estimate the unknown model parameters [13], [14], in order to get a better control performance. Techniques of back-stepping controller [15], [16] and sliding mode [17], [18] have also been applied for the control of pneumatic actuators. A comparative-study of some of these nonlinear controllers shows improvement over the conventional linear control techniques. However, in some cases, model-based adaptive control techniques demand an iterative process to identify the accurate model of a system, which also requires immense validation and verification [19]. The occurrence of chattering in sliding-mode control [18] causes the wear and tear of actuator components, and thus requires careful measure to preclude such a phenomenon. Besides this, some adaptive and modern control techniques require costly hardware equipment, capable of performing a number of computationally complex operations in a given time [20].

Recent developments in incremental nonlinear dynamic inversion (INDI) control have led to its widespread use for aerospace control applications [21], [22]. INDI combines the advantages of an incremental form with that of a model-based nonlinear dynamic inversion (NDI), to result in a robust controller that relies less on the system model and depends more on the accuracy of sensor feedback [22]. The implementation of INDI does not involve any complicated processors, unlike a few modern control techniques. INDI being a sensor-based technique relies more on the accuracy of sensor feedback, which contains information about the unmodelled system dynamics in the controller. Besides sensor accuracy, another crucial factor for the efficient performance of INDI is the time synchronisation of different time-delays in the plant model and sensors [9]. These factors make the implementation of INDI on a pneumatic actuator difficult and there is no available research work that exploited INDI control for such an application. This necessitates additional research on the components of pneumatic systems such as their two chambers, the inactive volumes at the end of each chambers, connecting tubes and their time-delay, valve and piston dynamics. Therefore, these characteristics of a pneumatic system are investigated in this research article, and INDI is implemented for such a system for position-tracking tasks, which is the major contribution of this research project. As mentioned previously, the SIMONA flight simulator [4] of Delft University currently utilizes six hydraulic cylinders for its actuation. However due to the previously mentioned issues of hydraulic actuation, an effort has been done in this research article to replace it with pneumatic technology. Therefore, this research article implements INDI controller for a pneumatic cylinder, such that it can actuate the SIMONA flight simulator, which also serves as a motivation for this research project. In order to ensure high-fidelity simulations of the SRS, the cylinder should be capable of generating long-strokes of up to one meter with precision, while showing robustness to sensor noises and external disturbances. A few pneumatic flight simulators exist, but they rely on short-strokes using small cylinders [23], [24]. This limits the range of motion that the simulator can demonstrate, thus making it obsolete for its commercial application in the flight simulator industry.

Currently, a number of industrial pneumatic actuators are being controlled by conventional PID controllers [10], [3], mainly due to its ease of implementation. However, the performance of linear controllers for a highly nonlinear system is likely to degrade under varying operating conditions [12]. Therefore, a conventional PID controller has been implemented here as a baseline controller and the second contribution of this research article is to highlight the advantages of incremental-control over a conventional linear-control strategy, in the context of a pneumatic system. Realistic sensor noises are introduced in the feedback of piston-position and chamber pressure sensor, which are further processed using first-order filters, before feeding it to the controller. The external load attached to the piston is also varied, besides increasing it by five times, in order to compare the robustness property between PID and the incremental approach. Absolute error and root mean square error are used as the measures for this comparison.

The organisation of this research article is as follows. First, a brief review of a pneumatic system dynamics and its various component is provided in Section II. This is followed by a description of the basic principles of a NDI and INDI controller in Section III. Thereafter, a cascaded structure of controller is designed for a pneumatic system in Section IV. After that, the simulation results for a given tracking task is provided in Section V. This section also compares the performance of the designed INDI based controller with a baseline PID controller, both under nominal and robust conditions. Next, Section VI validates the plant dynamics and design method used in this article. Following this, Section VII discusses some of the major findings and also suggest a few recommendations for future research. Finally, Section VIII summarizes the conclusion that can be drawn from this research article.

II. Pneumatic system dynamics

A. Working-Principle of a Pneumatic System

A schematic diagram of a pneumatic system is shown in fig. 1 [11]. It consists of an piston to connect an external load to the pneumatic cylinder. The piston divides the cylinder into two chambers, namely A and B. The inflow and outflow of air from the cylinder is controlled using a pneumatic valve. A pair of transmission tubes connects the pneumatic cylinder to a valve. A supply pressure P_s is supplied to the pneumatic valve from the air reservoir. Based on the position of the valve-spool, this supply-pressure is either connected to chamber A or chamber B. For instance in fig. 1, if a positive force F_c is applied then it displaces the valve-spool to the right, which is along positive X-axis, based on the axis convention in fig. 1. This results in the supply pressure being connected to chamber A, while chamber B to the exhaust, due to which the piston moves toward its right along the positive X-axis. Similarly if the direction of force F_c is reversed, then the piston moves left along the negative X-axis. Based on the magnitude of orifice opening in the valve as a result of the spool-displacement of valve, the pressure in each of the two chambers can be controlled, which is accomplished using the designed controllers in this article.

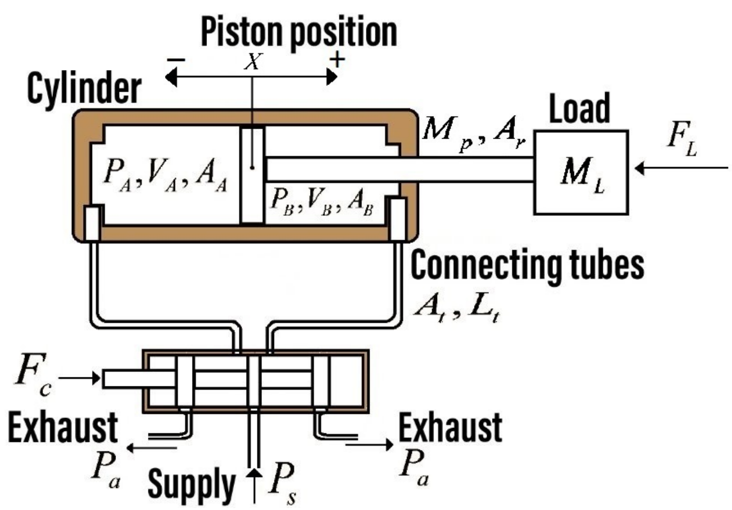

Fig. 1: Schematic diagram of a pneumatic system

B. Dynamical Equations of a Pneumatic System

A detailed mathematical model of a pneumatic system is given in [11], which considers most of the involved nonlinearities and physical phenomenon of a pneumatic system, such as the law of conservation of mass, friction of the piston-seal, attenuation and time-delay in connecting-tubes, inactive volume of air in both the cylinder chambers and different piston-area along the two chambers.

The dynamics of piston and the connected external-load can be described by the following equation:

$$(M_L + M_p)\,\ddot{x} + F_f + F_L = P_A A_A - P_B A_B - P_a A_r \tag{1}$$

In eq. (1), P_A and P_B are the pressures in chambers A and B, respectively, whereas A_A and A_B are the respective areas of chamber A and B, respectively. P_a is the ambient atmospheric-pressure, which is conventionally taken to be 101,325 pascal. M_L refers to the mass of the external-load and M_p denotes the mass of cylinder-piston. F_L refers to the force due to the external load and A_r is the cross-sectional area of the piston rod. These parameters are summarized in Table. I.

A Coulomb friction-force acts between the piston and the inner-surface of cylinder, which is represented by F_f and is expressed below by eq. (2) [11]. F_{sf} and F_{df} refers to the coefficient of static and dynamic friction-forces, respectively, whereas $\dot{x}$ is the velocity of cylinder-piston. The value of dynamic and static friction coefficients are considered as 4.47 N/m and 0.486 N, respectively [11].

$$F_f = \begin{cases} F_{sf} & \text{if } \dot{x} = 0 \\ F_{df}\text{sign}(\dot{x}) & \text{if } \dot{x} \neq 0 \end{cases} \tag{2}$$

Next, the rate of change of pressure across each cylinder-chambers is represented as follows [11]:

$$\dot{P}_i = \frac{RTk}{V_i}\left(\alpha_{in}\dot{m}_{\text{in,i}} - \alpha_{out}\dot{m}_{\text{out,i}}\right) - \frac{P_i k}{V_i}\dot{V}_i \tag{3}$$

In eq. (3), the subscript i can be either A or B, depending on the chamber. The ideal gas constant R is non-dimensional, whose value is taken as 287 and the temperature T is considered to be 293.15 K, which is the room-temperature. $\dot{m}_{\text{in,i}}$ and $\dot{m}_{\text{out,i}}$ respectively refers to the rate of mass-inflow and mass-outflow from the cylinder chamber i. α_{in} and α_{out} are the thermal coefficients that are characteristics of the compression and expansion process, respectively, during the motion of the piston. Both these constants are considered to be equal to the specific heat ratio of atmospheric air k, which is taken as 1.4 [10]. V_i refers to the volume of cylinder chamber i that can be expressed using eq. (4) [10] as follows:

$$V_i = V_{0i} + A_i\left(\frac{1}{2}L \pm x\right) \tag{4}$$

In eq. (4), V_{oi} and A_i refers to the inactive-volume and area of chamber i, respectively. L is the total length of one-complete stroke, summarized below in Table. I. The mass-flow rate from a pneumatic valve to the cylinder can be either classified as chocked or unchoked, depending on the ratio of down-stream to up-stream chamber-pressure [11]. Choked-flow is considered to have attained sonic velocity, whereas a subsonic velocity is attained during a unchoked-flow. It is summarized below in eq. (5).

$$\dot{m}_v = \begin{cases} C_f A_v C_1 \frac{P_u}{\sqrt{T}} & \text{if } \frac{P_d}{P_u} \leqslant P_{cr} \\ C_f A_v C_2 \frac{P_u}{\sqrt{T}}\left(\frac{P_d}{P_u}\right)^{1/k}\sqrt{1-\left(\frac{P_d}{P_u}\right)^{(k-1)/k}} & \text{if } \frac{P_d}{P_u} > P_{cr} \end{cases} \tag{5}$$

In eq. (5), the nondimensional discharge constant C_f is taken to be 0.25. The other constants, C_1 and C_2, which depend on the specific heat-ratio are both unitless and calculated to be 0.1562 and 0.0404, respectively [10]. P_u and P_d denotes the upstream and downstream pressure, respectively. For mass-inflow into chamber A, the upstream pressure P_u equals the supply-pressure P_s, whereas P_d equals the chamber pressure P_A. Similarly for mass-outflow from chamber A, P_u = P_A and P_d = P_a. For our simulation environment, the value of the critical pressure P_{cr}, which depends on the specific heat ratio, is a nondimensional quantity, and is found as 0.5823 [10]. Finally, A_v represents the orifice opening, which controls the flow of air through a pneumatic-valve. The orifice-opening can be changed by the action of force F_c, which is produced by the valve solenoid. In fig. 1, a positive force F_c results in a valve-spool displacement along the positive X-axis, and vice-versa. In our simulation studies, the orifice-opening and valve-spool displacement are related by the following relation [10]:

$$A_v = \text{sign}(X_s)\frac{\pi X_s^2}{4} \tag{6}$$

In eq. (6), X_s refers to the displacement of the valve-spool. Depending on the direction of spool movement along the X-axis, the orifice opening A_v can be either positive or negative. A positive opening A_v signifies that chamber A is connected to the supply pressure, whereas chamber B is connected to the atmosphere through an exhaust. Similarly, a negative area A_v signifies that chamber B is connected to the supply-pressure, whereas chamber A is connected to atmosphere. However, it is to be noted that the control surface used in this article is the orifice-opening of the valve, rather than the spool displacement as then the calculation of control-effectiveness becomes simpler by avoiding the signum function in eq. (6).

The dynamics of both pneumatic and a hydraulic valve can be modelled as a first-order or a second-order transfer function between the commanded control-input and the actual input, which is then fed to plant [9]. This research article uses a first-order error dynamics between the commanded orifice-opening (A_v) from the controller and the actual orifice-opening (A_{v_m}) that is supplied to the plant. It is summarized in eq. (7) as follows:

$$\frac{A_{v_m}(s)}{A_v(s)} = \frac{1}{\tau s + 1} \tag{7}$$

The time-constant τ is considered to be around 10 ms for our simulations and therefore, it should be ensured that the band-width of the final control-outcome should be below 100 Hz, which can be achieved by tuning the controller. The tuning parameters of the designed controllers and its tuning procedure are discussed in more details in Section V-C. To utilize eq. (7) in discrete form, it is transformed using bilinear transformation to obtain eq. (8). The simulations are run using Simulink®software at a sampling frequency of 10,000 Hz, which is selected by assuming it to be twice of that of SIMONA [9], besides aligning with the philosophy that INDI performs better at high sampling-rates [22]. In eq. (8), dt refers to the sampling time, which is the inverse of the sampling frequency in Hz.

$$\frac{A_{v_m}(z)}{A_v(z)} = \frac{dt\,(z+1)}{z\,(2\tau + dt) + (dt - 2\tau)} \tag{8}$$

III. Incremental Nonlinear Dynamic Inversion (INDI)

Nonlinear dynamic inversion (NDI) control is one of the popular control techniques in the aerospace community [25], [26]. NDI, which is also referred to as feedback-linearization, involves a process of state-feedback, due to which any involved nonlinearity gets cancelled and the final controlled dynamics can be guided by a linear-control law, such as PID. However, NDI requires an accurate knowledge of the system-states, as the presence of any external disturbances or an inaccurate plant-model will not result in an exact cancellation of the system-nonlinearity, thus reducing the efficiency of the controlled system. Incremental Nonlinear Dynamic Inversion (INDI) is a recently developed control-technique, which has been used widely for aerospace applications [21]. It is more robust compared to NDI in handling external disturbances and system uncertainties, due to its marginal dependency on the plant dynamics.

A. Basic Principles of INDI

The basic principle of INDI is that it combines the advantages of model inversion with that of incremental approach, to result in a control-command that relies mores on the accuracy of the sensor feedback and depends less on the system-dynamics. The block diagram of an INDI controller is shown below in fig. 2, where $\mathbf{x}_d$ refers to the desired system-state and $\mathbf{x}$ is the actual state. In order to frame an INDI control, a general nonlinear plant is defined as follows:

$$\dot{\mathbf{x}} = f(\mathbf{x}, \mathbf{u}) \tag{9}$$

In eq. (9), $\mathbf{x}$ and $\mathbf{u}$ refers to the state vector and the supplied control-input, respectively. Taylor-series expansion can be used to expand $f(\mathbf{x}, \mathbf{u})$ as follows:

$$\dot{\mathbf{x}} = f\left(\mathbf{x}_0, \mathbf{u}_0\right) + \left.\frac{\partial f(\mathbf{x}, \mathbf{u})}{\partial \mathbf{x}}\right|_{\mathbf{x}=\mathbf{x}_0, \mathbf{u}=\mathbf{u}_0} (\mathbf{x} - \mathbf{x}_0) + \left.\frac{\partial f(\mathbf{x}, \mathbf{u})}{\partial \mathbf{u}}\right|_{\mathbf{x}=\mathbf{x}_0, \mathbf{u}=\mathbf{u}_0} (\mathbf{u} - \mathbf{u}_0) + \text{H.O.T.} \tag{10}$$

In eq. (10), H.O.T. refers to higher-order terms which are neglected to obtain an simplified expression as follows:

$$\dot{\mathbf{x}} \simeq \dot{\mathbf{x}}_0 + F\left(\mathbf{x}_0, \mathbf{u}_0\right) \Delta\mathbf{x} + G\left(\mathbf{x}_0, \mathbf{u}_0\right) \Delta\mathbf{u} \tag{11}$$

$F\left(\mathbf{x}_0, \mathbf{u}_0\right)$ and $G\left(\mathbf{x}_0, \mathbf{u}_0\right)$ refers to the Jacobian operation, defined as $F\left(\mathbf{x}_0, \mathbf{u}_0\right) = \left.\frac{\partial f(\mathbf{x}, \mathbf{u})}{\partial \mathbf{x}}\right|_{\mathbf{x}=\mathbf{x}_0, \mathbf{u}=\mathbf{u}_0}$ and $G\left(\mathbf{x}_0, \mathbf{u}_0\right) = \left.\frac{\partial f(\mathbf{x}, \mathbf{u})}{\partial \mathbf{u}}\right|_{\mathbf{x}=\mathbf{x}_0, \mathbf{u}=\mathbf{u}_0}$. The incremental quantities $\Delta\mathbf{u} = \mathbf{u} - \mathbf{u}_0$ and $\Delta\mathbf{x} = \mathbf{x} - \mathbf{x}_0$ refers to the deviation of variable $\mathbf{x}$ and $\mathbf{u}$ at the current sampling-instant, from its previous sampling-instant. Next, considering a high sampling-rate of the state and using time-scale separation principle, it is assumed that the update-rate of the control-command $\mathbf{u}$ is much higher than that of the state $\mathbf{x}$. Therefore, the state-Jacobian term is dropped, resulting in the following expression:

$$\dot{\mathbf{x}} \simeq \dot{\mathbf{x}}_0 + G\left(\mathbf{x}_0, \mathbf{u}_0\right) \Delta\mathbf{u} \tag{12}$$

Eq. (12) can be linearized by the following incremental control law:

$$\Delta\mathbf{u} = G\left(\mathbf{x}_0, \mathbf{u}_0\right)^{-1} \left(\mathbf{v} - \dot{\mathbf{x}}_0\right) \tag{13}$$

By equating eq. (13) in eq. (12), the linear enforcement-dynamics is obtained as $\dot{\mathbf{x}} = \mathbf{v}$. The chosen linear-law $\mathbf{v}$ will guarantee an asymptotic stability of the plant-output error, and it will be discussed in more details in Section IV-C. Therefore, the total control-command generated from INDI is summarized in eq. (14).

$$\mathbf{u} = \mathbf{u}_0 + G\left(\mathbf{x}_0, \mathbf{u}_0\right)^{-1} \left(\mathbf{v} - \dot{\mathbf{x}}_0\right) \tag{14}$$

It can be observed from eq. (14) that the final expression of control-command does not contain any information of the state-transition matrix $F(\mathbf{x_0}, \mathbf{u_0})$, and is thus less-dependent on the system dynamics. However, it is dependent on the feedback of the state-derivative, and thus an erroneous feedback of $\dot{\mathbf{x}}_0$ can reduce the efficiency of INDI.

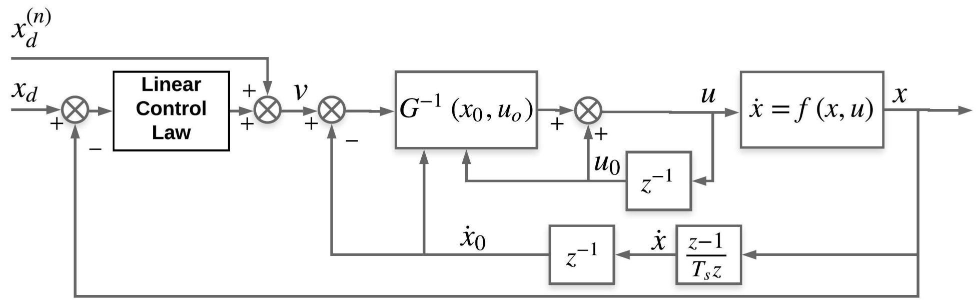

Fig. 2: Block diagram of an INDI controller

B. Robustness of INDI

As mentioned previously, INDI is robust compared to NDI because it can handle uncertainties in the plant model. The robust property of INDI will be demonstrated by the following analysis. In eq. (14), some uncertainty is assumed to be present in the control-effectiveness matrix, which is represented as follows:

$$G(\mathbf{x}, \mathbf{u}) = G_n(\mathbf{x}_0, \mathbf{u}_0) + \Delta G(\mathbf{x}_0, \mathbf{u}_0) \tag{15}$$

The nominal control-effectiveness is represented as $G_n(\mathbf{x}_0, \mathbf{u}_0)$ and uncertainties are represented as $\Delta G(\mathbf{x}_0, \mathbf{u}_0)$. The uncertainties in the control effectiveness are not known and thus the final INDI command will be framed based only on the nominal part, as represented by eq. (16).

$$\mathbf{u} = \mathbf{u}_0 + G_n\left(\mathbf{x}_0, \mathbf{u}_0\right)^{-1}\left(\mathbf{v} - \dot{\mathbf{x}}_0\right) \tag{16}$$

Next, utilizing eq. (15) and eq. (16) in eq. (12), the following relation is obtained:

$$\dot{\mathbf{x}} = -\Delta G\left(\mathbf{x}_0\right) G_n^{-1}\left(\mathbf{x}_0\right) \dot{\mathbf{x}}_0 + \left(I_{n\times n} + \Delta G\left(\mathbf{x}_0\right) G_n^{-1}\left(\mathbf{x}_0\right)\right) \mathbf{v} \tag{17}$$

By assuming a high sampling-rate of the system, the state-derivative $\dot{\mathbf{x}}_0$ at the previous sampling-instant is considered equal to the corresponding variable in the present instant $\dot{\mathbf{x}}$. Thus, making this change of variable in eq. (17), the following relation is obtained:

$$\left(I_{n\times n} + \Delta G\left(\mathbf{x}_0\right) G_n^{-1}\left(\mathbf{x}_0\right)\right) \dot{\mathbf{x}} = \left(I_{n\times n} + \Delta G\left(\mathbf{x}_0\right) G_n^{-1}\left(\mathbf{x}_0\right)\right) \mathbf{v} \tag{18}$$

Cancelling the similar terms along both sides of eq. (18) results in the simplified relation $\dot{\mathbf{x}} = \mathbf{v}$. This is similar to the linear enforcement dynamics for the nominal case [22]. Therefore, it can be concluded that if the considered system has a high sampling-rate, then uncertainties in control-effectiveness does not influence the performance of the incremental control approach INDI. The stability and robustness analysis of INDI can be found in more details in [27].

IV. Controller Design

A. Cascaded Structure of Pneumatic Controller

A cascaded strategy of pneumatic control is discussed in this section. It is similar in principle to that of a cascaded hydraulic controller [5] which is summarized in fig. 3.

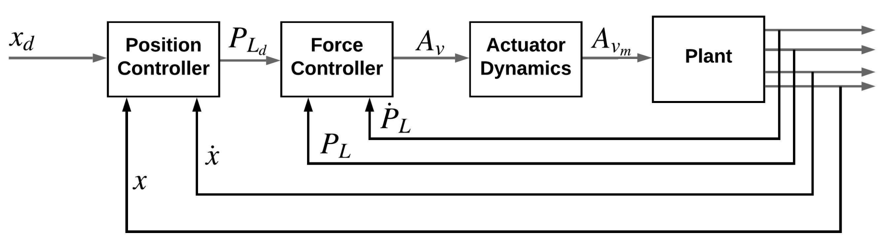

Fig. 3: Block diagram of a cascaded control approach

The outer-loop is known as the position control loop which is fed with the desired piston-position x_d. It also receives the feedback of the actual piston-position x and its velocity $\dot{x}$. Based on their error, the desired pressure-difference P_{L_d} across the two chambers is calculated, which is further fed to the inner-loop force controller. The inner-loop receives the feedback of actual pressure-difference P_L across the two chambers, and also its derivative $\dot{P}_L$. The output of inner-loop controller is the commanded orifice-opening A_v of pneumatic valve (see fig. 1), which is then acted upon by a valve-dynamics (eq. (8)). Finally, the output A_{v_m} of the valve dynamics is fed to the pneumatic plant, described previously in Section II.

In the following sections, two different cascaded control approaches are discussed. The first uses NDI as the outer-loop controller, whereas INDI acts as the inner-loop controller. This approach is called as incremental control approach in this research article, as the final control-command issued to the plant is calculated using INDI. The outer-loop of incremental approach is designed using NDI as its involved dynamics of piston-load combination (eq. (1)) is simple in formulation and marginally prone to uncertainties, compared to the dynamics of inner-loop. Therefore, the inner-loop incremental approach is framed using INDI which involves a number of system-states that are prone to abrupt variations and uncertainties. The goal of inner-loop INDI is primarily to control the dynamics, defined by eq. (3) and eq. (5). It can be observed that the dynamics of both the chamber-pressure and air-flow are comparatively nonlinear and thus, more sensitive than the piston-position dynamics. INDI, being less dependent on the system dynamics, will thus be a better-fit for the inner-loop dynamics, whereas NDI is best suited for a more certain dynamics, such as that of the cylinder-piston. A second cascaded approach is then designed for the pneumatic system, where both the inner-loop and outer-loop are based on PID. It will be used as the baseline controller for comparing with the incremental control approach. PID is chosen as the baseline controller for comparison because a number of industrial pneumatic actuation systems use this conventional control technique [3], [10] and thus, any advantage of incremental approach over PID will be be beneficial for a number of industries that utilizes pneumatic actuator technology.

B. Outer-Loop Position Control using NDI

The outer-loop command is computed using NDI, by utilizing the dynamics of piston and external-load. The area of chamber B is A_B which can be related to that of chamber A as A_B=A_A-A_r, where A_r refers to the piston-area. Using this relation in eq. (1), the following equation is obtained:

$$(M_L + M_p)\,\ddot{x} + F_f + F_L = (P_A - P_B)A_A + P_B A_r - P_a A_r \tag{19}$$

Before proceeding to model inversion, the friction force F_f is ignored, as they can be highly oscillatory for some part of the trajectory, which will then be reflected in the final NDI output. Thus, the designed NDI controller in this research article does not involve a complete inversion. This partial dynamic inversion is usually implemented when a small perturbation in some system-states result in a vast variation of the control command [28]. Next, by introducing the linear control law $\ddot{x} = v_1$ in eq. (19), the expression for desired pressure-difference across the chambers is calculated as follows:

$$P_{L_d} = \frac{(M_p + M_L)\,v_1 + P_a A_r - P_B A_r + F_l}{A_a} \tag{20}$$

P_{L_d} refers to the difference of pressure between the two chambers of cylinder. The linear control law v_1 is chosen as follows:

$$v_1 = K_{p_1}\,(x_d - x) - K_{d_1}(\dot{x}_d - \dot{x}) + K_{i_1}\sum dt(x_d - x) \tag{21}$$

In eq. (21), x_d refers to the desired piston-position, x is the actual piston-position and the tuning parameters are denoted by K_{p_1}, K_{d_1} and K_{i_1}. The tuning procedure and the parameters are summarized in the next section.

C. Inner-Loop Force Control using INDI

The inner-loop control is based on INDI and is also known as a force control loop [5]. In order to derive the INDI control law, the mass-flow rates in eq. (3) and the chamber pressure in eq. (4) are both equated in eq. (5). Furthermore, by utilizing the expression for the differential-pressure P_L, the following equation of motion is obtained:

$$\dot{P}_L = f(A_v, \text{Other Parameters}) \tag{22}$$

The other parameters in eq. (22) refer to the flow-rate constants C_f, C_1 and C_2, the ideal-gas constant R, the temperature T, the specific heat-ratio k, the complete stroke-length L, the inactive chamber-volume V_0, the area of chambers A_A and A_B, and the position of the piston x. Next, simplifying eq. (22) and utilizing a high-sampling rate of the system, the following relation is obtained:

$$\dot{P}_L = \dot{P}_{L_0} + G(A_v - A_{v_0}) \tag{23}$$

In eq. (23), $\dot{P}_{L_0}$ refers to the derivative of actual pressure-difference across the chambers at the previous sampling-instant. A_v and A_{v_0} denote the orifice opening of the valve, measured at the current and previous sampling-instant, respectively. INDI assumes that the commanded orifice-opening is achieved instantaneously, and is thus equal to the actual orifice-opening of plant. However, in reality it is acted upon by actuator-dynamics, which is represented as a first-order lag (eq. (8)). The control-effectiveness G is calculated by using the following relation:

$$G = \frac{\partial \dot{P}_L}{\partial A_v} \tag{24}$$

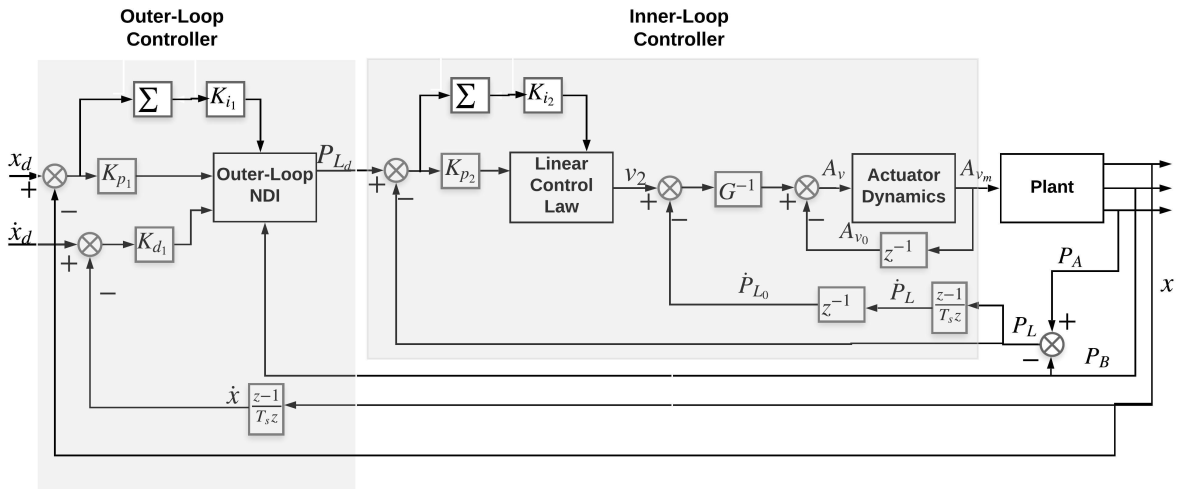

Fig. 4: Block diagram of incremental control approach

As mentioned in Section III-B, INDI is robust to variations in the control-effectiveness. Therefore, a fixed control-effectiveness of magnitude $3 \cdot 10^8$ is used here, which is chosen after carefully analyzing the time-domain response of the INDI-controlled system, and then averaging the value of G over the whole simulation period. Next, by introducing the linear control law $\dot{P}_L$ = v_2 and by inverting eq. (23), the following relation is obtained for the final INDI control-output:

$$A_v = A_{v_0} + G^{-1}\left(v_2 - \dot{P}_{L_0}\right) \tag{25}$$

The linear control-law v_2 is summarized below in eq. (26). K_{p_2} and K_{i_2} are the tuning parameters, which will be discussed in Section V-C.

$$v_2 = \dot{P}_{L_d} + K_{p_2}\left(P_{L_d} - P_L\right) + K_{i_2}\sum dt(P_{L_d} - P_L) \tag{26}$$

The block diagram of the cascaded incremental approach is shown in fig. 4. It is to be noted that the desired derivative component for the inner-loop linear control law $\dot{P}_{L_d}$ is considered as zero in order to minimize any noise, which is obtained by numerically differentiating the chamber pressure. This aligns with the philosophy of partial inversion, as discussed previously.

D. Outer-Loop Position Control using PID

The outer-loop of the cascaded PID control approach is discussed in this section, which will then be combined with an appropriate inner-loop. The input signal to outer-loop is the error in piston-position and its time-derivatives. The output of this loop is the desired pressure difference across the cylinder chambers, which is then fed to the inner-loop controller. It is summarized below in eq. (27). K_{p_3}, K_{d_3} and K_{i_3} denotes the proportional, derivative and integral constants of the PID, respectively, which will be discussed in Section V-C.

$$P_{L_d} = K_{p_3}\left(x_d - x\right) + K_{d_3}(\dot{x}_d - \dot{x}) + K_{i_3}\sum dt(x_d - x) \tag{27}$$

E. Inner-Loop Force Control using PID

The inner-loop of the cascaded PID approach controls the differential-pressure across the chambers, by calculating the required orifice-opening of the pneumatic valve. It is summarized below in eq. (28), where K_{p_4}, K_{d_4} and K_{i_4} are the tuning parameters.

$$A_v = K_{d_4}(\dot{P}_{L_d} - \dot{P}_L) + K_{p_4}\left(P_{L_d} - P_L\right) + K_{i_4}\sum dt(P_{L_d} - P_L) \tag{28}$$

The block diagram of the cascaded PID approach is shown in fig. 5. Similar to the incremental approach, the derivative component of PID for the inner-loop is also considered as zero, in order to minimize any high-frequency oscillations due to the numerical differentiation of chamber pressure.

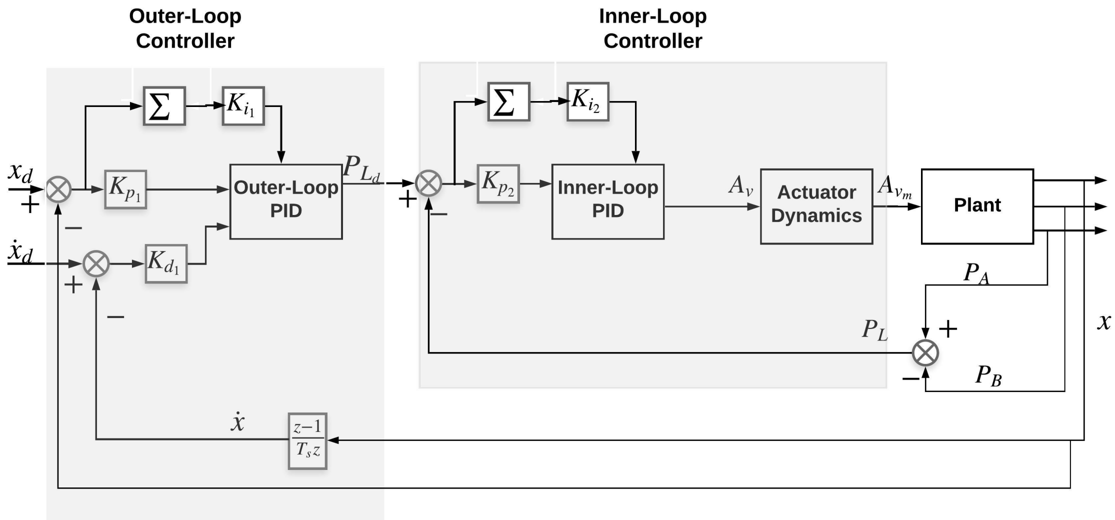

Fig. 5: Block diagram of cascaded PID approach

V. Simulation Results

A. Selection of Actuator Dimensions

The motion-base of the SIMONA flight simulator [4] currently uses six hydraulic cylinders for its actuation. As mentioned previously, this research article designs an incremental controller for a pneumatic system that is capable of actuating SIMONA and therefore, the dimensions of the pneumatic cylinder are selected by considering the actuation requirements of SIMONA. The actuation of a high-fidelity flight simulator requires a cylinder capable of generating long-strokes. For SIMONA, the maximum stroke-length is 1.25 m and its maximum speed of operation is 0.9 m/s[1]. Its total payload is around 4,500 kg, which also includes the weight of two test-pilots. Utilizing this total weight of payload and the desired speed of operation, the dimensions of the pneumatic system are then calculated. The available models of SMC[2] and Festo[3] are used, to provide the best matching dimensions of a pneumatic cylinder.

The total load of SIMONA when considering it to be directly perpendicular to the ground, is roughly 45,000 N. This weight has to be distributed amongst the six cylinders, which are acting as its legs. Dividing the weight uniformly across its legs, the load on each cylinder is 7,500 N. However, this load will not always be uniformly distributed amongst its six legs, as it depends on the maneuver that the simulator is executing. Therefore, after considering around 33% extra load, the thrust that each cylinder should be capable of generating is considered as 10,000 N. The maximum supply pressure from the air reservoir is taken as 10 bar, and it is assumed that around 70% of maximum supply pressure is utilized for most of the tracking operation. The atmospheric pressure is considered to be 1 bar and the pneumatic cylinder is directly connected to the atmosphere through an exhaust. So, the approximate driving pressure that propels the piston for most of its operation is 6 bar, which is obtained by subtracting the atmospheric pressure from 70% of the maximum supply pressure. Next, the required area of cylinder-bore is calculated as follows:

$$\text{Bore Area} = \frac{\text{Thrust Needed}}{\text{Driving Pressure} \times \text{Efficiency}} = \frac{10,000\ \text{N}}{600,000\ \text{Pa} \times 0.9} = 0.0185\ m^2 \tag{29}$$

An efficiency of 90% is considered for the pneumatic cylinder after analyzing a series of commercially available actuators[4]. A bore area of 0.0185 m^2 corresponds to a cylinder of inner diameter 15.4 cm. Pneumatic cylinders of such a dimension is not available in the market and therefore, the next available cylinder diameter[5] is considered in this research article, which is 16 cm.

Next, the consumption-rate of air is calculated that can generate the desired stroke in a given time. If a cylinder stroke of 0.5 m is to be completed in 1 seconds, then the total air-consumption every second is found by multiplying the area of cylinder

[1]T. Delft, “Flight deck·simona.” [Online]. Available: http://cs.lr.tudelft.nl/simona/facility/flight-deck

[2]SMC, ”CP96-C ISO15552 Cylinders” [Online]. Available: https://www.pneumatiek.nl/pneumatiek/smc-pneumatics/cilinders/cp96-iso-32-t-m-100/cp96-c-iso15552/

[3]Festo, ”Normcilinder DSBG Cylinders” [Online]. Available:https://shop.eriks.nl/nl/pneumatische-componenten-cilinders-zuigerstang-cilinders-standaard-cilinders/normcilinder-dsbg-pr455266037361155/

[4]SMC, ”The Pneubook” [Online]. Available: https://www.scribd.com/document/126820448/SMC-the-Pneubook

[5]SMC, ”Datasheet of SMC SY Series Pneumatic Cylinders.” [Online]. Available: https://content2.smcetech.com/pdf/SY3.5.7.9000.pdf

with its stroke length, which in our case is found to be around 9.3 l/s. Boyle's law [29] is then utilized which is summarized as follows:

$$P_1V_1 = P_2V_2 \tag{30}$$

In eq. (30), P_1 refers to the actual driving force of the system plus the atmospheric pressure, which comes to be 8 bar. V_1 refers to total air consumption calculated previously as 9.3 l/s. P_2 is the atmospheric pressure and V_2 is the amount of air consumed during a full-stroke, by the cylinder. Thus the air consumed by the cylinder is found to be 74.4 litre, which is needed in 1 second to complete a stroke of 0.5 m. In minutes, the air-consumption rate is calculated as 4,464 l/min, which its corresponding pneumatic valve should be capable of generating. In our simulation experiments, it has been found that the maximum mass-flow rate into both chamber A and B is 0.32 kg/s (fig. 8), which after conversion comes to around 1,683 l/min. Therefore, the air-consumption rates obtained for the nominal case are much below the maximum limit of the valve. Moreover, the external mass for the nominal case is considered as 200 kg, which is 5 times less than the maximum external mass of 1,000 kg and therefore, the corresponding air-consumption rate of the valve is found to be less than the maximum limit by a similar factor. Some of the other rating[4] for the air-consumption rate that are used commercially are Cv value, kv and S. The parameters of a big pneumatic system that is used for this research article is summarized below in Table. I. The maximum orifice opening $A_{v_{max}}$ is not found in the manufacturer's datasheet[5] and is therefore selected in a way that enables the cylinder to attain a maximum piston velocity, as specified in its data-sheet. It is also found in our analysis that lowering $A_{v_{max}}$ reduced the maximum speed attainable by the cylinder due to less air-flow through it and vice-versa. The maximum supply pressure P_s is obtained from the manufacturer[5], and exceeding this limit is against the standard approvals set by ISO[4], which is followed worldwide for certification of pneumatic cylinders.

TABLE I: Dimensions of a big pneumatic system

Parameter	Long-stroke pneumatic system
Piston Length (L)	1.2 m
Piston Ineffective Length (L_0)	0.1 m
Chamber Diameter (d_c)	0.16 m
Piston Diameter (d_p)	0.032 m
External load mass (M_L)	200 kg
Piston Rod Mass (M_p)	2 kg
Maximum Orifice opening ($A_{v_{\max}}$)	$2.2062 \cdot 10^{-3}$ m^2
Maximum supply pressure (P_s)	10 bar

This research article initially demonstrates the working of incremental control approach for a low external-load of mass 200 kg, following which the load is increased. It is found after a preliminary research that when a heavy load is attached to the piston, then at some points of our sinusoidal tracking-trajectory, the pressure in either of the two chambers saturated. Techniques such as PCH [30] can be implemented later to take this saturation into account, but it is beyond the scope of this research article. However, the incremental control approach is implemented later in this article for a heavy load of 10,000 N, in order to analyze this phenomenon of pressure-saturation. Furthermore, the initial pressure in both the chambers is set according to the total external load that is needed to balance it. This ensures that the piston-position does not displace initially in the opposite direction, similar to a non-minimum phase behaviour. In order to calculate the initial pressures, the following two equations are solved:

$$P_AA_A - P_BA_B = F_L + P_aA_r \tag{31}$$

$$P_A + P_B = P_s \tag{32}$$

eq. (31) is obtained by equation eq. (19) to zero. Moreover, the piston acceleration $\ddot{x}$, and the Coulomb friction forces are both assumed to be zero at the initial sampling-instant. eq. (32) assumes that the sum of the pressure across the two chambers is equal to the maximum supply pressure at the initial time-instant. However, the sum of the chamber pressure is not always less than the maximum supply pressure because of compressing effect due to heavy external-loads, which is discussed in Section VII. The initial chamber-pressures P_{A0} and P_{B0} corresponding to three different external loads are summarized in Table. II. P_{A0} is usually greater than P_{B0} due to the asymmetric nature of our simulation setup, where the pneumatic cylinder is kept parallel to gravity, with the chamber A directly below chamber B. If the cylinder is kept perpendicular to gravity, then it requires the initial pressures P_{A0} and P_{B0} to be similar, which can concluded by solving eq. (31) and eq. (32), and also after equating F_L to zero due to the symmetric placement of pneumatic cylinder that is attached to a static external load.

B. Controller Tuning

The incremental control approach and the PID are initially tuned to result in similar time-domain unit-step responses. Then, these tuned coefficients are used to track the above-mentioned sinusoidal reference trajectory. This ensures a "fair" and "unbiased" comparison of both the control approaches. In order to tune the INDI controller, the proportional and derivative

TABLE II: Initial pressure in the cylinder chambers for different external loads

External load	P_{A0}	P_{B0}
10 N	$5{\cdot}10^5$ Pa	$5{\cdot}10^5$ Pa
2,000 N	$5.68{\cdot}10^5$ Pa	$4.32{\cdot}10^5$ Pa
10,000 N	$7.45{\cdot}10^5$ Pa	$2.54{\cdot}10^5$ Pa

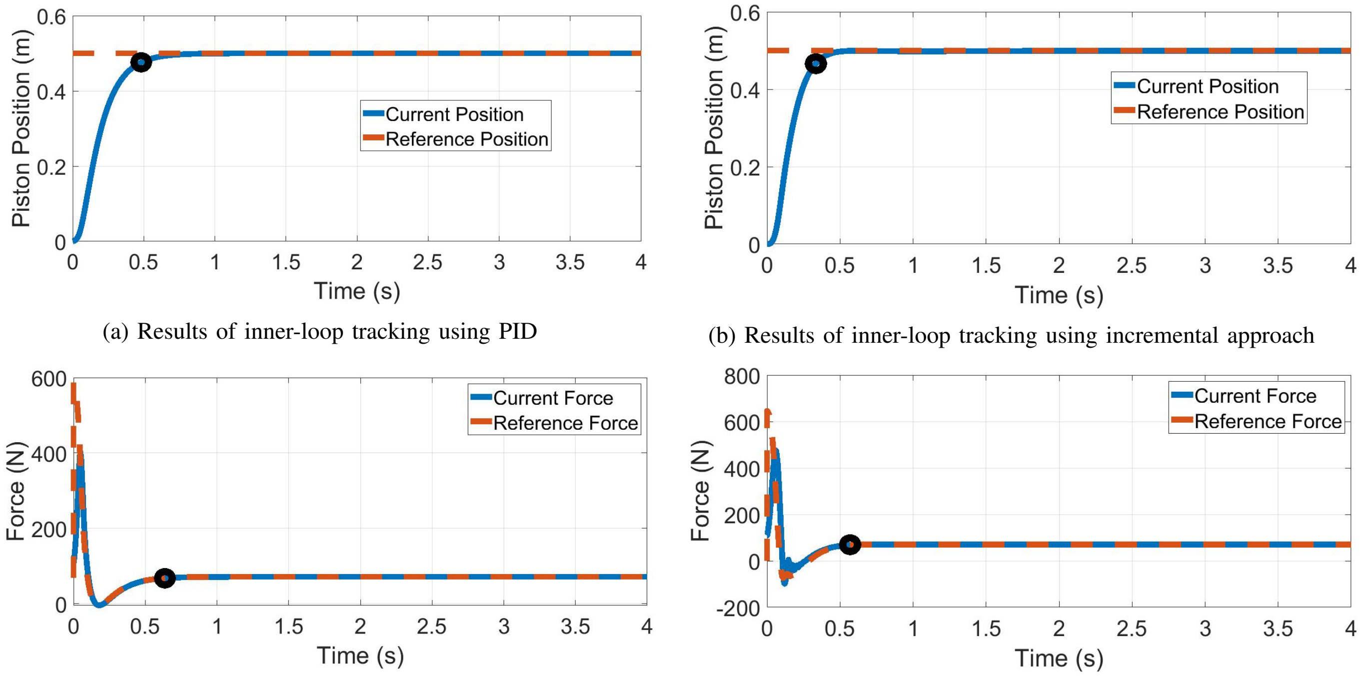

(a) Results of inner-loop tracking using PID

(b) Results of inner-loop tracking using incremental approach

(c) Results of outer-loop tracking using PID

(d) Results of outer-loop tracking using incremental approach

Fig. 6: Tuning of PID and incremental approach for a unit-step command

components are both initialized with zero. Next, the proportional gain is increased until an overshoot and a corresponding reduction in rise-time is seen. Sometimes, the overshoot can also lead to multiple visible peaks. The derivative component is then increased to damp the overshoot, which results in an increase in the rise time. This process is repeated until a desired time-domain tracking performance is obtained, as summarized in Table. III. The integral component is considered to be zero for the incremental control approach, as it assumes first-order error dynamics in its formulations, which results in zero steady-state error. The error converges to zero in an asymptotic sense by the use of a suitable error-dynamics, as described by eq. (26).

TABLE III: Controller coefficients for PID and incremental control approach

	K_p	K_d	K_I
Outer-Loop (NDI)	135	25	0
Inner-Loop (INDI)	175	0	0
Outer-Loop (PID)	1,605,000	250,000	0.01
Inner-Loop (PID)	$1{\cdot}10^{-6}$	0	$1{\cdot}10^{-14}$

For tuning the PID controller, the proportional and derivative components are both initialized with 1. Then, the proportional and derivative components are increased sequentially, similar to the previously mentioned approach for incremental control. However in this case, the integral component is increased by a factor of around 0.01 times the proportional component, when the time-domain response improves due to P and D component but it settles down with some steady-state error. Introducing the integral component changes the time-domain behaviour of the system's response, which requires further tuning of the proportional and derivative component. It is done in a iterative way as mentioned previously in this section. The final obtained controller coefficients are summarized in Table. III. The proportional, derivative and integral coefficients are represented as K_p, K_d and K_I, respectively. We can observe that both the controller responses are over-damped with no overshoot. Besides overshoot, rise-time is chosen as the other measure for tuning the outer-loop, and the tuning is performed such that this time-domain specification is similar for both the control approaches. The rise-time can have many interpretation, and in this research article it is considered as the time to reach from 0% to 95% of its steady-state value. Their step-responses are plotted in fig. 6 and the points corresponding to these specifications are marked on the graph with black circles. It is observed that there is a difference of around 0.08 seconds between their rise-times, which is acceptable for our pneumatic application.

The inner-loop gains are then tuned such that both the control approaches are able to achieve a similar settling-time, which is defined as the time required to settle from 0% to 95% of its steady-state value. The inner-loop tracking for the step response is plotted in fig. 6 and the settling-time of both the controllers is marked in the graph using black circles. The tuning guidelines for the inner-loop are the same as outer-loop that is mentioned previously, and finally the difference between settling time of the two approaches is found to be 0.6 seconds. It is also to be noted from Table. III that the proportional and the derivative gains of PID are much higher for the outer-loop, when compared with the incremental approach. The reason for this observation is that the output of the outer-loop PID is a linear control law that depends only on position error of the piston. The maximum magnitude of the piston-position is around 0.5 m, whereas output of the outer-loop is the desired differential pressure, whose magnitude is around 10^5 Pa. Therefore, high gains are needed in PID to bring such a noticeable change in its output. However, this is not the case with the incremental approach, as the linear control law of its outer-loop is further acted upon, both by the chamber pressure B and atmospheric pressure P_a, as described by eq. (20). Besides these outer-loop gains, an opposite trend is observed for the inner-loop gains, where the gains of PID are much higher than that of the incremental approach. This is because the linear control law of the inner-loop incremental approach is acted upon by the control effectiveness, whereas for the PID approach, the output of linear control law directly serves as the input to the plant. The control effectiveness in our case is very high, i.e. $3{\cdot}10^8$ and moreover, the output of inner-loop is the required orifice-opening of the valve whose maximum amplitude is around $2.21{\cdot}10^{-3}\ m^2$. So both these factors contribute to the high gain and the low gain of the inner-loop PID and inner-loop incremental approach, respectively.

C. Controller Analysis under Nominal Conditions

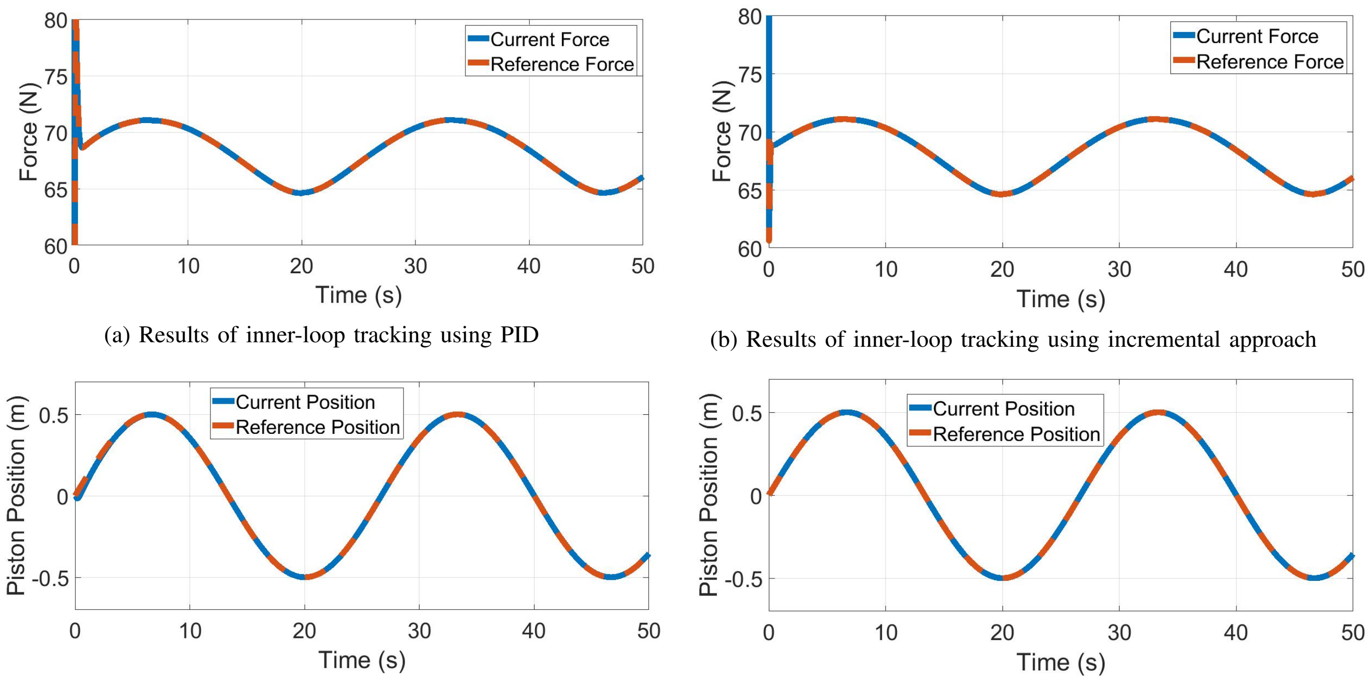

(a) Results of inner-loop tracking using PID

(b) Results of inner-loop tracking using incremental approach

(c) Results of outer-loop tracking using PID

(d) Results of outer-loop tracking using incremental approach

Fig. 7: Nominal case tracking results of incremental control approach and PID for an external load of F_L=2,000N

The controller is initially analyzed under nominal conditions, where sensor noises are not added and the external-load is considered as 2,000 N. The nominal case is then followed by a robust case in the next section in which sensor noises are introduced and the external load is increased to 10,000 N, besides making it variable. A sinusoidal trajectory is chosen as the reference for analyzing the controller response, as such a trajectory ensures that a long-stroke motion of the cylinder is possible at a given speed. Moreover, a sinusoidal trajectory also ensures that a few turn-around points exist so that the robustness of both the control approaches can be tested in such regions. These turn-around points and the controller response for such regions are discussed later in this section. It is to be noted that other reference trajectories such as a staircase reference signal can also meet these objectives, but it is beyond the scope of this article. Moreover, the reference-velocity for a sine trajectory is simple to obtain by backward differentiation, unlike a staircase reference which involves discontinuities while differentiating

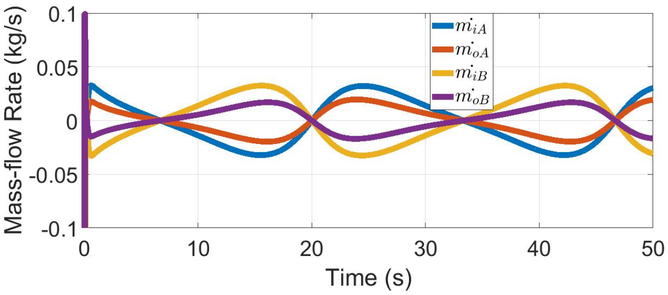

(a) Mass-flow rates for PID approach

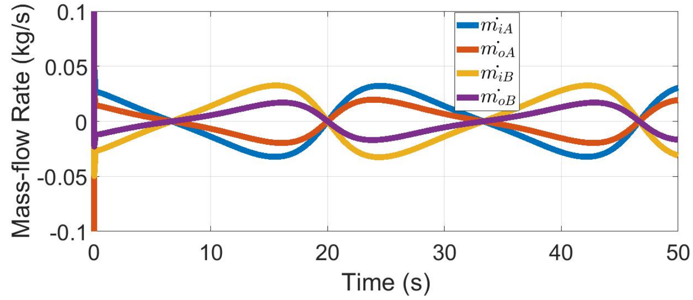

(b) Mass-flow rates for incremental approach

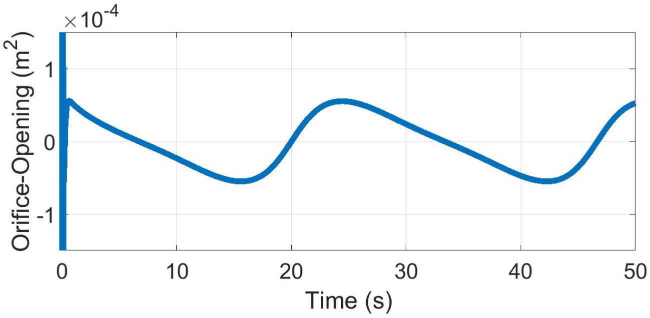

(c) Control-input issued to the plant for PID approach

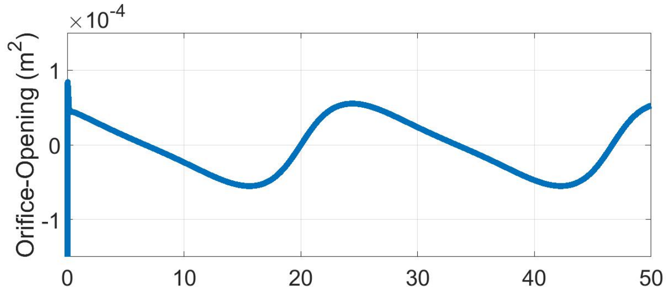

(d) Control-input issued to the plant for incremental approach

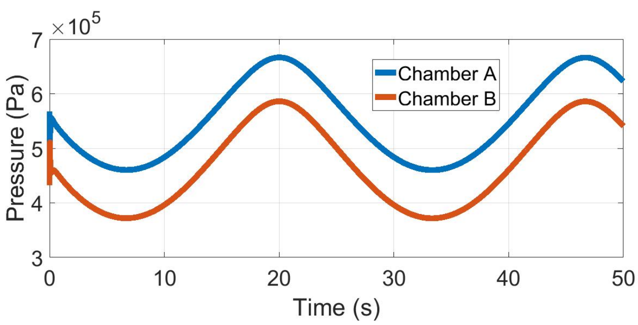

(e) Chamber-pressures for PID approach

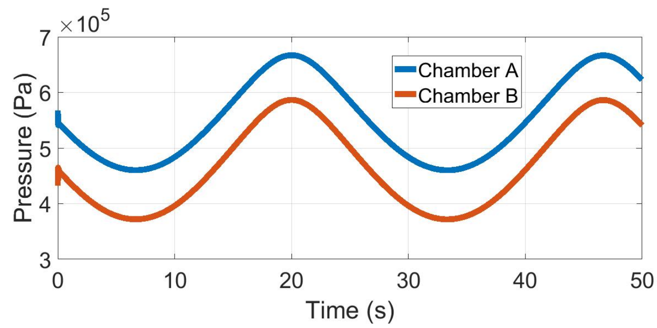

(f) Chamber-pressures for incremental approach

Fig. 8: Mass flow-rates, chamber pressure and orifice-openings of valve for the nominal case of external load F_L=2,000 N

it. The amplitude and frequency of this reference sinusoidal signal are chosen as 0.5 m and 0.2356 rad/s, respectively. The amplitude of 0.5 m is selected such that the pneumatic cylinder can complete a stroke of one meter length, as long-stroke pneumatic actuation is one of the motivations of this research article. The frequency of reference signal is chosen in a way such that the pneumatic cylinder can achieve a speed close to its maximum-limit that is specified in its data-sheet. Besides this, errors measures such as root mean square error (RMSE) and absolute error [31] are used for the comparison of incremental approach with the baseline PID controller. According to sign convention in fig. 1, the position of cylinder-piston can be both positive as well as negative, besides the error in the piston-position tracking, which can also be both positive as well as negative. Therefore, considering absolute error for comparing both the controllers ensures that the above-mentioned positive and negative components do not cancel each other, and thus provide a better sense of the prevailing errors in the system. Next, RMSE is chosen as another measure for comparing the controllers. In RMSE, the errors are squared before taking its average, which ensures that any large error in the system is highlighted with a higher priority and the designed controllers can be augmented to tackle such high errors. Moreover, RMSE also ensures that the positive and the negative components of the error do not cancel each other, similar to absolute error.

The tracking results for the nominal-case are plotted in fig. 7, where initial peaks are observed in the inner-loop tracking of both the control approaches. For the PID approach, it happens because the inner-loop PID receives a desired pressure-difference from its outer-loop controller, which is also a PID controller and therefore, the desired pressure-difference (P_{L_d}) which is dependent on the error of piston-position gradually increases from zero. However, this is not the case with the initial pressure-difference (P_L) across the chambers and therefore a large overshoot in the inner-loop tracking is observed. For the case of incremental approach, the peak in the inner-loop tracking error happens due to a incorrect initialization of the initial pressure-derivative v_0 across the cylinder chambers. However, both these initial transients converges to the actual reference, in a minimal time of around 10 ms. Besides the initial peak in the inner-loop tracking, initial transients are also observed in the control-input of the two controllers (fig. 8), due to similar reasons. fig. 8 also shows the variation of the mass-flow rate with the opening of valve orifice. We observe that for a positive orifice-opening, the rate of mass-inflow is positive for chamber A, while it is negative for chamber B. Similarly, the mass-flow rate out of chamber A is positive, while negative for chamber B. However, the positive rate of mass-inflow into chamber A is more than its positive mass outflow-rate, thus resulting in a net mass inflow into chamber A, and vice-versa for chamber B.

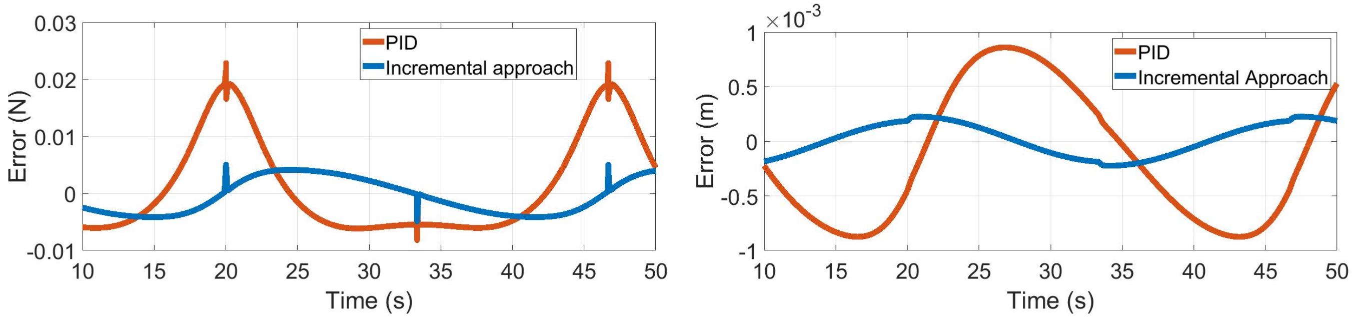

(a) Inner-loop tracking errors of PID and incremental approach (b) Outer-loop tracking errors of PID and incremental approach

Fig. 9: Tracking errors of incremental control approach and PID for a nominal case of external load F_L=2,000 N

TABLE IV: Error comparison of incremental control approach with a baseline controller for the nominal case of external load F_L=2,000 N

	Maximum Absolute Error	Mean Absolute Error	Root Mean Square Error
Outer-loop incremental approach	$2.25{\cdot}10^{-4}$ m	$1.34{\cdot}10^{-4}$ m	$1.49{\cdot}10^{-4}$ m
Inner-loop incremental approach	$5{\cdot}10^{-3}$ N	$2.8{\cdot}10^{-3}$ N	$3.1{\cdot}10^{-3}$ N
Outer-loop PID	$8.75{\cdot}10^{-4}$ m	$5.66{\cdot}10^{-4}$ m	$6.24{\cdot}10^{-4}$ m
Inner-loop PID	$1.95{\cdot}10^{-2}$ N	$7.2{\cdot}10^{-3}$ N	$8.8{\cdot}10^{-3}$ N

The errors for comparing the two controllers are calculated only after their control inputs stabilize, i.e. all the simulation transients have died out. For this research project, some extra margin is considered and thus, a time range of 10-50 seconds is used for calculating the errors of both the controllers. It is observed that for both the outer-loop position controllers, all the three error measures are minimal. For instance, the RMSE of outer loop PID is 0.62 mm, whereas the RMSE of outer-loop incremental approach is 0.14 mm. However, the maximum absolute error, mean absolute error and root mean square error of outer-loop PID are 74.3%, 76.32% and 76.1% higher than the corresponding outer-loop incremental approach, respectively. The inner-loop tracking errors of PID are also higher than that of its incremental counterpart. For instance, the RMSE of PID is 64.7% higher than its incremental counterpart. The tracking errors of both the control approaches are shown in fig. 9. and summarized in Table. IV. We also observe that for the inner-loop tracking error of incremental approach, peaks are observed at 20, 33 and 47 seconds. The reason for this observation is that these points mark the turn-around points of the reference trajectory to be tracked, where the rate of change chamber-pressure changes its direction. This further causes a jump in the calculated pressure-derivative due to this discontinuity, which is then reflected in the output of incremental approach and finally in the inner-loop error. However, no conclusions are deduced from these nominal-case tracking results, as the errors in piston-position tracking using both the control approaches are below 1% of the maximum amplitude of the sinusoidal reference signal.

D. Robustness-Study in Presence of Sensor Noise

In order to test the robustness property of both the control approaches, normally distributed zero-mean Gaussian noise are introduced in both the simulated piston-position and the chamber-pressure. The accuracy of the position and chamber-pressure feedback is found after the survey of a few widely available sensors [32], [33]. The feedback of piston-velocity and the chamber pressure-derivative are obtained using numerical-differentiation of their parent variable. The noise properties are summarized in Table. V whereas both the noise in pressure sensor and its normal distribution are plotted in fig. 10.

The tracking-errors for the time-frame of 10-50 seconds are plotted in fig. 11. The three error-measures that are used for comparison are summarized in Table. VI. It is observed that the tracking errors of both the outer-loop controllers are satisfactory but however, the RMSE of outer-loop PID is lower than that of incremental approach by 56.2%. Unlike the nominal case, the inner-loop RMSE for the robust case is a lot higher by 99.99% and 99.98%, respectively for the incremental approach and PID. The reason for such a high-error using incremental approach is that it relies heavily on the accuracy of sensor feedback,

TABLE V: Summary of simulated sensor noise

Sensor	Piston-Position	Chamber-Pressure
Mean error	-9$\cdot10^{-9}$ m	0.09 Pa
Maximum error	1.1 $\cdot10^{-4}$ m	1,114.3 Pa
Standard-deviation of error	2.49 $\cdot10^{-5}$ m	249.8 Pa

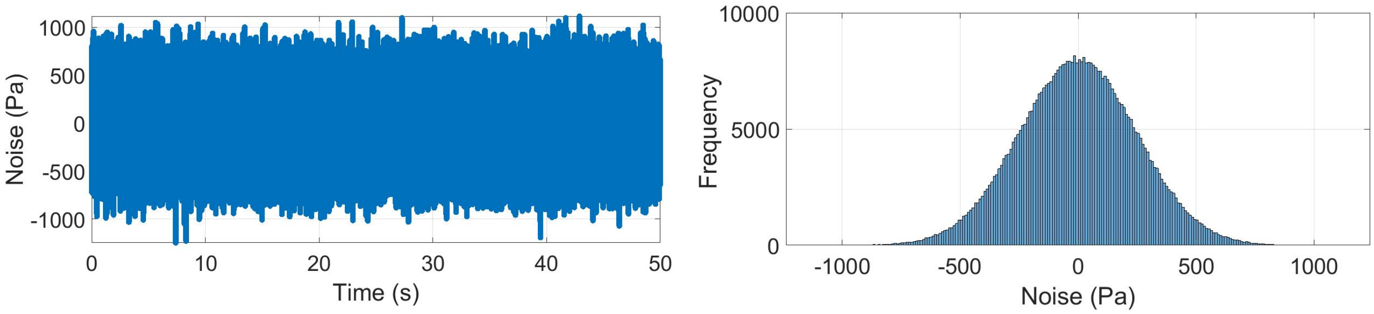

(a) Simulated pressure-sensor noise

(b) Histogram of pressure-sensor noise

Fig. 10: Simulated noise in pressure-sensor and its histogram

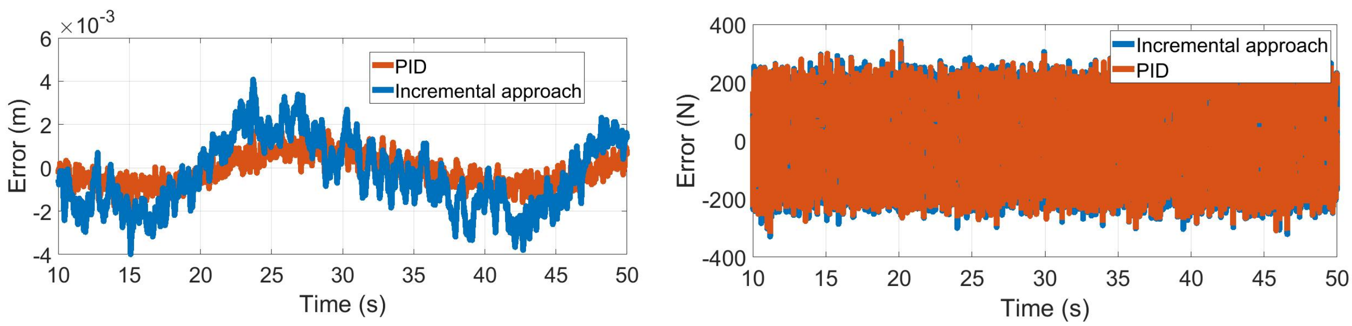

(a) Outer-loop tracking errors of PID and incremental approach with no filtering

(b) Inner-loop tracking errors of PID and incremental approach with no filtering

Fig. 11: Robust-case tracking errors of PID and incremental approach with no filtering for low load of F_L=2,000 N

and the sensor noise introduced in both the chamber-pressure and piston-position are not filtered, before feeding them to the controller. It has also been found that the errors of the inner-loop PID are almost similar to that of inner-loop incremental approach, with very little difference of 0.34%. Furthermore, numerical differentiation is performed to obtain the requested feedback signals of piston-velocity and chamber-pressure-derivative, which further amplifies the noise. In order to tackle this issue, low-pass filters are implemented to attenuate any high-frequency noise from sensor. A first-order lag filter is implemented whose transfer function is summarized in eq. (33) as follows:

$$G(s) = \frac{a}{s+a} \tag{33}$$

In eq. (33), a denotes the cut-off frequency. In this research article, two sets of filtering scheme are imposed for filtering the high-frequency noise, which are named as moderate-filtering and high-filtering. The cut-off of high-filtering scheme is set to be lower than the moderate-filtering schemes. A filter with very low-cutoff ensures that besides noise, a lot of useful information from the plant dynamics is also filtered out. However for the moderate-filtering scheme, a lot of useful information is retained along with a lot of noise, compared to the previous scheme. Thus, these two schemes involve a trade-off between more information content and less sensor noise, which is used for comparing the two control schemes. Therefore, the cut-off frequencies of the two schemes is chosen with the sole objective of rejecting more noise using one scheme, whereas retaining more noise from the other. Power spectral density (PSD) plots are first used for finding the power of the system-states x and $\dot{P}_L$ as a function of frequency and then the cut-off frequency for the inner-loop and outer-loop are set at 4 Hz and 6 Hz, respectively for the moderate filtering scheme, which ensures that enough noise is retained for comparing it with the high filtering scheme. The cut-off frequency of the moderate scheme is chosen close to the frequency with the maximum power in control input, which is around 8 Hz. However, rigorous techniques can also be applied for deciding the exact cut-off frequency, required to cancel a given noise source [34], but it is beyond the scope of this research article, whose one of the main objectives

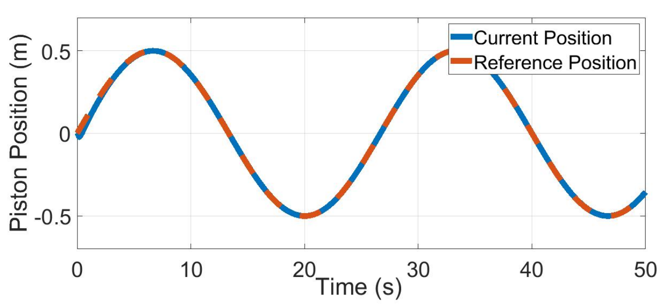

(a) Results of outer-loop tracking using PID with moderate-filtering

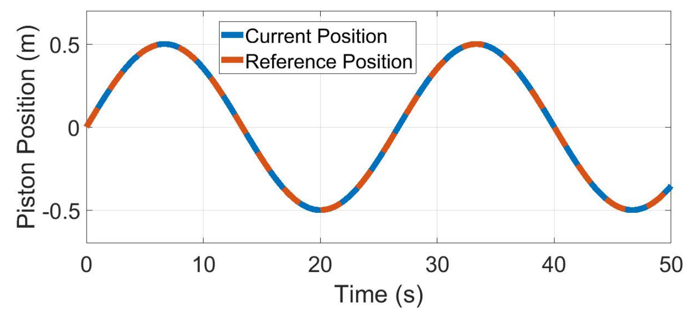

(b) Results of outer-loop tracking using incremental approach with moderate-filtering

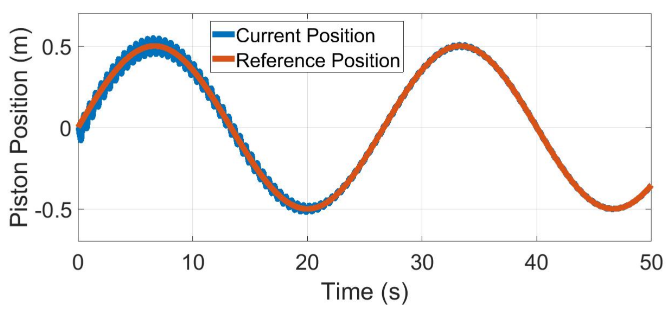

(c) Results of outer-loop tracking using PID with high-filtering

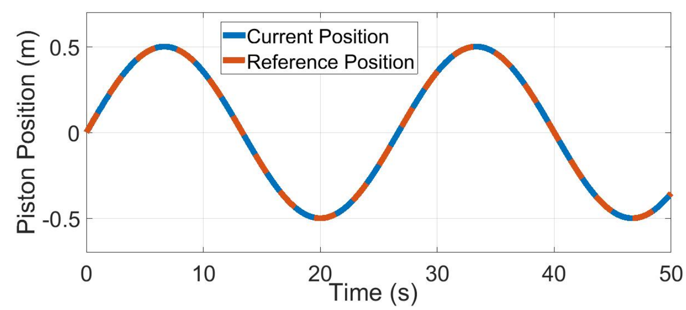

(d) Results of outer-loop tracking using incremental approach with high-filtering

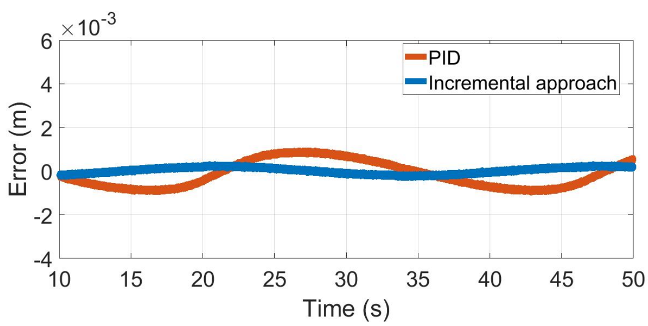

(e) Outer-loop tracking errors of PID and incremental approach with moderate-filtering

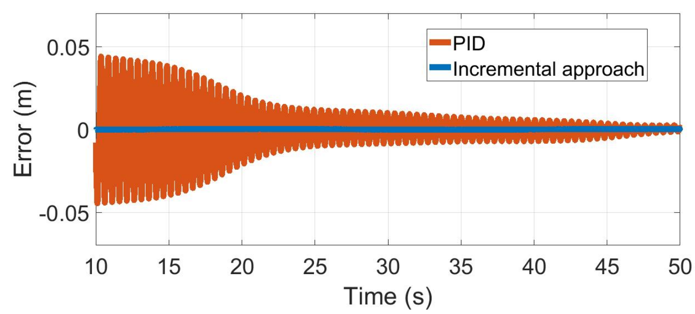

(f) Outer-loop tracking errors of PID and incremental approach with high-filtering

Fig. 12: Robust-case outer-loop tracking results with filter implementation for low load of F_L=2,000 N

is to compare the performance of the incremental control approach with PID in the context of a pneumatic system. The cut-off frequency for the high-filtering scheme is chosen as 1.05 Hz, for both the inner-loop and outer-loop. This frequency is chosen by assuming it to be more than 4 times lower than the previous case, which ensures that more information content is lost in the high-filtering scheme, as compared to moderate-filtering. For the inner-loop, two filters are used with the same dynamics in order to obtain the feedback signals of both the chamber pressure-derivative and orifice-area of the valve. This ensures that the inner-loops of controller are synchronised and thus eliminate the presence of any RHP poles [9].

The tracking results and errors of the inner-loop and outer-loop are plotted in fig. 13 and fig. 12, respectively. Table. VI summarizes the tracking-errors obtained using both the filtering schemes. It is observed that the errors significantly reduced after the introduction of low-pass filters. For instance, the outer-loop mean absolute tracking error using moderate-filtering reduced by over 10 times, as compared to the corresponding unfiltered scenario of the incremental approach. It is also found that the RMSE of outer-loop incremental approach is lower than the outer-loop PID by 75.84$\%$ but however, the RMSE of inner-loop incremental approach is higher than inner-loop PID by 26.3%, for the moderate filtering scheme. Similarly, the absolute tracking error of inner-loop PID is lower than inner-loop incremental approach by 26.6%, for the moderate-filtering scheme. Therefore, nothing can be concluded from these observations, as the inner-loop and outer-loop errors do not show a similar trend for both the control approaches. Following the moderate-filtering scheme, the introduction of high-filtering further reduced the inner-loop tracking errors of incremental approach by around 83$\%$ as compared to its corresponding error using moderate filtering. However, with the high-filtering scheme, PID showed degradation, with the error rising by 57$\%$ as compared to the

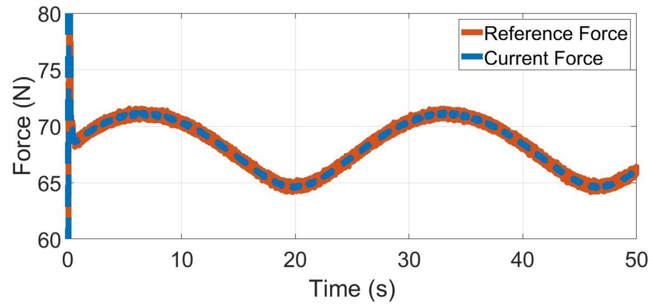

(a) Results of inner-Loop tracking using PID with moderate-filtering

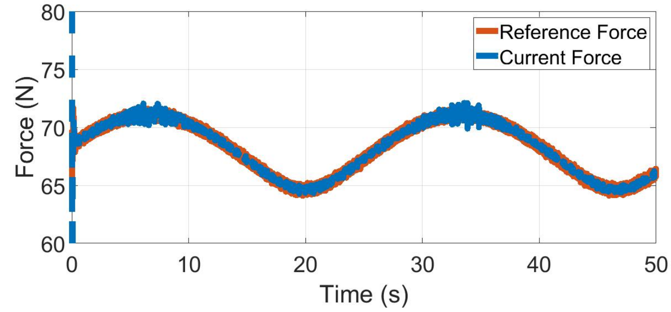

(b) Results of inner-Loop tracking using incremental results with moderate-filtering

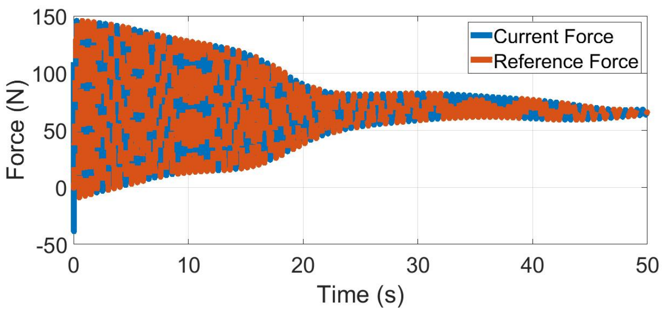

(c) Results of inner-Loop tracking using PID with high-filtering

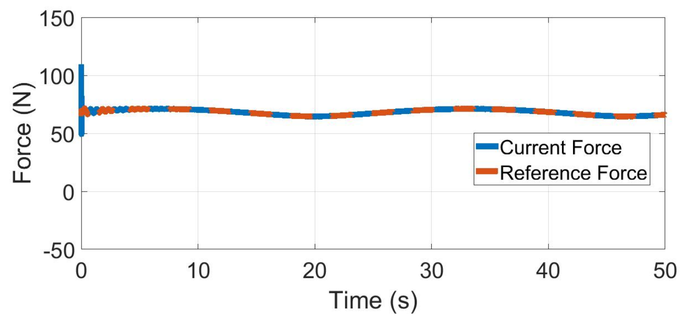

(d) Results of inner-loop tracking using incremental approach with high-filtering

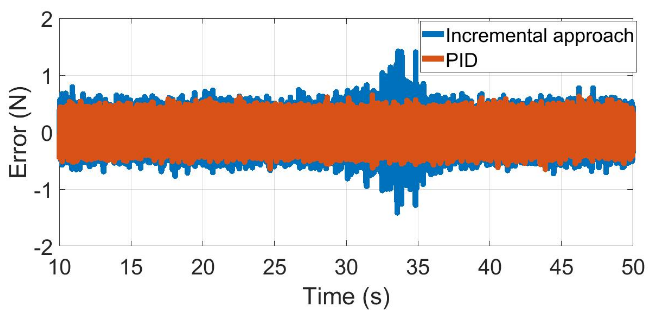

(e) Inner-loop tracking errors of PID and incremental approach with moderate-filtering

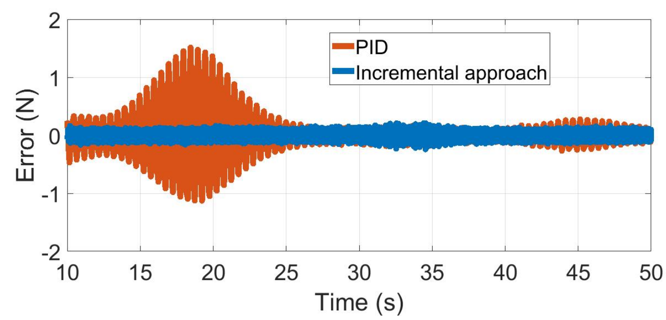

(f) Inner-loop tracking errors of PID and incremental approach with high-filtering

Fig. 13: Robust-case inner-loop tracking results with filter implementation for low load of F_L=2,000 N

TABLE VI: Robust-case error comparison of incremental control approach with a baseline controller for a low load of F_L=2,000 N

	Maximum Absolute Error	Mean Absolute Error	Root Mean Square Error
Outer-loop incremental approach (no-filtering)	$4.1\cdot10^{-3}$ m	$1.4\cdot10^{-3}$ m	$1.6\cdot10^{-3}$ m
Outer-loop incremental approach (moderate-filtering)	$3.2\cdot10^{-4}$ m	$1.34\cdot10^{-4}$ m	$1.51\cdot10^{-4}$ m
Outer-loop incremental approach (high-filtering)	$3.48\cdot10^{-4}$ m	$1.35\cdot10^{-4}$ m	$1.53\cdot10^{-4}$ m
Outer-loop PID (no-filtering)	$1.8\cdot10^{-3}$ m	$5.98\cdot10^{-4}$ m	$7\cdot10^{-4}$ m
Outer-loop PID (moderate-filtering)	$9.86\cdot10^{-4}$ m	$5.67\cdot10^{-4}$ m	$6.25\cdot10^{-4}$ m
Outer-loop PID (high-filtering)	$4.47\cdot10^{-2}$ m	$9.6\cdot10^{-3}$ m	$1.42\cdot10^{-2}$ m
Inner-loop incremental approach (no-filtering)	341 N	57.1 N	71.5 N
Inner-loop incremental approach (moderate-filtering)	1.41 N	0.15 N	0.19 N
Inner-loop incremental approach (high-filtering)	0.24 N	$3.1\cdot10^{-2}$ N	$3.94\cdot10^{-2}$ N
Inner-loop PID (no-filtering)	334.4 N	56.86 N	71.25 N
Inner-loop PID (moderate-filtering)	0.65 N	0.11 N	0.14 N
Inner-loop PID (high-filtering)	1.51 N	0.19 N	0.32 N

corresponding moderate filtering case. It can also be seen from Table. VI that RMSE of the inner-loop incremental approach is 87.69% lower than that of the corresponding inner-loop PID. A similar trend is also found in the outer-loop, where the RMSE of PID is higher than the incremental approach by 98.9%. Therefore, it can be concluded from these results that if the cut-off frequency of filter is increased to attenuate more sensor noise, similar to our high-filtering scheme, then the incremental approach performs better than PID. But in the absence of any filters or with the moderate-filtering scheme, lucid conclusions about the advantage of any particular control approach in the presence of sensor noise is difficult to deduce. Moreover, more analysis is needed to find the minimum bound of this cut-off frequency that ensures better performance for the incremental approach, as compared with the obtained results in this article. Besides this, more study is required for finding the instability conditions in the designed controlled system due to low-pass filtering [35], which is to be done in the later stages of this project.

E. Robustness-Study with Changes in External Load

The robustness property of both these control approaches is then tested by increasing the external load from 2,000 N to 10,000 N. The controller coefficients for this case are considered to be same as the nominal case and the results are plotted in fig. 14, where fig. 14b and fig. 14d plots the variation of chamber pressures for the tracking tasks involving a heavy load, using PID and incremental control approach, respectively. It is observed that for some parts of the tracking-trajectory such as between 12 and 21 seconds, and also between 39 and 48 seconds, the pressure in chamber A has saturated to 10 bar, which is the maximum supply pressure. It is also to be noted that the variation in pressure of chamber B is very minimal, once the pressure in chamber A saturates to its maximum limit. This happens because the chambers of a pneumatic cylinder (see fig. 1) form a closed system, and thus pressure in chamber B cannot change independently without impacting the chamber A. A important observation to be noted in fig. 14b is that for the inner-loop tracking using PID, high frequency oscillations are observed in the pressure feedback of both chamber A and B. These oscillations happens in the same time-frame as the saturation of chamber pressure, which are not observed for the incremental approach. The reason for such an anomaly is that close to the bottom turning-point of the tracking trajectory, it becomes difficult for PID to track it, as the velocity of such a heavy load starts changing its direction. However, the incremental approach is able to reduce the piston-velocity from its maximum value to zero, without any high-frequency pressure component in the cylinder chamber. The oscillations in piston-position due to PID control is further reflected in the outer-loop law, which is then propagated to the final controller output, only to be reflected in the chamber pressures, approximately between 12 and 21 seconds. This trend is also repeated when the piston again reaches the bottom turning-point of the trajectory, i.e. between 38 and 47 seconds.

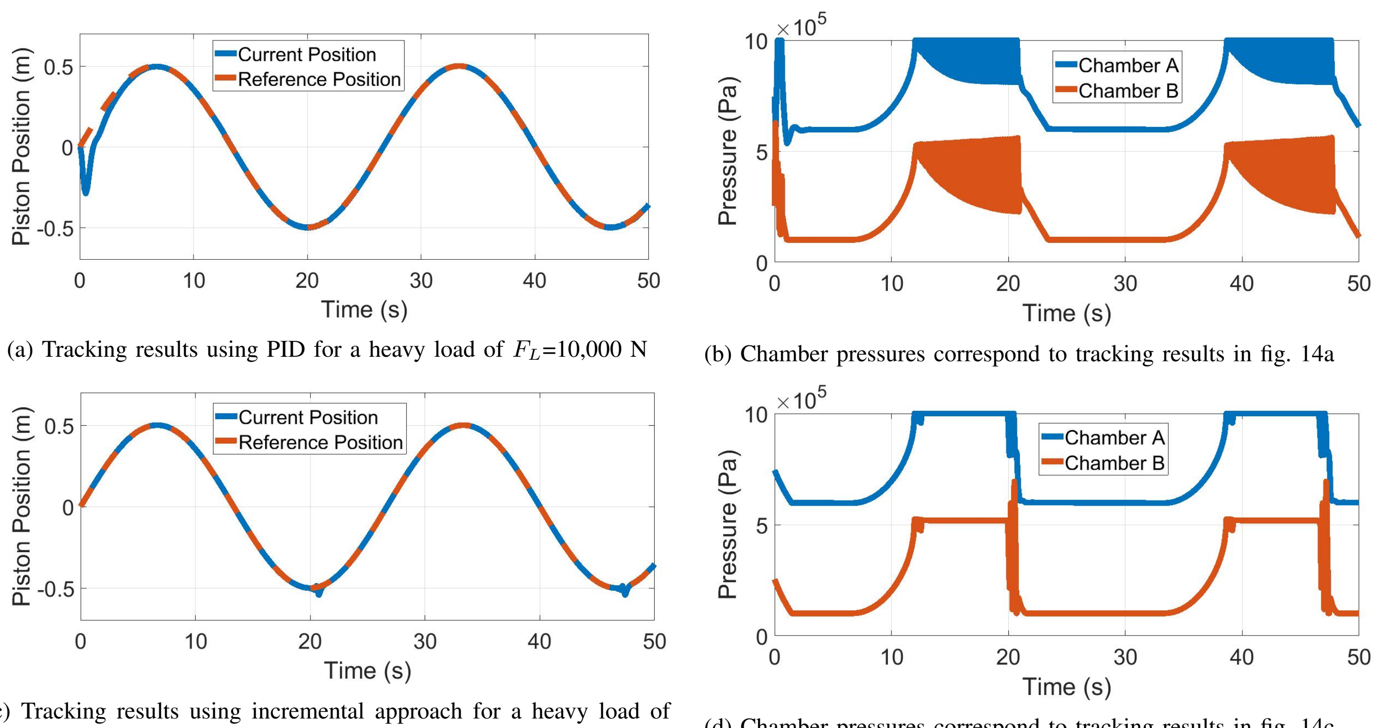

(a) Tracking results using PID for a heavy load of F_L=10,000 N

(b) Chamber pressures correspond to tracking results in fig. 14a

(c) Tracking results using incremental approach for a heavy load of F_L=10,000 N

(d) Chamber pressures correspond to tracking results in fig. 14c

Fig. 14: Tracking results for heavy load of F_L=10,000 N

Moreover, chamber A saturates due to the asymmetric structure of external load, as chamber A is directly below chamber B in a vertically upright position of the cylinder. In addition to asymmetry, the external load for this case is high as a result of which it is much easier for chamber B to push the piston downwards when compared to chamber A pushing the piston upwards. This phenomenon of pressure saturation is not observed previously for the case of low external-load as the cylinder did not require high differential pressure for moving the load. However, this is not the case with heavy external load, which requires a high pressure difference across the chambers of cylinder, as shown in fig. 14b and fig. 14d. It has also been observed in our simulation experiments that reversing the position of the pneumatic cylinder causes a similar pressure saturation in chamber B rather than in chamber A, as observed previously. Therefore, it can be concluded that the phenomenon of pressure-saturation in fig. 14 is both due of the effect of the heavy-load and the asymmetrical structure of our simulation set-up. Besides this, fig. 14 shows an initial downward-peak in the response of PID control, which is not observed in the incremental control approach. This happens because even though the external load has increased by five times, the controller coefficients are still same as a result of which old PID coefficients are too low to handle the transients produced by the heavy load. In order to counteract this initialization problem, the control gain needs to be increased, especially the proportional component. However, by utilizing the same INDI control coefficients for heavy load as tuned for the low load, it has been demonstrated that INDI is robust to initial transients due to a heavy external load. We also observe slight oscillations at the bottom turn-around point of the trajectory at around 20 seconds and 47 seconds, which are not observed in top turn-around points of the graph. This happens because at these points, the pressure in chamber A comes out of saturation, forcing a large pressure-derivative which is then reflected in both the controller outputs. This impact is more evident in the incremental control approach as it explicitly uses this variable for calculating the control command, does highlighting one of the downfalls of incremental approach for the case of saturated chamber pressures in a pneumatic cylinder.

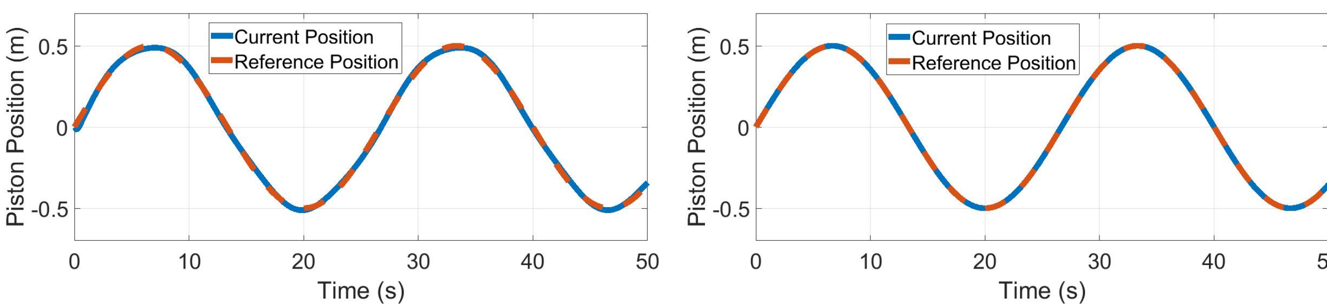

(a) Outer-loop tracking results for PID

(b) Outer-loop tracking results for incremental approach

Fig. 15: Tracking results for varying load

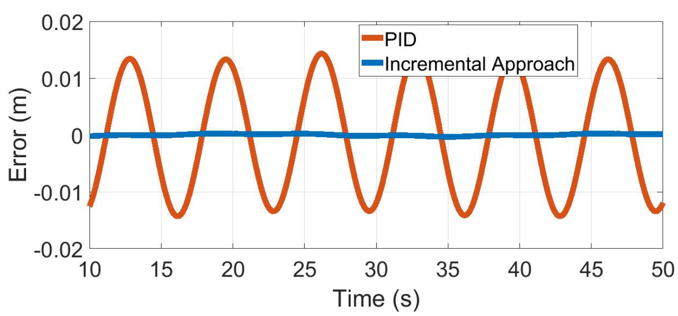

Fig. 16: Nominal-case tracking errors of PID and incremental approach for varying load

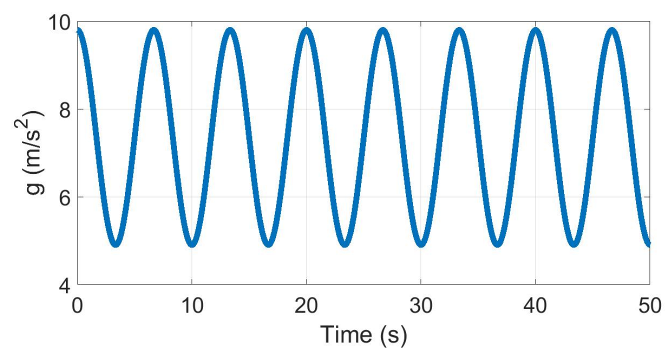

Fig. 17: Variation of gravitational-constant for the tracking results in fig. 16

Following a heavy load, the robustness property of both these approaches is tested using a varying external load. The nominal mass is considered to be 200 kg and the value of gravitational constant g is taken as 9.8 m/s^2. The variation of g is done by considering a sinusoidal motion about a base point that is fixed on the ground. The axis of rotation is directly perpendicular to the axis of motion of the cylinder which ensures a two-dimensional motion of the cylinder, besides ensuring that the component of gravity acting directly along the axis of cylinder keeps changing throughout the tracking trajectory, as plotted in fig. 17. The outer-loop tracking results for PID and incremental approach are plotted in fig. 15a and fig. 15b, respectively. The outer-loop tracking RMSE of incremental approach is 98.4$\%$ lower than that of the PID. The reason for such a disparity in the tracking errors is because the incremental approach considers the varying load in its controller formulation, as is expressed using eq. (20). However, the output of corresponding PID control does not directly depend on the varying load, but rather only on the piston-position error and its time-derivative, as expressed in eq. (27). Therefore, it can be concluded from these experiments that the incremental approach is better at handling the variations in external load, when compared with PID.

F. Recommendations for Time-Delay in Tubes

In pneumatic systems, a set of tubes connect the pneumatic valve with the cylinder. These tubes can be mathematically expressed using eq. (34) [11], where R_t refers to the resistance of connecting-tube, R is the ideal gas constant, c refers to the speed of air, P is the pressure at the end of the tube, L_t refers to the total length of the connecting-tubes and the function $h(t)$ refers to the original mass-flow rate released from the valve at time-instant t. Therefore, we observe that when air passes through the connecting-tubes, it suffers from a attenuation factor and a time delay, both of which are directly dependent on the length of connecting-tubes, as expressed below:

$$\dot{m}_t\left(L_t, t\right) = \begin{cases} 0 & \text{if} \quad t < L_t/c \\ e^{-R_t RT/2P} L_t/c \quad h\left(t - \frac{L_t}{c}\right) & \text{if} \quad t > L_t/c \end{cases} \tag{34}$$

The results of inner-loop tracking using incremental approach in the presence of connecting-tube dynamics is plotted in fig. 18. The time-delay in the considered tube of length 0.5 m results in high-frequency oscillations, which increased the outer-loop absolute error by over 4 times, as compared to the nominal case. The deterioration in the inner-loop is worse, with both the RMSE and absolute error rising by over 99% as compared to their corresponding nominal case. Next, from the power-spectral density of the previous state-derivative v_0 (fig. 19), it is found that multiple resonance modes can be linked with this transmission dynamics at 155 Hz, 306 Hz, 474 Hz and so on. These peaks can be further eliminated by the use of a notch-filter with appropriate damping, notch frequency and gain, which is a recommendation for the next stages of this research project.

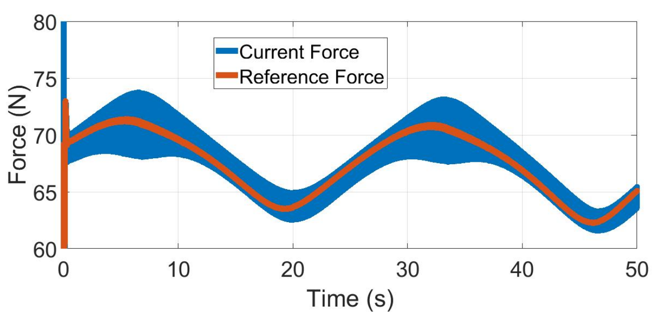

Fig. 18: Inner-loop tracking errors of incremental approach in the presence of connecting-tube dynamics

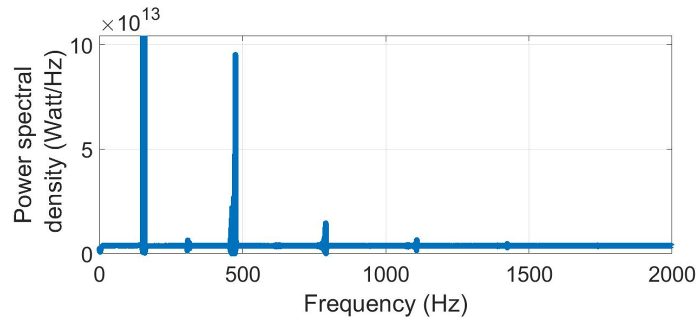

Fig. 19: Power spectral density of chamber pressure-derivatives for tracking response in fig. 19

VI. Validation of plant-model and control-methods

An open-loop analysis can be an important tool for validating a given plant dynamics. The plant model described previously by eq. (1) - eq. (5) can be validated prior to controller testing using open-loop analysis, as described here. Open-loop analysis of an erroneous controlled system can also be used to verify if any error is either due to issues in controller or issues in plant-dynamics. In order to eliminate any additional effect of heavy load and to verify only the dynamical formulation, an open-loop analysis is performed for a low-load of 0.1 N. First, an open-loop command is issued to keep the orifice-opening completely closed and it can be observed from fig. 20a that the piston demonstrates initial oscillations, after which it converges to 0.08 m. Moreover, both the chambers are initialized with a pressure of 5 bar each, but as the time progresses, the pressure in chamber B converges to a value higher than that of chamber A. The reason for these observations is that the piston is connected to the side of cylinder containing chamber B (see fig. 1), due to which the effective area of chamber B reduces. Therefore, more pressure is required from chamber B to produce a similar force as chamber A, which is necessary for balancing the mass of both the external load and piston. Next, an oscillatory command is issued to the orifice opening of the valve and it can be observed from fig. 20 that the piston-position and the chamber pressures are both oscillatory, which corresponds with the issued open-loop valve command. However, a phase lag can be observed between the piston-position and the open-loop command, due to the low-bandwidth of the considered pneumatic system. This phase-lag can be decreased by reducing the frequency of the open-loop command.

The controlled systems in this research article is implemented with the piston-position kept fixed at the middle of the stroke, similar to [36]. However, the external load considered in our case ranges from 200 kg to 1000 kg, unlike a low-external load of 1 kg in [36]. Therefore, it is necessary to trim the cylinder with the correct initial condition of the chamber pressures, as is calculated using eq. (31) and eq. (32). This is required to prevent the initial downward movement of the piston, due to the gravitational force of the heavy load. The initial chamber pressures are summarized in Table. II, which aligns with the fact that the initial pressure in chamber A keeps getting higher than chamber B, as the external load increases. In [36], the

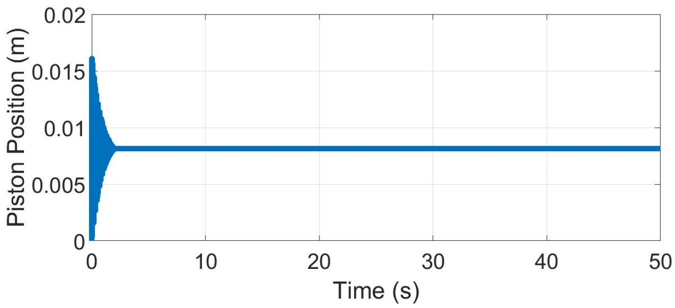

(a) Piston position for a zero input

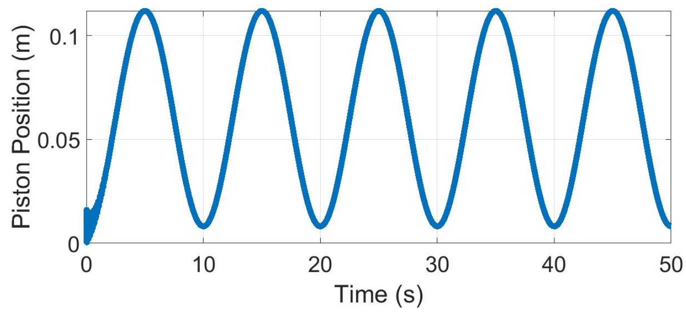

(b) Piston position for a oscillating input

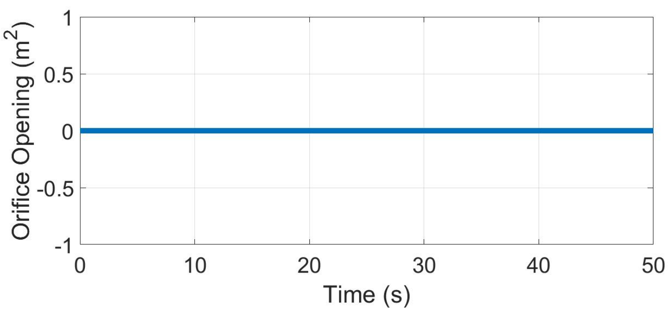

(c) Input used for fig. 20a

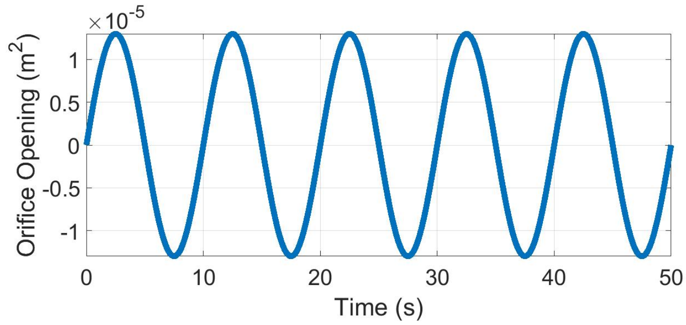

(d) Input used for fig. 20b

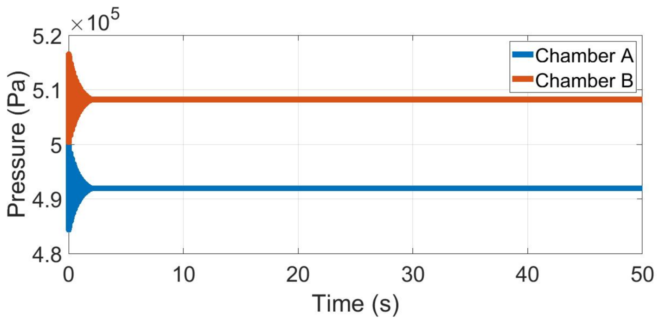

(e) Chamber pressure corresponding to piston positions in fig. 20a

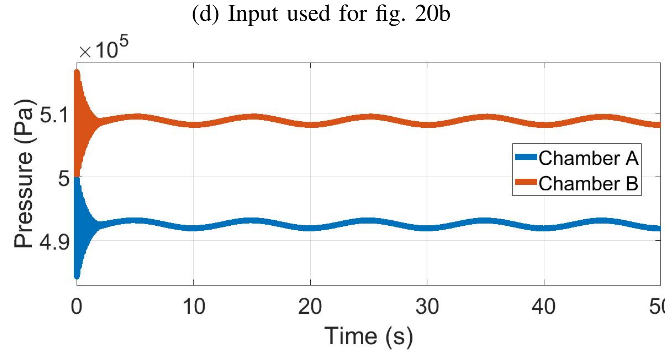

(f) Chamber pressure corresponding to piston positions in fig. 20b

Fig. 20: Open-loop analysis

pneumatic cylinder is used for tracking a reference force whereas in this research article, tracking a reference position is the goal. However, a similar sinusoidal profile of force tracking is observed in our analysis (fig. 7a and fig. 7b) as in [36]. The range of this sinusoidal variation of the system force is different for the two cases, as in our analysis an outer-loop position controller generates the desired force profile, which is absent in [36]. Moreover for the nominal case tracking results (fig 7), significant improvements are observed in the steady-state tracking errors of cylinder force, as compared with the results in [36]. Besides this, the maximum force tracked in our analysis for the nominal case is around 71 N, whereas it is 75 N in [36]. These forces are comparable to each other even though the external load is much higher in our analysis. A possible explanation for this observation is that the frequency of the reference signal in our analysis is 0.03 Hz, whereas it is considered as 75 Hz and 20 Hz in [36], which creates a similar demand of piston force. Moreover, our analysis considers a big pneumatic cylinder of bore diameter 0.16 m and maximum stroke-length 1 m, whereas [36] considers a small cylinder of maximum stroke-length 0.076 m and bore diameter of around 0.01 m. Therefore, high frequency movement of a small pneumatic cylinders requires a similar force, as required by a big pneumatic cylinder for low frequency movement

The bandwidth of the designed sliding mode controller in [36] ranges from 25 Hz to 60 Hz, depending on the length of the tube and order of the controller, whereas the bandwidth of our designed incremental control also falls in the similar range, with the maximum power of the signal occurring at around 8 Hz. It is also observed that in the presence of time-delays due to the connecting tubes (fig. 18), the inner-loop tracking results of the incremental approach deteriorated, with a lot of high-frequency components. In [36], these high-frequency components in the force-tracking response are absent, but however, there is a steady-state error in its sliding-mode approach, which is not observed for the incremental approach. It is also found in our analysis that similar to [36], the performance of the controlled system deteriorated with the increase in the length of the connecting-tubes, due to more signal-attenuation and time-delays, as described previously by eq. (34).

VII. DISCUSSION

In this research article, the characteristics of pneumatic system dynamics is studied and an incremental control approach is successfully implemented to control such a highly nonlinear system [11]. A cascaded control strategy is implemented here, where the inner-loop controls the force exerted by the system and the outer-loop tracks the desired piston-position. In addition, some of the advantages of incremental control over a conventional linear control strategy are highlighted, with respect to the considered pneumatic system. For instance, for the nominal tracking scenario with an external load of F_L=2,000 N and without any added-noise in the sensor feedback, the RMSE of outer-loop incremental approach is 76.1% lower than the outer-loop PID. However, the maximum absolute errors of both the control approaches are much below 1% of the amplitude of reference sine signal. Thus, significant conclusions with respect to comparison of the two control approaches cannot be made from such an observation. For the robust case without any filter-implementation, the inner-loop errors are above 99% for both the control approaches, when compared with the corresponding nominal-case results. These tracking errors significantly reduced after the introduction of moderate-filtering scheme, with the RMSE of tracking errors dropping by over 99.8% and 99.7% for PID and incremental approach, respectively, as compared to their corresponding unfiltered case. However, the the RMSE of PID is 26.3% lower than incremental approach, thus glorifying the ineffectiveness of incremental approach in the presence of noisy sensor feedback. But after implementing high-filtering scheme, the maximum absolute error of outer-loop tracking using incremental approach dropped to less than 1% of the reference sine signal's amplitude, whereas it is 9% for PID. Therefore, it can be concluded that in the presence of realistic sensor noise, a high-filtering scheme of incremental approach gives better performance than a conventional linear controller by utilizing less plant information. Similarly, in the presence of a varying external load, the mean absolute error of the outer-loop of incremental approach is 98.5% less than that of PID. Moreover, the maximum absolute error for the case of a varying load using PID is found to be around 3% of the reference sine's amplitude, thus highlighting one of the benefits of incremental control approach over PID. Therefore, all these error analysis strengthens the argument that even though the performance of both the control approaches are equally satisfactory for a nominal case, but for a few realistic and robust-case simulation scenarios, the performance of incremental approach is better than PID.

The designed NDI for the outer-loop incremental approach does not involve an exact model inversion because the Coulomb force is dropped from the final NDI output, in order to minimize any oscillations due to it. Besides this, the control-effectiveness term of INDI control is not obtained by the conventional Jacobian operation, but rather kept as constant in order to minimize any oscillations due to the switching dynamics of pneumatic mass-flow rate. It is found out later that even after fixing the control-effectiveness, the performance of INDI is very satisfactory, with the maximum absolute error of the outer-loop tracking for the nominal case being less than 1% of the reference signal's amplitude of 0.5 m. As mentioned previously, the outer-loop of the incremental approach is based on partial dynamic inversion, as some of the components of the outer-loop dynamics are prone to high-frequency oscillations. Designing this outer-loop using INDI will involve differentiating eq. (19), which can induce discontinuities in the control effectiveness matrix due to the high-frequency oscillation components in piston dynamics. This can be tackled by using a fixed control-effectiveness, similar to the inner-loop of incremental approach used here. The resultant INDI law can be described by eq. (35), where $\tilde{G}$ denotes the control effectiveness and v is a suitable linear control law. Such a control law depends on the jerk of the piston-position, which can be obtained by differentiating it thrice. Appropriate filters might be necessary to cancel sensor noise, as is used in this research article and the output of the overall incremental approach is expected to improve due to its reduced dependency on the system states, and is thus a recommendation for the next stages of this research project.

$$P_L = P_{L_0} + \tilde{G}(v - \dddot{x}) \tag{35}$$

Both the control approaches are tuned using a step-response command to result in similar time-domain specifications such as rise-time and settling-time. This ensured a "fair" comparison of both control approaches but however in the later stages of this project, controller tuning can be performed more efficiently using tools such as MOPS [30], which optimizes a given set of design criterion. It would be interesting to see how both the controller reacts with optimised controller coefficients. Based on the performed simulation study, it can be predicted that the performance of both the controllers might improve marginally for the nominal case. However, for the robust-case scenario with added sensor noise and no filter, the tracking performance of PID might improve with respect to the incremental approach. Moreover, optimized PID coefficient might as well reduce the steady-state error that is observed for the case of varying load. In this article, a sinusoidal signal of amplitude 0.5 m and frequency 0.24 rad/s is used for generating the reference trajectory. Even though this article uses a sinusoidal reference trajectory for its tracking tasks, but in the later stages of this research project, both the developed control approaches will be used to track other realistic reference signals that are used in a high-fidelity flight simulator [5]. Based on the obtained results, it can be interpolated that PID will perform worse that the incremental approach while tracking high-frequency reference signals. But in such cases, it should be ensured that time-derivatives of such a signal should be filtered with an appropriate filter to prevent it from reflecting in the desired state-derivatives, which is then utilized in the final control output of incremental control approach. Besides this, the effect of compression and expansion, also termed as charging and discharging are observed in our tracking results. For instance, during the downward motion of piston connected to a load of F_L=2,000 N, the pressure in the cylinder chambers compressed by 2.5 bar more than the maximum supply pressure. However, this compressibility effect did not affect the nominal case tracking performance, which is then analyzed for the heavy load.

For the simulation studies with heavy external load, an initial negative peak of amplitude 0.29 m is observed for the PID response, which is not found in the corresponding response by the incremental control approach, which proves its robustness to initial transients due to the heavy external load. Similar to the incremental approach, the final steady-state error is zero for PID, but with a higher settling time. In order to prevent such an initial transient and also to reduce the settling time, the gains of PID needs to be tuned according to the external load, which is a recommendation for future works. It is also observed that the pressure in the cylinder chamber saturated for the case of heavy load tracking (fig. 14), which can be reduced by increasing the maximum supply pressure, if necessary. PCH [30] can also be used to tackle such a saturation phenomenon, besides handling valve saturation, which might occur while tracking a heavy load with a high frequency of the reference signal, as observed in some of our investigations.

Besides the effects of pressure saturation in the chambers, compressibiility effect is observed while tracking the heavy load. The sum of the chamber pressures at some parts of the tracking trajectory is found to be around 50% higher than the maximum supply pressure, whereas it is around 25% for the nominal case of load 2,000 N. Therefore, it can be concluded that these compressibility effects are dependent on the external load, which needs to be studied in details in the later stages of this research project. Moreover, the compression and expansion effects in this article are both described using the same thermal constant k=1.4 [10]. However, its needs to be analyzed later if such effects of a long-stroke pneumatic cylinder can be modelled using k=1.2 [11] or if they can be described better using separate coefficients for the charging and the discharging process [37]. These effects of compressibility in a pneumatic system are assumed to be independent of the chamber volumes but however in a hydraulic system, the compressibility effect is represented using oil stiffness C_m, which depends on the volumes of the two cylinder chambers [5]. Therefore, further investigation is required in the designed pneumatic controlled system, in order to find any dependence of the compressibility coefficients on the chamber volumes.

Moreover, based on our analysis with a heavy external load and varying external load, it can be deduced that the initial transients in the PID response increase with the external load, which necessitates re-tuning of the controller gains. Moreover, from results obtained for the varying load (fig. 15), it can be concluded that a particular controller gain for PID will not give efficient tracking performance across all operating conditions, which might require re-tuning. But this is not the case with the incremental control approach. Besides this, the tracking errors of incremental approach are not impacted by variation of gravitational acceleration from 0.5 g-force to 1 g-force (fig. 17). However, nothing can be concluded for variations beyond this limit, which necessitates further investigation in the later stages of this research project.

VIII. Conclusion

A cascaded-control strategy based on incremental nonlinear dynamic inversion control is successfully designed in this research article, for position-tracking tasks using a long-stroke pneumatic cylinder. The outer-loop is based on NDI that outputs a desired chamber pressure-difference to the inner-loop, which is based on INDI. The inner-loop commands a desired orifice-opening to the pneumatic valve in order perform the given tracking task. The dimensions of the pneumatic system are selected by considering the requirements of SIMONA flight simulator, whereas the pneumatic valve is approximated using a first-order lag. A sinusoidal signal is chosen as the reference trajectory for the tracking tasks, whose amplitude and frequency are selected based on our application. The performance of both the controllers is found to be similar and satisfactory for the nominal case, with the maximum absolute error being less than 1% of the reference sine wave's maximum amplitude, for both the controllers. Furthermore, realistic sensor noises are introduced in the system, which are then filtered using two different filtering schemes as a result of which the performance of both the control approaches increased. The mean absolute error of the moderate-filtering scheme reduced by over 90%, when compared with the unfiltered incremental control approach. The cut-off frequency of the moderate-filtering is then further reduced by over 75%, which resulted in a significant decrease of over 99% in the RMSE of the inner-loop tracking using incremental approach as compared to its corresponding unfiltered case. However, this is not the case with the response obtained from PID, thus glorifying the robustness of incremental control approach in the presence of realistic sensor noise, by utilizing comparatively less information of the plant dynamics due to the implemented filters. Finally, for the case of a heavy external-load, a few initial transients as well as high-frequency oscillations in the cylinder chamber are observed for PID, which are not seen in the incremental approach. It is also found that for the case of varying external load, the RMSE of outer-loop tracking error for the incremental approach is around 98% lower than PID. Therefore, it can be concluded that incremental control approach has potential in increasing the tracking performance of commercial pneumatic actuators, as observed from a number of realistic simulation scenarios in this research article.

References

[1] Y. Huang, D. Pool, O. Stroosma, and Q. Chu, "Incremental nonlinear dynamic inversion control for hydraulic hexapod flight simulator motion systems," *IFAC-PapersOnLine*, vol. 50, no. 1, pp. 4294–4299, 2017.

[2] I. Boldea and S. A. Nasar, "Linear electric actuators and generators," *IEEE Transactions on Energy Conversion*, vol. 14, no. 3, pp. 712–717, 1999.

[3] H. I. Ali, S. Noor, S. Bashi, and M. Marhaban, "A review of pneumatic actuators (modeling and control)," *Australian Journal of Basic and Applied Sciences*, vol. 3, no. 2, pp. 440–454, 2009.

[4] O. Stroosma, M. Van Paassen, and M. Mulder, "Using the simona research simulator for human-machine interaction research," in *AIAA modeling and simulation technologies conference and exhibit*, 2003, p. 5525.

[5] Y. Huang, D. M. Pool, O. Stroosma, and Q. Chu, "Long-stroke hydraulic robot motion control with incremental nonlinear dynamic inversion," *IEEE/ASME Transactions on Mechatronics*, vol. 24, no. 1, pp. 304–314, 2019.

[6] H.-P. Ren and C. Huang, "Adaptive backstepping control of pneumatic servo system," in *2013 IEEE International Symposium on Industrial Electronics*. IEEE, 2013, pp. 1–6.

[7] L. An and N. Sepehri, "Hydraulic actuator leakage fault detection using extended kalman filter," *International Journal of Fluid Power*, vol. 6, no. 1, pp. 41–51, 2005.

[8] P. Szczepaniak, G. Jastrzebski, and M. Jóźko, "A method of investigating internal leakages in aircraft hydraulic units," *Journal of KONES*, vol. 21, 2014.

[9] L. van Litsenburg, "Challenges and solutions for sensor-based incremental nonlinear control of hydraulically actuated parallel robots," Masters thesis, Delft University of Technology, 2020.

[10] M. Malaysia, "Non-linear modeling and cascade control of an industrial pneumatic actuator system," *Australian Journal of Basic and Applied Sciences*, vol. 5, no. 8, pp. 465–477, 2011.

[11] E. Richer and Y. Hurmuzlu, "A high performance pneumatic force actuator system: Part i—nonlinear mathematical model," *J. dyn. sys., meas., control*, vol. 122, no. 3, pp. 416–425, 1999.

[12] S. Liu and J. Bobrow, "An analysis of a pneumatic servo system and its application to a computer-controlled robot," *Journal of dynamic systems, measurement, and control*, vol. 110, no. 3, pp. 228–235, 1988.

[13] J. E. Bobrow and F. Jabbari, "Adaptive pneumatic force actuation and position control," in *1989 American Control Conference*. IEEE, 1989, pp. 1508–1513.

[14] S. R. Pandian, Y. Hayakawa, Y. Kamoyama, and S. Kawamura, "Practical design of adaptive model-based sliding mode control of pneumatic actuators," in *Proceedings of IEEE/ASME International Conference on Advanced Intelligent Mechatronics*. IEEE, 1997, p. 140.

[15] Z. Rao and G. M. Bone, "Modeling and control of a miniature servo pneumatic actuator," in *Proceedings 2006 IEEE International Conference on Robotics and Automation, 2006. ICRA 2006.* IEEE, 2006, pp. 1806–1811.

[16] M. Smaoui, X. Brun, and D. Thomasset, "A study on tracking position control of an electropneumatic system using backstepping design," *Control Engineering Practice*, vol. 14, no. 8, pp. 923–933, 2006.

[17] H.-P. Ren, X. Wang, J.-T. Fan, and O. Kaynak, "Fractional order sliding mode control of a pneumatic position servo system," *Journal of the Franklin Institute*, 2019.

[18] A. K. Paul, J. Mishra, and M. Radke, "Reduced order sliding mode control for pneumatic actuator," *IEEE Transactions on Control Systems Technology*, vol. 2, no. 3, pp. 271–276, 1994.

[19] S. Jacklin, J. Schumann, P. Gupta, M. Lowry, J. Bosworth, E. Zavala, K. Hayhurst, C. Belcastro, and C. Belcastro, "Verification, validation, and certification challenges for adaptive flight-critical control system software," in *AIAA Guidance, Navigation, and Control Conference and Exhibit*, 2004, p. 5258.

[20] Y. Liao, "Neural networks in hardware: A survey," *Department of Computer Science, University of California*, 2001.

[21] S. Sieberling, Q. Chu, and J. Mulder, "Robust flight control using incremental nonlinear dynamic inversion and angular acceleration prediction," *Journal of guidance, control, and dynamics*, vol. 33, no. 6, pp. 1732–1742, 2010.

[22] P. Simplício, M. Pavel, E. Van Kampen, and Q. Chu, "An acceleration measurements-based approach for helicopter nonlinear flight control using incremental nonlinear dynamic inversion," *Control Engineering Practice*, vol. 21, no. 8, pp. 1065–1077, 2013.

[23] B. Andrievsky, D. V. Kazunin, D. M. Kostygova, N. V. Kuznetsov, G. A. Leonov, P. Lobanov, and A. A. Volkov, "Control of pneumatically actuated 6-dof stewart platform for driving simulator," in *2014 19th International Conference on Methods and Models in Automation and Robotics (MMAR)*. IEEE, 2014, pp. 663–668.

[24] A. S. Lafmejani, M. T. Masouleh, and A. Kalhor, "Trajectory tracking control of a pneumatically actuated 6-dof gough–stewart parallel robot using backstepping-sliding mode controller and geometry-based quasi forward kinematic method," *Robotics and Computer-Integrated Manufacturing*, vol. 54, pp. 96–114, 2018.

[25] H. Das, "Dynamic inversion control of quadrotor with a suspended load," *IFAC-PapersOnLine*, vol. 51, no. 1, pp. 172–177, 2018.

[26] R. Da Costa, Q. Chu, and J. Mulder, "Reentry flight controller design using nonlinear dynamic inversion," *Journal of Spacecraft and Rockets*, vol. 40, no. 1, pp. 64–71, 2003.

[27] X. Wang, E.-J. Van Kampen, Q. Chu, and P. Lu, "Stability analysis for incremental nonlinear dynamic inversion control," *Journal of Guidance, Control, and Dynamics*, vol. 42, no. 5, pp. 1116–1129, 2019.

[28] S. S. Mulgund and R. F. Stengel, "Aircraft flight control in wind shear using partial dynamic inversion," in *1993 American Control Conference*. IEEE, 1993, pp. 400–404.

[29] J. B. West, "The original presentation of boyle's law," *Journal of applied physiology*, vol. 87, no. 4, pp. 1543–1545, 1999.

[30] F. Grondman, G. Looye, R. O. Kuchar, Q. P. Chu, and E.-J. Van Kampen, "Design and flight testing of incremental nonlinear dynamic inversion-based control laws for a passenger aircraft," in *2018 AIAA Guidance, Navigation, and Control Conference*, 2018, p. 0385.

[31] T. Chai and R. R. Draxler, "Root mean square error (rmse) or mean absolute error (mae)?" *GMDD*, vol. 7, no. 1, pp. 1525–1534, 2014.

[32] I. L. Krivts and G. V. Krejnin, *Pneumatic actuating systems for automatic equipment: structure and design*. Crc Press, 2016.

[33] P. Rohner, *Fluid Power Logic Circuit Design: Analysis, Design Methods and Worked Examples*. Macmillan International Higher Education, 1979.

[34] B. Yu, D. Gabriel, L. Noble, and K.-N. An, "Estimate of the optimum cutoff frequency for the butterworth low-pass digital filter," *Journal of Applied Biomechanics*, vol. 15, no. 3, pp. 318–329, 1999.

[35] H. Qian and J. De Schutter, "The role of damping and low pass filtering in the stability of discrete time implemented robot force control," in *Proceedings 1992 IEEE International Conference on Robotics and Automation*. IEEE Computer Society, 1992, pp. 1368–1369.

[36] E. Richer and Y. Hurmuzlu, "A high performance pneumatic force actuator system: part ii—nonlinear controller design," *J. Dyn. Sys., Meas., Control*, vol. 122, no. 3, pp. 426–434, 2000.

[37] A. M. Al-Ibrahim, *Transient air temperature and pressure measurements during the charging and discharging processes of an actuating pneumatic cylinder*. University of Wisconsin–Madison, 1991.

II

Preliminary Report

This part of the thesis is included only for convenience and has already been graded for the literature study.

2

Pneumatic Actuators

This chapter provides a state-of-the-art review of the available literature on pneumatic actuators. A number of different controllers were critically analyzed, to decipher the advantages and also the shortcomings of each one of them. This chapter introduces the basic theory and principles of a pneumatic system, which will be used in this research project. An accurate model of a pneumatic system is described, which is driven by a proportional spool-valve.

Firstly, section 2.1 explains the basic principles of a pneumatic system and the various mathematical relations expressing its physical processes. Following this, section 2.2 describes the the dynamical equations of a parallel robot using Newton-Euler equation. Finally, section 2.3 presents the state-of-art-review on pneumatic controllers. Some of the widely-used conventional controllers were analyzed, such as pole placement, PID, sliding mode, backstepping, adaptive control and modern control techniques. A brief review of the control techniques for a flight simulator is also provided.

2.1. Basic Principles of a pneumatic system

Modern pneumatic systems come in various types and sizes, but a typical system will consists of the following components.

- Piston to connect the cylinder to an external load
- Pneumatic cylinder with different chambers in it
- Valve to control the inflow and outflow of air
- Tubes to connect valve with cylinder
- Sensors to measure position, pressure and force

A schematic diagram of a pneumatic system is shown in Fig.2.1. P_1, A_1 and V_1 refers to the pressure, volume and area of chamber A respectively, whereas subscript 2 refers to the corresponding variables of chamber B. The supply pressure P_s comes from a cylinder of compressed air. The valve in figure 2.1 is a 4-way 3-position valve. It is driven by a current-carrying solenoid which produces a force F_c to move the valve-spool. When the valve-spool is shifted to its left, then chamber B is connected to the supply pressure and chamber A is directly in contact with the atmosphere, whose pressure is around $1.01325 \times 10^5\ Pa$. Such a configuration of the valve will force the piston to move to its left. Similarly, if the current in the solenoid is now reversed, then the direction of force F_c changes. It now starts pushing the valve-spool towards its right, due to which chamber A now gets connected to the supply pressure and chamber B is connected to the atmosphere. The connecting tubes transfer air from a valve to the cylinder chambers. It plays a major role in the controller design as the connecting tubes are a source of time-delays and attenuation in the air-flow.

A mathematical model of a pneumatic system is highly nonlinear due to the air-flow and also its compressibility property. The other aspects in modelling are the attenuation and time delays caused, when the air flows through the connecting tubes. The model of a pneumatic system considered in this research project uses concepts from [73] and [54]. They depict a very accurate representation of the pneumatic system and takes into account the involved nonlinearities, that are listed below.

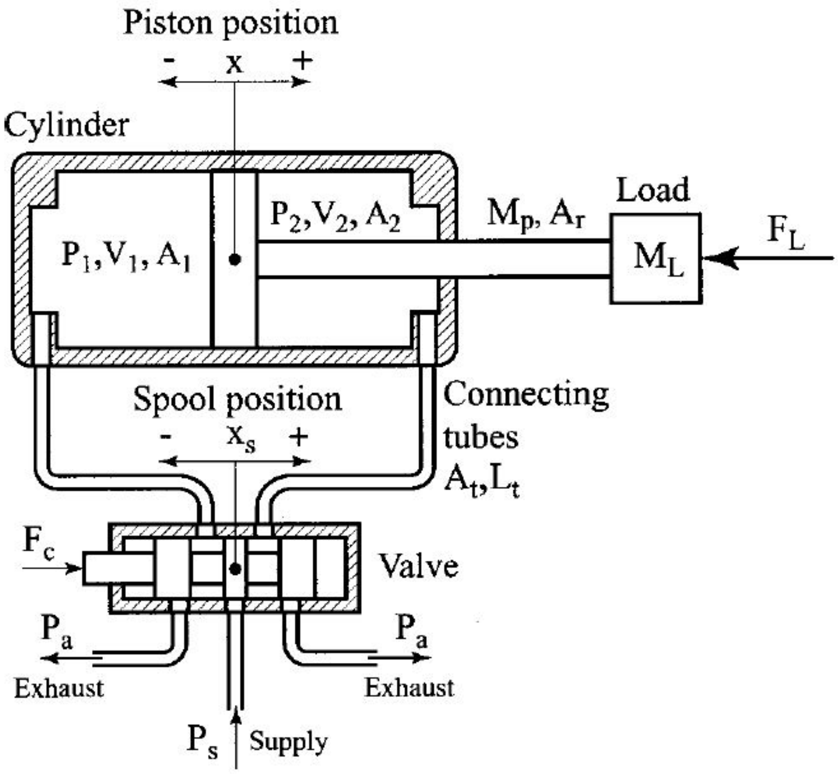

Figure 2.1: Schematic diagram of a pneumatic system [73]

- Attenuation and time delays in the connecting tubes
- Leakage between the two cylinder chambers
- Friction of the piston seal
- Difference of piston areas in the two chambers
- Inactive volume of air in both the ends of the cylinder
- Valve dynamics and nonlinear air-flow though the valve orifice

2.1.1. Dynamics of Piston and Load

The driving force for a pneumatic piston is the difference of pressure in the two chambers. Friction forces play a major role in the piston dynamics and the entire process can be summarized using the equation given below.

$$\left(M_L + M_p\right)\ddot{x}' + \beta\dot{x} + F_f + F_L = P_A A_A - P_B A_B - P_a A_r \tag{2.1}$$

In the above equation, M_L refers to the mass of the external load, M_p is the mass of the piston, x is the piston position, F_f is the Coulomb friction force, β is the coefficient of viscous force, F_L is the external force of the load, P_A and P_B refers to the pressure of the two chambers A and B respectively, A_A refers to the area of the piston in chamber A and A_B is the area of the piston in chamber B, P_a refers to the ambient atmospheric pressure and A_r is the cross-sectional area of piston rod.

The friction force F_f is derived using the LuGre friction model [54]. It is summarized as follows.

$$F_f = \sigma_0 z + \sigma_1 \dot{z} + \sigma_2 \dot{x} + F_{df}\frac{\dot{x}}{|\dot{x}|} \tag{2.2}$$

In the above equation, σ_0 is the stiffness coefficient, σ_1 and σ_2 are the damping coefficients and z is the internal state of friction which is propagated using the equation given below.

$$\dot{z} = \dot{x} - \frac{|\dot{x}|z}{g} \tag{2.3}$$

In Eq.(2.3), g is the stribeck function which is computed as follows

$$g = \frac{F_c + (F_s - F_c)e^{(-\dot{x}/v_s)^2}}{\sigma_0} \tag{2.4}$$

In the above equation F_c is the coulumb friction coefficient, F_s is the static friction coefficient, F_{df} is the dynamic friction coefficient. v_S is the velocity at which the stribeck friction is calculated .

2.1.2. Model of cylinder chambers

The differential equations that describes the change of pressure in the cylinder chambers can be derived using some general models, concerning the flow of gas. The ideal gas law, energy equation and law of conservation of mass were first used by Hullender and Woods [42] to derive such differential equations. The ideal gas law is summarized as follows.

$$P = \rho RT \tag{2.5}$$

In Eq.(2.5), P is the pressure exerted by gas, ρ is the density of the gas, R is the ideal gas constant and T is the temperature. The law of conservation of mass also known as continuity equation, can be summarized as given below.

$$\dot{m} = \frac{d}{dt}(\rho V) \tag{2.6}$$

In Eq.(2.6), V is the volume of the gas and $\dot{m}$ represents the rate of change of mass. Finally, a third equation which describes the energy of the system is summarized below.

$$q_{\text{in}} - q_{\text{out}} + kC_v(\dot{m}_{\text{in}} T_{\text{in}} - \dot{m}_{\text{out}} T) - \dot{W} = \dot{U} \tag{2.7}$$

In Eq.(2.7), q_{in} and q_{out} refers to the amount of heat entering and leaving the system respectively, k is the specific heat ratio, C_v is the specific heat at a constant volume, $\dot{m}_{\text{in}}$ and $\dot{m}_{\text{out}}$ refers to the mass flow-rate going into and out of the chamber respectively, T_{in} refers to the temperature of the incoming gas , W is the amount of work done and U is the internal energy of the system. The rate of change in internal energy and work done can be expressed as follows.

$$\dot{U} = \frac{d}{dt}(C_v mT) = \frac{1}{k-1}\left(V\dot{P} + P\dot{V}\right) \tag{2.8}$$

$$\dot{W} = P\dot{V} \tag{2.9}$$

Now substituting Eqs.(2.8) and (2.9) in Eq.(2.7), and by assuming that the incoming gas temperature T_{in} is the same as room temperature T, the following relation is obtained.

$$\frac{k-1}{k}\left(q_{\text{in}} - q_{\text{out}}\right) + \frac{1}{\rho}(\dot{m}_{\text{in}} - \dot{m}_{\text{out}}) - \dot{V} = \frac{V}{kP}\dot{P} \tag{2.10}$$

Some research on pneumatic system considers this whole process to be adiabatic such as [52], [11] and [72], whereas some researchers consider the discharging process of the chamber to be isothermal and the charging stage to be adiabatic [4]. Considering an adiabatic assumption ($q_{\text{in}} = q_{\text{out}}$), the rate of change of chamber pressure can be expressed as follows.

$$\dot{P} = k\frac{RT}{V}(\dot{m}_{\text{in}} - \dot{m}_{\text{out}}) - k\frac{P}{V}\dot{V} \tag{2.11}$$

By assuming a isothermal equation (constant T), the rate of change of pressure becomes

$$\dot{P} = \frac{RT}{V}(\dot{m}_{\text{in}} - \dot{m}_{\text{out}}) - \frac{P}{V}\dot{V} \tag{2.12}$$

Therefore, the general expression for the rate of change in pressure can be expressed as follows.

$$\dot{P} = \frac{RT}{V}(\alpha_{\text{in}}\dot{m}_{\text{in}} - \alpha_{\text{out}}\dot{m}_{\text{out}}) - \alpha\frac{P}{V}\dot{V} \tag{2.13}$$

In above equation, α_{in} and α_{out} can acquire any value ranging from 1 to the specific heat ratio k, depending on the characteristics of heat transfer. The volume V of the chamber can be expressed as

$$V_i = V_{0i} + A_i\left(\frac{1}{2}L \pm x\right) \tag{2.14}$$

In the above equation, i can be either A or B depending on the chamber, A_i denotes the area of i^{th} chamber, x is the position of piston which is 0 in the neutral position and V_{oi} is the inactive volume at the end of the cylinder, which remains in the cylinder ever after the completion of a full-stroke.

2.1.3. Mass Flow-Rate through pneumatic valve

The air flow through the valve can be either classified as choked or under-choked [54]. For the flow to be classified as choked, the ratio of upstream pressure P_u to downstream pressure P_d is more than the critical pressure ratio P_{cr} which is given by

$$P_{cr} = \left(\frac{2}{k+1}\right)^{k/k-1} \tag{2.15}$$

The equation of mass-flow rate $\dot{m}_v$ for the two kinds of flow [11] can be expressed as follows.

$$\dot{m}_v = \begin{cases} C_f A_v C_1 \frac{P_u}{\sqrt{T}} & \text{if } \frac{P_d}{P_u} \leqslant P_{cr} \\ C_f A_v C_2 \frac{P_u}{\sqrt{T}} \left(\frac{P_d}{P_u}\right)^{1/k} \sqrt{1-\left(\frac{P_d}{P_u}\right)^{(k-1)/k}} & \text{if } \frac{P_d}{P_u} > P_{cr} \end{cases} \tag{2.16}$$

In Eq.(2.16), C_f is the discharge constant, A_v is the area of orifice, P_u is the upstream pressure and P_d is the downstream pressure. The constants C_1 and C_2 are defined as:

$$C_1 = \sqrt{\frac{k}{R}\left(\frac{2}{k+1}\right)^{k+1/k-1}} \tag{2.17}$$

$$C_2 = \sqrt{\frac{2k}{R(k-1)}} \tag{2.18}$$

The valve area A_v can be expressed as a simple function of the spool displacement x_s [54] as follows.

$$A_v = \left(\frac{\pi}{4}\right) x_s^2 \tag{2.19}$$

Richer and Hurmuzlu [73] have considered the valve area to be derived from the radial holes. The area is first expressed for one hole, which is then integrated for the total number of active holes. In Fig.2.2, x_e is the

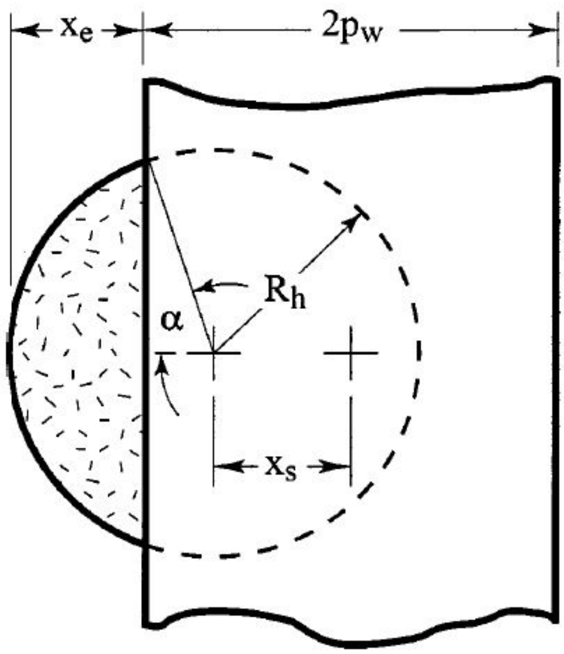

Figure 2.2: Spool position and orifice area [73]

effective displacement of the valve-spool. The total width of valve-spool $2p_w$ is considered to be double of the hole radius R_h, in order to ensure that even small misalignment of the spool will immediately close any air paths. Therefore the actual spool displacement x_s is different from its effective displacement x_e, which are related by $x_e = x_s - (p_w - R_h)$. The effective area of orifice by accounting only one opening can be expressed as follows.

$$A_e = 2\int_0^{x_e}\sqrt{R_h^2 - (\xi - R_h)^2}\,d\xi = 2\int_0^{x_e}\sqrt{\xi\,(2R_h - \xi)}\,d\xi \tag{2.20}$$

Now by considering all the available active holes n_h, the effective area of the valve [73] for the exhaust ($A_{v_{ex}}$) and input path ($A_{v_{in}}$) can be expressed as follows.

$$A_{v_{\text{ex}}} = \begin{cases} \pi n_h R_h^2 & \text{if } x_s \leqslant -p_w - R_h \\ n_h\left[2R_h^2 \arctan\left(\sqrt{\frac{R_h - p_w + |x_s|}{R_h + p_w - |x_s|}}\right| - (p_w - |x_s|)\sqrt{R_h^2 - (p_w - |x_s|)^2}\right] & \text{if } -p_w - R_h < x_s < R_h - p_w \\ 0 & \text{if } x_s \geqslant R_h - p_w \end{cases} \tag{2.21}$$

$$A_{v_{in}} = \begin{cases} 0 \quad \text{if } x_s \leqslant p_w - R_h \\ n_h\left[2R_h^2 \arctan(\sqrt{\frac{R_h - p_w + x_s}{R_h + p_w - x_s}}) - (p_w - x_s)\sqrt{R_h^2 - (p_w - x_s)^2}\right] & \text{if } p_w - R_h < x_s < p_w + R_h \\ \pi n_h R_h^2 \quad \text{if } x_s \geqslant p_w + R_h \end{cases} \tag{2.22}$$

The variation of input and exhaust valve area with the spool-displacement is plotted below in Fig.2.3.

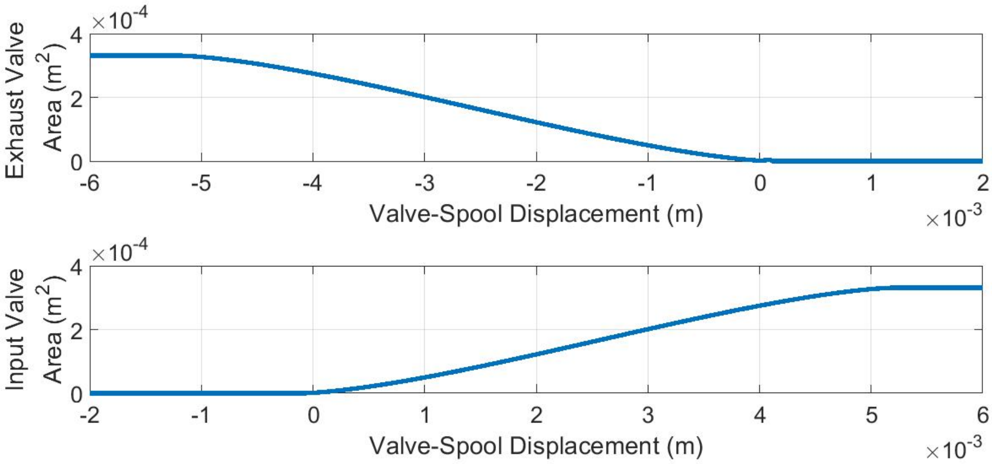

Figure 2.3: Variation of orifice-opening with the valve-spool displacement

Eq.(2.16) describes the mass-flow rate from the valve, but by the time it reaches the cylinder through a connecting tube, affects of flow attenuation and time-delays are clearly visible. These effects are highly dependent on the length of tube. Increasing the length of the tube will increase these nonlinear effects and vice-versa. The equations given below summarizes these effects and it is derived by solving the one-dimensional wave equation.

$$\dot{m}_t(L_t, t) = \begin{cases} 0 & \text{if } t < L_t/c \\ e^{-R_t RT/2P} L_t/c \quad h\left(t - \frac{L_t}{c}\right) & \text{if } t > L_t/c \end{cases} \tag{2.23}$$

In Eq.(2.23), L_t is the length of the tube, c is the speed of sound, R_t is the resistance of tube and P is the end pressure. The tube resistance for a laminar flow can be written as follows.

$$R_t = \frac{32\mu}{D^2} \tag{2.24}$$

In Eq.(2.24), μ is the atmospheric air's dynamic viscosity and D is the diameter of the tube. For a turbulent flow, this resistance R_t changes [54], and can be expressed as follows.

$$R_t = 0.158\frac{\mu}{D^2}Re^{3/4} \tag{2.25}$$

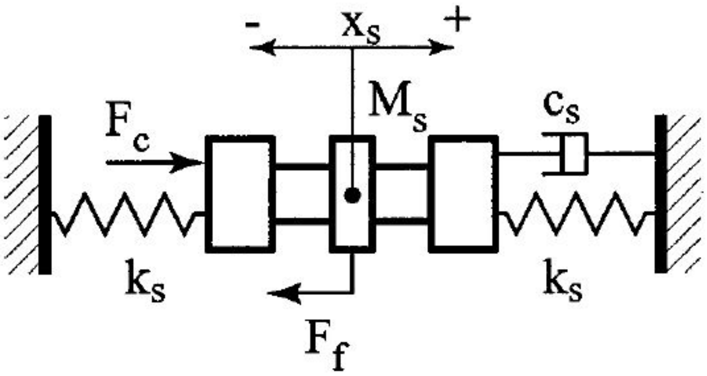

Figure 2.4: A typical valve spool [73]

2.1.4. Valve spool dynamics

The equations of motion [73] for the valve spool can be derived using Newton's second law as follows.

$$M_s \ddot{x}_s = -c_s \dot{x}_s - F_f + k_s (x_{so} - x_s) - k_s (x_{so} + x_s) F_c \tag{2.26}$$

In Eq.(2.26), F_c is the force produced by the solenoid coil of the valve, c_s is the coefficient of viscous force, k_s is the spring constant and F_c is the Coulomb force of friction. The above expression can be simplified as follows.

$$M_s \ddot{x}_s + c_s \dot{x}_s + F_f + 2k_s x_s = F_c \tag{2.27}$$

The frictional force F_f is usually neglected due to the small magnitudes of current in the coil. The force F_c can be expressed as $F_c = K_{fc} i_c$, where K_{fc} is the force coefficient of the coil. Besides the frictional force, in some case the mass M_s is also neglected as it is very low compared to the mass of piston or the external load, thus leaving us with the following first-order equation.

$$c_s \dot{x}_s + k_s x_s = K_f i_c \tag{2.28}$$

In [54], a controller was designed by considering the spool displacement to be directly proportional to input voltage, i.e. $x_s = C_v u$, where C_v is the proportionality constant and u is the supply voltage.

2.2. Basic Principles of a general Stewart platform

The general Stewart platform is used for most flight simulators ([7], [8], [21]). It falls under the category of parallel robots, where certain constraint relations needs to be satisfied. Contrary to it, serial robots are much simpler in formulations, but a few of its disadvantages compared to the parallel structure are less precision in positioning, performance degradation under high loads and less structural strength. A Stewart platform can be either of SPS or UPS form [38]. In SPS form, the joint connecting the platform to the leg and the joint connecting the base to the leg are both spherical. They can rotate across all three axis. For the UPS form, the base has a universal joint which cannot rotate around one axis and the other joints are spherical. Huang et al. [39] used a formulation similar to [26], in order to derive the dynamics of hydraulic Stewart platform which will be used in this report. Two frames of reference are very crucial in the dynamic formulation, which are summarized as follows.

- E_a: Body frame attached to the platform, which is moving
- E_b: Inertial frame attached to the inertial base, which is static

The state-space equations for this linear model considers six states, which are the position and orientation of frame E_a with respect to E_b. The position between two frames is measured by the use of vector **c**, which connects the origin of the two frames E_a and E_b. The orientation is represented by the use of Euler angle Φ which consists of roll (ϕ), pitch (θ) and yaw angle (ψ). Vector **c** consists of the three inertial positions x, y and z. The state vector X is summarized as follows.

$$X = \begin{bmatrix} c^T & \Phi^T \end{bmatrix}^T = \begin{bmatrix} x & y & z & \phi & \theta & \psi \end{bmatrix}^T \tag{2.29}$$

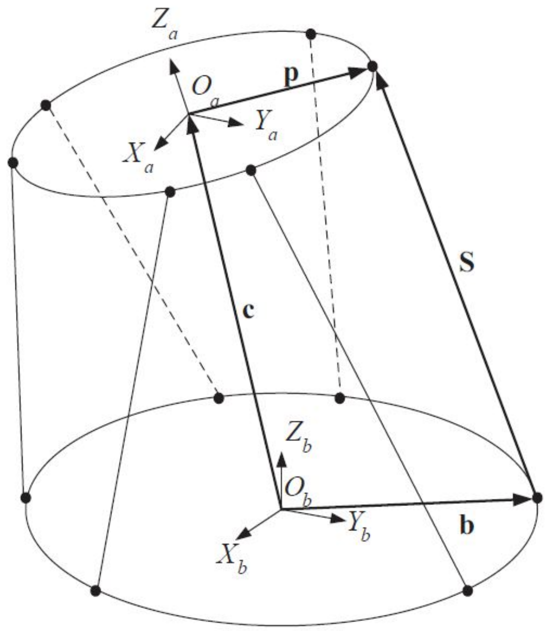

Figure 2.5: General Stewart Platform Eq.[39]

The state-derivative consists of the velocity vector $\dot{\mathbf{c}}$ and also the angular velocity vector ω_p of the platform. One of the legs is represented as **S** in Fig.2.5, which is the vector extending from the lower joint to the upper. **S** is measured in the inertial frame and can be expressed as follows.

$$\mathbf{S} = Ls = c + T_{ba}p - b \tag{2.30}$$

In Eq.(2.30), L is the length of the vector **S** and s is its unit vector. T_{ba} is the transformation matrix from frame E_a to E_b, p is the platform connection point to the leg expressed in E_b and b is position of the lower gimbal point expressed in E_b. Next, the dynamical equations for one leg can be expressed by using the constraint force $\mathbf{F}_p$ acting on the upper joint [39] as follows.

$$L\mathbf{s} \times \mathbf{F}_p = -(m_1\mathbf{r}_1 + m_2\mathbf{r}_2) \times \mathbf{g} + m_1\mathbf{r}_1 \times \mathbf{a}_1 + m_2\mathbf{r}_2 \times \mathbf{a}_2 + (\mathbf{I}_1 + \mathbf{I}_2)\dot{\mathbf{W}} + \mathbf{W} \times (\mathbf{I}_1 + \mathbf{I}_2)\mathbf{W} \tag{2.31}$$

In Eq.(2.31), m_1 and m_2 are the masses of the lower and upper parts of the leg respectively. Similarly $\mathbf{r}_1$, a_1 and $\mathbf{I}_1$ denotes the center of gravity, its acceleration and the moment of inertia of the lower leg respectively and the corresponding variables with subscript 2 are for the upper leg. **W** denotes the angular velocity of the leg and the gravitational acceleration is represented by **g**. Next, simplifying Eq.(2.31) by taking its cross product with **s** on both the sides of equation we obtain:

$$\mathbf{F}_p = \left(\mathbf{s} \cdot \mathbf{F}_p\right)\mathbf{s} + \mathbf{D} \times \mathbf{s}/L \tag{2.32}$$

In Eq.(2.32), **D** refers to the right hand side of Eq.(2.31). Next, Newtons's equation is used to derive the dynamics of the upper leg as follows.

$$F + s \cdot \mathbf{F}_p + m_2 s \cdot \mathbf{g} = m_2 s \cdot \mathbf{a}_2 \tag{2.33}$$

In Eq.(2.33), F is the translational force applied by the actuator. The inner-loop INDI controller designed in the later sections will try to track this reference force, in order to obtain a desired orientation of the platform. Next, combining Eqs.(2.32) and (2.33) we obtain

$$\mathbf{F}_p = \left(m_2 s \cdot a_2 - m_2 s \cdot g\right) + \mathbf{D} \times s/\mathbf{L} - Fs = \mathbf{K} - Fs \tag{2.34}$$

Dasgupta et al. [26] defined **K** using **Q** and **V**, and the final expression for the force acting on one of the upper joint is summarized as follows.

$$\mathbf{F}_p = \mathbf{Q}\left(\ddot{c} + \dot{\omega}_p \times q\right) + \mathbf{V} - Fs \tag{2.35}$$

The expression for **Q** and **V** in Eq.(2.35) are obtained from [26]. The constraint force acting on one leg is summed up over the six legs, and the translational dynamics is obtained using Newtons's equation as follows.

$$\sum_{n=1}^{6} (\mathbf{F}_s)_i + M_p\mathbf{g} = M_p a_p \tag{2.36}$$

In Eq.(2.36), M_p is the mass of the platform and a_p is the acceleration of center of gravity of the platform which is expressed as follows.

$$a_p = \dot{\omega}_p \times \mathbf{R} + \omega_p \times (\omega_p \times \mathbf{R}) + \ddot{c} \tag{2.37}$$

Next, using Euler's approach, the rotational dynamics is expressed as follows [39].

$$\sum_{n=1}^{6} (q_i \times \mathbf{F}_s)_i + M_p\mathbf{R} \times g = M_p\mathbf{R} \times a_p + \mathbf{I}_p\dot{\omega}_p + \omega_p \times \mathbf{I}_p\omega_p \tag{2.38}$$

In Eq.(2.38), $\mathbf{I}_p$ is the moment of inertia of the platform and **R** is the position of the center of gravity of the platform which is expressed in the inertial frame. Finally combining Eqs.(2.35)-(2.38), the complete equations of motion for an UPS-Stewart platform is summarized as given below [39].

$$\mathbf{M} = \begin{bmatrix} M\mathbf{E}_3 & -M\tilde{\mathbf{R}} \\ M\tilde{\mathbf{R}} & \mathbf{I}_p + M\left(R^2\mathbf{E}_3 - \mathbf{R}\mathbf{R}^T\right) \end{bmatrix} + \sum_{n=1}^{6} \begin{bmatrix} \mathbf{Q}_i & -\mathbf{Q}_i\tilde{\mathbf{q}}_i \\ \tilde{\mathbf{q}}_i\mathbf{Q}_i & -\tilde{\mathbf{q}}_i\mathbf{Q}_i\tilde{\mathbf{q}}_i \end{bmatrix} \tag{2.39}$$

$$\eta = \begin{bmatrix} M\{\omega_p \times (\omega_p \times \mathbf{R}) - \mathrm{g}\} \\ \omega_p \times \mathbf{I}_p + M\mathbf{R} \times \{(\omega_p \cdot \mathbf{R})\,\omega_p - \mathbf{g}\} \end{bmatrix} + \sum_{n=1}^{6} \begin{bmatrix} \mathbf{V}_i \\ \mathbf{q}_i \times \mathbf{V}_i \end{bmatrix} \tag{2.40}$$

$$\mathbf{F} = \begin{bmatrix} F_1 & F_2 & F_3 & F_4 & F_5 & F_6 \end{bmatrix} \tag{2.41}$$

$$\mathbf{H} = \begin{bmatrix} s_1 & s_2 & s_3 & s_4 & s_5 & s_6 \\ \mathrm{q}_1 \times s_1 & \mathrm{q}_2 \times s_2 & \mathrm{q}_3 \times s_3 & \mathrm{q}_4 \times s_4 & \mathrm{q}_5 \times s_5 & \mathrm{q}_6 \times s_6 \end{bmatrix} \tag{2.42}$$

The subscript i ranges from one to six, which signifies one of the six legs of the platform. E_3 refers to identity matrix of size 3×3 and $\tilde{q}_i$ refers to the skew-symmetric vector component of q_i.

2.3. State-of-the-Art Review on Pneumatic Controllers

Pneumatic actuators are being widely used in industrial and robotic automation-based processes such as haptic interfaces, drilling, gripping, teleoperation and various other applications. These applications usually demand a high output of force for every unit weight of the object, on which it is applied [6]. Pneumatic actuators are much safer to work with, as compared to their electrical counterparts due to its low requirement of current supply. They help in keeping the environment clean by reducing any harmful leakage into it. Hydraulic actuators, on the other hand, require hydraulic fluids for its operation which are prone to constant leakage into the surroundings [40]. Besides this, pneumatic actuators require less maintenance than a hydraulic actuator. Geared electric actuators have a high impedance and friction due to which they are usually not suited for accurate and fast response [14]. The components of a pneumatic actuator are highly durable and lightweight, thus making it a very cost-effective solution to many industrial and robotic applications [70].

Pneumatic actuators however have certain issues which does not make them compatible for everyday life applications ([70], [73]). One of such issues with a pneumatic system is the air-compressibility which does not exist for hydraulic systems, as hydraulic fluids are incompressible. The second major problem is the non-linearity in the mass flow-rate across the valve and the connecting tubes [54]. These pneumatic tubes are prone to attenuation and time-delays, thus lowering the bandwidth of operation. Moreover, the two chambers in the pneumatic cylinder are not perfectly isolated from each other, which causes air to leak from one chamber to the other. This phenomenons must be taken into account while designing a controller for such systems. The Coulomb friction forces [73] existing in the cylinder piston constantly switches near the zero piston velocity and can cause oscillations in the control command. Therefore, a pneumatic controller should be capable of handling such disturbances.

2.3.1. Controller Design

One of the first well-known references for the dynamic modelling of pneumatic systems was written by Shearer [76], where the charging and discharging process of a pneumatic cylinder was described using the equations of involved air-flow and its thermodynamics. The developed model is linearized around the mid-stroke position and is thus valid only for such a configuration. This paper also presents one of the very important concepts of pneumatic system, regarding the mass flow-rate through a pneumatic valve. If the ratio of the downstream to upstream pressure is less than a critical value, then the flow is classified as choked and the air moves with the speed of sound. Burrows [15] augmented the mathematical model developed in [76], by considering all the actuator positions possible while performing linearization. However, the models developed in these papers were not validated experimentally.

Liu and Bobrow [52] were the first to develop and also experimentally verify a mathematical model of a pneumatic system. A pole-placement controller was implemented on the developed state-space model. It was concluded in this research work that the flow-chocking effect and the limited orifice-opening demanded large feedback gains, which is needed to shift the poles to left-half of the complex plane. The developed controller can be used for various force-feedback applications. The notion of pressure-feedback and the corresponding improvement in the controller performance was first presented by Mannetje [55]. This idea was implemented in [52] and it clearly demonstrated that on introducing an additional feedback term of pressure, the closed-loop poles are shifted further right which improved the performance of the system. The system's response time is further minimized by formulating a linear quadratic Gaussian (LQG) problem to determine the controller gains. Some of the other works that involved designing linear controller with fixed gains are [47], [49] and [65]. A demerit of a linear controller is that the order of the system might get reduced while linearizing, due to pole-zero cancellation. For instance, in [52] the order of the system was reduced from fourth order to third order when the system was linearized about the mid-stroke position. Thus it can be concluded that due to various underlying assumptions, linear controllers do not provide good performance for highly nonlinear systems like a pneumatic actuator.

Currently, proportional integral derivative (PID) controllers are one of the most commonly used conventional controllers for controlling pneumatic actuators, for various industrial applications. One of the first applications of PID for pneumatic actuators was done by Kunt and Singh [47], where it was applied for a simple on-off solenoid valve. A friction model based on Coulomb was used for compensating the friction and it was deactivated every time the steady-state error falls within a tolerance bound. A feed-forward controller was also implemented to reduce the tracking error. Following them, Wang et al. [97] modified the conventional PID by adding acceleration feedback, which improved the system stability. Moreover, two other compensations imposed on the controller were for minimizing the null-offset and also time-delays. To increase the accuracy of linear controllers for pneumatic systems, Saleem et al. [74] added a feedback as well as feed-forward of velocity information to their PID control, which they referred to as PID-VF control. In [92], Mandani-based fuzzy rules were combined with a PD controller and the resulting controller was shown to be stable and capable of rejecting disturbances in the system. Fractional order PID-type controllers are explored in [63] and [44] to tackle the issues of slow actuator bandwidth and high non-linearities in pneumatic systems. Some of the other applications of PID-type controller for pneumatic systems are shown in [56], [75] and [90]. The performance of fixed-gain PID controllers degrades, when subjected to a large and abrupt variations in the external load and the supply pressure. This usually necessitates the integration of conventional PID controllers with various other techniques, as explained previously in this section. Multi-model control system [90] is a very good alternative for linear PID controllers, but it involves an accurate identification of different models, by varying the operating conditions of the plant. Then at every instant, the controller will choose the best-fitting model from its set of available models and thus involves a lot of switching. It also leads to a trade-off between the speed of response and number of unwanted switching.

Various techniques of adaptive control theory have also been explored to control pneumatic systems. Some of the early research done in this field are by Bobrow and Jabbari [12], Kim and Gibson [46] and Mcdonell and Bobrow [58]. In [12], a standard least squares approach was used in a linear ARMA (Autoregressive moving average) model to estimate the model coefficients. The software programme to implement this adaptive control used INT 60H software interrupt, which allows the control gains to change at any time of the process. One of the important observations made in [12], is that using a lower-order model approximation for the pneumatic system results in a better system response as compared with a higher order model. This is because the uncertainties increase with the order of system. Recursive least squares was used in both [46] and [58] to experimentally estimate the unknown parameters, but many physical effects were not accounted in these papers such as the valve dead-band, effects of friction, resolution of feedback sensors and the nonlinearity of air-flow in valve. Adaptive control techniques usually cannot handle the transients produced by any abrupt changes in external load, and thus these methods lag in tracking any fast parameter variations of pneumatic systems. Some of the other applications of adaptive control for pneumatic systems are demonstrated in [62], [88], [59] and [19]. The current research on pneumatic muscle actuators is increasing and various adaptive control strategies are applied to harness this technology such as [101] and [100].

The concept of sliding mode control for pneumatic systems was first described by Paul et al. [64]. A two-way ON-OFF solenoid valve was used for controlling the position of a pneumatic system. A potentiometer was used to measure the position of piston, which acted as the only available sensor information and its corresponding velocity was derived by sampling the position data using a 8088 microprocessor. Due to this limited sensor feedback, the designed sliding surface was of a lower order which complicated the reachability condition. To counteract the low bandwidth of such a system, current drive amplifiers were used to reduce the time-constant of solenoid valve. Pandipan et al. [62] used differential-pressure as one of the state variables, which circumvents the use of any noisy acceleration feedback in their sliding mode formulation. Large control gains were needed when the variation of parameters such as supply pressure and mass of payload are high, thus introducing chattering effects. High frequency chattering can lead to wear and tear of the actuator components. The valve opening in this formulation is simply assumed to be proportional to the applied voltage and it has been found-out by them that this unmodelled dynamics acts as a filter which dampens the chattering. The controller was imposed experimentally on an industrial actuator with a sampling period of 18 ms. Some of the other applications of sliding mode control for pneumatic systems are shown in [17], [71], [31] and [22]. Fractional order sliding mode control [71] can reduce the chattering issue and also consume less power, thus giving a better performance than its integer order counterpart.

Techniques of backstepping control have also been exploited for controlling pneumatic systems, some of which are [35], [80], [69], [9] and [70]. Smaoui et al. [80] designed a backstepping controller to track the position of a electropneumatic system, and their experimental results performed better than classical linear control strategy. A nonlinear friction model was considered by them while designing the controller, and one of the major advantages of this controller is the stability proof using lyapunuov method. The other advantage of this technique is that useful nonlinearities can be considered for the controller design, while the other nonlinearities can be cancelled. Rao and Bone [69] implemented backstepping controller on a 9.5 mm bore miniature pneumatic actuator. The tracking performance was compared with a proportional plus velocity plus acceleration (PVA) control using root mean square (RMSE), for the position error. Backstepping control performed better than PVA, but for tracking certain trajectories like a S-curve, the performance of PVA was better. Besides this, it was also observed that on decreasing the total external mass, the bandwidth of the system increases which causes any high frequency unmodelled dynamics to be excited by high frequency noise. Ren and Huang [70] designed an adaptive backstepping controller for a 25 mm bore double-acting cylinder, which does not require any pressure feedback.

The recent developments in modern control theory led to its application in the field of pneumatic actuators. [95] was one of the first well-known works to implement neural networks for controlling a pneumatic arm. Following this work, in [36] a network of around 200 neurons were used for controlling a robotic arm. It was shown by them, that only pressure input alone is sufficient to control a robotic arm. Visual information from camera was used for the controller feedback, but it is limited by the resolution of the camera. In [99], certain features of neural networks were exploited such as the ones related to preserving the topology, and it resulted in a path planning algorithm to avoid obstacles. Tanaka et al. [93] combined the benefits of neural networks with model reference adaptive control for a system involving electropneumatic servo. In [43] and [86], the benefits of fuzzy logic and neural networks were exploited together for controlling a pneumatic system. Some of the other applications of neural networks in the domain of pneumatic systems are [94], [20], [3] and [57]. Besides neural networks, genetic algorithms have also been used to control pneumatic actuators such as in [45], [18] and [96]. These modern control techniques require highly efficient and computationally intensive hardware for its implementation. Moreover, the current offline-control techniques are giving satisfactory performance with much cheaper hardware, as compared to the ones required for implementing some of the modern control techniques. These becomes a problem for small research organisations to dedicate funds for high-end processors and graphics cards required for some of the modern control techniques. The other important reason is that a number of research and experiments are currently being conducted for improving these control techniques and making it implementable for various offline and online applications in the near future. It is one of the hot topics of research for many interdisciplinary branches like Aerospace Engineering and Computer Science.

2.3.2. Parallel Robots

Flight simulators use parallel structure for increasing the fidelity of their simulation. Parallel manipulators are also termed as closed-link robots, and most commonly known as the Stewart-Gough platform. They offer a number of advantages when compared with its serial counterparts, and are currently being used in a number of industries such as automotive, aerospace, defence, bridge-construction, satellite dishes. Some of its advantages include increased load-to-weight ratio, higher load-carrying capability and more structural strength [33]. Electric and hydraulic actuators are one of the most common means of actuation for these structures but in the recent times, pneumatic actuators are being explored for its use in Stewart-Gough platforms due to some of its advantages mentioned previously.

Grewal et al. [33] were one of the first to implement an advanced control technique for a pneumatically driven Stewart-Gough platform, where they implemented a linear quadratic gaussian (LQG) controller. They verified their control technique experimentally on a miniature Stewart platform with the sampling time of the whole process being 400 Hz. They successfully tracked a sinusoidal wave of frequency 0.1 Hz and amplitude 20 mm. An anti-windup scheme was imposed for the integral control and they verified that their controller is robust to varying external load. Sliding-mode controller was implemented for controlling a six degree-of-freedom Stewart platform [8], where its tracking performance was five times better than a conventional on-off controller. Pradipta et al. [66] modified the conventional Stewart structure by augmenting the structure with an extra cylinder, whose main function was to lift the platform. A compensator for striction friction was introduced while designing the immersion and invariance controller. It was experimentally verified by them that such a control structure resulted in a fast response-rate. In [67], a cascaded PID controller was designed for a pneumatically driven Stewart platform and firefly algorithm was further used to optimise the controller parameters. Gattringer et al. [29] also implemented a PID controller but in combination with inverse dynamics feedforward control. Some of the other control mechanisms for pneumatically driven motion simulator platforms are given in [21], [48], [7] and [37]. These research works mostly focused on small pneumatic structures with cylinder strokes of less than 0.3 m. Big cylinders with larger strokes take a longer time to complete the stroke. The air consumption rate is much higher for bigger systems and it also becomes difficult to track a reference trajectory of frequency higher than 1 Hz due to the limitations of hardware and increased nonlinearity. Therefore, most applications which require higher tracking speed usually relies on small pneumatic actuators with strokes ranging from 1 cm to 30 cm.

Besides the widespread application of Stewart platform as flight simulators, they are also used for other applications. For instance in [32], Girone et al. designed a haptic interface based on a Stewart platform for the purpose of rehabilitation. The platform was constructed using pneumatic cylinders, force and position sensors. The developed system which uses a force control and a position control loop, was named as "Rutgers ankle" and it helps in the effective and fun exercising of damaged ankles. Similarly in [61], Onodera et al. designed a controller for a pneumatically driven Stewart platform for assisting rehabilitation of ankle-foot. The controller is based on viscous damping, stiffness and force. A pneumatically driven wearable device was designed in [91] based on Stewart platform, for the rehabilitation of foot and ankle. Some of the other works on pneumatically driven Stewart platforms acting as ankle and foot devices are given in [13] and [60]. Stewart platform is also used for the purpose of vibration isolation, where the vibration produced by two structures are isolated from one another. Such Stewart platform which are driven by pneumatic actuators can be found in [30] and [50].

2.4. Conclusion and Recommendations

In the recent times, the research community in the field of industrial manipulators and flight simulators are focusing on harnessing the benefits of pneumatic actuators, due to the few edges it has over its electric and hydraulic counterparts. Investing on pneumatic technology to make it applicable as industrial actuators can be economically very beneficial, as it takes very less resource to operate when compared with an equivalent hydraulic or electric actuator. The maintenance required for an pneumatic actuator is very minimal and its average lifespan is usually higher than electric and hydraulic actuators. The hydraulic actuators are prone to oil-leakage from the cylinders and connecting-tubes, which is a major source of concern for the environment. A pneumatic actuator requires the consumption of air from the atmosphere, which makes it one of the safest possible means of actuation. Air being agile, can flow very fast through the cylinders and the connecting tubes. This makes the operating speed of a pneumatic cylinder very high, whereas hydraulic oil has more viscosity than air which makes the response of the system slower than its pneumatic counterpart. This is only applicable to small pneumatic cylinders, as the speed of a large pneumatic cylinder is slower than a similar hydraulic cylinder.

There are a few issues of pneumatic actuator which makes it difficult to apply conventional control techniques on them. Two of such issues are the compressibility of air and time-delays in the connecting-tubes, which makes the system dynamics highly nonlinear. This creates problem in designing controllers that can track the reference positions with high precision. As mentioned previously, switching of the mass-flow rate between chocked and un-choked flow conditions is a major nonlinear behaviour and must be taken into account. Implementing a model-based controller for a pneumatic system is difficult due to unavailability of an accurate model and also due to the variations of different parameters like friction, external load, etc. Some of the control techniques for pneumatic systems discussed in this chapter are pole placement, LQG, robust, sliding mode, backstepping, neural networks and genetic algorithms. It can be concluded after the literature review, that accounting various factors such as a time-varying friction model, pressure feedback, piston viscosity and friction parameters can increase the accuracy of the controller output.

Pneumatic actuators are used in a number of Stewart platforms due to a few of its advantages over other actuation mechanisms. Such structures offer an increased power-to-weight ratio without compromising precision in tracking the desired trajectory. Installing pneumatic actuators on Stewart platforms takes less effort and such structure can function in a wide range of temperature variation. Stewart platforms which are used for the application of flight simulators, should be capable of responding to different reference trajectories of frequency up to 10 Hz, but the inherent nonlinearity of pneumatic systems along with a limitation of available hardware, makes most of the pneumatic controlled systems degrade its performance over 1 Hz.

3

Incremental Nonlinear Dynamic Inversion (INDI)

This chapter presents he fundamentals of Nonlinear Dynamic Inversion (NDI) controller in section 3.1. This is followed by section 3.2, which discusses the fundamentals of Incremental Nonlinear Dynamic Inversion (INDI). Various concepts concerning INDI are also discussed in this section such as the time-scale separation and the effects of model-uncertainty on the system-response. Finally, a state-of-art-review on incremental control is discussed in section 3.3. It discuses some of the applications, issues and a few augmentations done, in order to improve INDI control.

3.1. Basic Principles of NDI

The basic principle of Nonlinear Dynamic Inversion (NDI) controller is that inverting a nonlinear system using state feedback results in a linear structure [25]. Once the nonlinearities are cancelled, almost any conventional linear controller can be designed for the system. NDI is also sometimes referred to as feedback linearization. In order to fully cancel any nonlinearity in system, a exact model of the system is very necessary. The presence of external disturbances and noises will not cancel the nonlinear terms completely and thus making the linear control laws less effective. The known model of the system is termed as nominal model, based on which the NDI law is designed. NDI is a state-feedback technique and thus it requires information of the system states. In this section, the concept of NDI is first demonstrated for a SISO system, following which it will be shown for a MIMO system.

3.1.1. NDI for SISO systems

We consider a general system to be consisting of a single input u and a single output y. The dynamics of the system can be represented as follows.

$$\begin{aligned} \dot{x} &= f(x) + G(x)u \\ y &= h(x) \end{aligned} \tag{3.1}$$

In the above equation, y is kept differentiating, until a explicit form of u appears [79]. For the above system (Eq.(3.1)), a single differentiation is sufficient which is shown below.

$$\dot{y} = \nabla h(x)\,\dot{x} = \nabla h(x)\left(f(x) + g(x)\,u\right) \tag{3.2}$$

In Eq.(3.2), $\nabla h(x)$ is the gradient of $h(x)$ with respect to x, i.e. $\nabla h(x) = \frac{\partial h(x)}{\partial x}$. Eq. (3.2) can be further simplified by the use of lie-derivatives as follows.

$$\dot{y} = L_f h(x) + L_g h(x)u \tag{3.3}$$

$$u = \frac{1}{L_g h(x)}\left(-L_f h(x) + v\right) = a^{-1}(x)\,(v - b(x)) \tag{3.4}$$

In Eq.(3.3), $L_f h(x) = \nabla h(x) f(x)$, $L_g h(x) = \nabla h(x) g(x)$, $a = L_g h(x)$ and $b = L_f h(x)$. The control law for u in Eq.(3.4) is obtained by inverting the system dynamics, which results in the linearizing control law $\dot{y} = v$. v can be expressed as given below.

$$v = \dot{y}_d + k\left(y_d - y\right) \tag{3.5}$$

If the error is defined as $E(t) = y_d - y$, then the linear law is guaranteed to achieve achieve asymptotic stability, which is shown by solving the following linear differential equation.

$$\dot{E}(t) + kE(t) = 0 \tag{3.6}$$

$$E(t) = E_0 e^{-kt} \tag{3.7}$$

In Eq.(3.7), $\lim_{t\to\infty} E(t) \to 0$ and thus the stability of system is guaranteed. For other system models, it might be needed to differentiate the output a number of times, until an explicit expression of u similar to Eq.(3.4) appears. r is defined as the relative degree of the system and the differentiation is done until $L_g L_f^{r-1} h(x) \neq 0$. For such cases, the linear control law becomes the following.

$$v = y_d^{(r)} + k_{r-1}\left(y_d^{(r-1)} - y^{(r-1)}\right) + k_{r-2}\left(y_d^{(r-2)} - y^{(r-2)}\right)\cdots + k_0\left(y_d - y\right) \tag{3.8}$$

In Eq.(3.8), $y_d^{(r)}$ is the rth order differentiation of y_d. For a few simple systems, r is usually equal to the order of the system n and for those systems with $r < n$, the number of internal state equals $n - r$. Internal stability should be ensured while designing a NDI controller. The controller structure is depicted below in Fig.3.1.

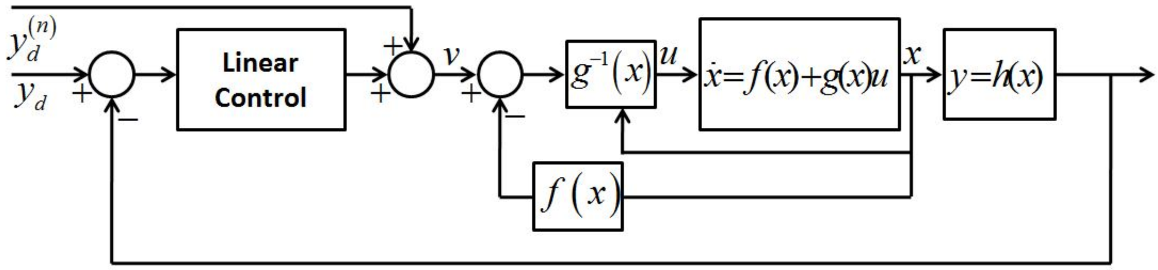

Figure 3.1: Block diagram of NDI controller

3.1.2. NDI for MIMO systems

NDI control methodology can be extended to a general Multiple Input Multiple Output (MIMO) system, in a similar way. The number of inputs x is considered as m, which is also the number of total outputs y. A MIMO system in control-affine form can be expressed as follows.

$$\dot{x} = f(x) + G(x)u \tag{3.9}$$

$$y = h(x) \tag{3.10}$$

The dimensions of x, $f(x)$, y and $h(x)$ are all $m \times 1$ and the dimension of $G(x)$ is $m \times m$. We can express these set of vectors as follows.

$$u = \begin{bmatrix} u_1 & \cdots & u_m \end{bmatrix}^T \tag{3.11}$$

$$x = \begin{bmatrix} x_1 & \cdots & x_m \end{bmatrix}^T \tag{3.12}$$

$$h = \begin{bmatrix} h_1 & \cdots & h_m \end{bmatrix}^T \tag{3.13}$$

$$y = \begin{bmatrix} y_1 & \cdots & y_m \end{bmatrix}^T \tag{3.14}$$

$$G = \begin{bmatrix} G_1 & \cdots & G_m \end{bmatrix}^T \tag{3.15}$$

In Eq.(3.15), all the elements of G have a dimension of $1 \times m$. An explicit relation between the output and the control input is found out by differentiating y [79]. Every output y_j is differentiated r_j number of times, which is known as the relative degree of that output. The sum of all such relative degrees is termed as the total relative degree. For MIMO systems, this differentiation is expressed using lie derivatives as follows.

$$y_j^{(r_j)} = L_f^{r_j} h_j(x) + \left[L_{G_1} L_f^{r_i-1} h_j(x) \cdots L_{G_m} L_f^{r_j-1} h_j(x)\right] \begin{bmatrix} u_1 \\ \vdots \\ u_m \end{bmatrix} \tag{3.16}$$

Next, Eq.(3.16) is inverted in order to find the control input vector u as follows.

$$u = A^{-1}(x)[v - b(x)] \text{ with } v = \begin{bmatrix} v_1 \\ \vdots \\ v_m \end{bmatrix} = \begin{bmatrix} y_1^{(r_1)} \\ \vdots \\ y_m^{(r_m)} \end{bmatrix} \tag{3.17}$$

The matrices $A(x)$ and the vector b are expressed as follows.

$$A(x) = \begin{bmatrix} L_{G_1} L_f^{r_1-1} h_1(x) & \cdots & L_{G_m} L_f^{r_1-1} h_1(x) \\ \vdots & \ddots & \vdots \\ L_{G_1} L_f^{r_m-1} h_1(x) & \cdots & L_{G_m} L_f^{r_m-1} h_1(x) \end{bmatrix}; b(x) = \begin{bmatrix} L_{f^{r_1}}^{r_1} h_1(x) \\ \vdots \\ L_f^{r_m} h_m(x) \end{bmatrix} \tag{3.18}$$

3.2. Basic Principles of INDI

Incremental Nonlinear Dynamic Inversion (INDI) control is a robust control technique, as compared to NDI. INDI has reduced dependency on the system dynamics and relies more on sensor measurement [77]. INDI combines the advantages of an incremental form with NDI and calculates the increments for the control commands, which is then added to the issued command in the previous sampling instant [77]. A general nonlinear system $\dot{x} = f(x,u)$ is considered, while framing INDI control. It is approximated using Taylor's series expansion as follows.

$$\dot{x} = f(x_0, u_0) + \left.\frac{\partial f(x,u)}{\partial x}\right|_{x=x_0, u=u_0} (x - x_0) + \left.\frac{\partial f(x,u)}{\partial u}\right|_{x=x_0, u=u_0} (u - u_0) + H.O.T. \tag{3.19}$$

The higher-order terms denoted as $H.O.T.$ are neglected and a simplified expression is obtained as follows.

$$\dot{x} \simeq \dot{x}_0 + F(x_0, u_0)\,\Delta x + G(x_0, u_0)\,\Delta u \tag{3.20}$$

In Eq.(3.20), $F(x_0, u_0) = \left.\frac{\partial f(x,u)}{\partial x}\right|_{x=x_0, u=u_0}$, $G(x_0, u_0) = \left.\frac{\partial f(x,u)}{\partial u}\right|_{x=x_0, u=u_0}$, $\Delta u = u - u_0$ and $\Delta x = x - x_0$. Now considering a very high update-rate for the control input u and also assuming a small sampling time, the current state x approaches the previous state x_0. Next, using this concept and simplifying Eq.(3.20), the following relation is obtained.

$$\dot{x} \simeq \dot{x}_0 + G(x_0, u_0)\,\Delta u \tag{3.21}$$

Eq. (3.21) is linearized by using the following control law, which results in $\dot{x} = v$

$$\Delta u = G(x_0, u_0)^{-1}\,(v - \dot{x}_0) \tag{3.22}$$

The linear control law can be selected in a similar way as Eq.(3.8). The final control input is thus calculated as given below. The block diagram for an INDI controller is shown in Fig. 3.2.

$$u = u_0 + G(x_0, u_0)^{-1}\,(v - \dot{x}_0) \tag{3.23}$$

The dependency on the system model $f(x,u)$ is reduced for an INDI controller. Instead, the information of this model $f(x,u)$ is reflected in the measurements of $\dot{x}_0$. This makes INDI control techniques to highly rely on the accuracy of sensor feedback [1]. $\dot{x}_0$ can also be derived from the state measurements, as will be discussed in chapter 3. It is also crucial to have an accurate and a complete knowledge of the system states, which is needed for the calculation of control effectiveness $G(x_0, u_0)$. The synchronisation of the feedback signal should be taken care of, such that both x_0 and u_0 are from the previous sampling instant.

As mentioned previously in this chapter, INDI is robust to model uncertainties which can be shown by the following analysis. The control effectiveness matrix G might contain some uncertainties represented as below.

$$G(x,u) = G_n(x,u) + \Delta G(x,u) \tag{3.24}$$

In Eq.(3.24), G_n is the nominal effectiveness and ΔG denotes its uncertainties. Eq.(3.20) can be now represented as follows.

$$\dot{x} \simeq \dot{x}_0 + (G_n(x_0, u_0) + \Delta G(x_0, u_0))\,\Delta u \tag{3.25}$$

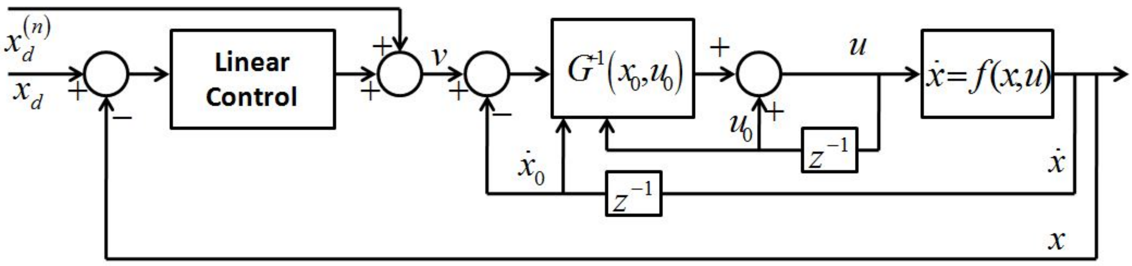

Figure 3.2: Block diagram of INDI controller

The designed control law will be based only on the nominal part, as the knowledge of the uncertainties is not always known, i.e. $u = G_n^{-1}(x_0)(v - \dot{x}_0) + u_0$. Next, replacing this control law in Eq.(3.25), the following relation is obtained.

$$\dot{x} = -\Delta G(x_0)\, G_n^{-1}(x_0)\, \dot{x}_0 + \left(I_{n\times n} + \Delta G(x_0)\, G_n^{-1}(x_0)\right) v \tag{3.26}$$

From Eq.(3.26), it can be observed that only if the uncertainty ΔG is zero, then $\dot{x} = v$. However, if the sampling time of controller is considered to very less, then the difference between the current state derivative $\dot{x}$ and previous state derivative $\dot{x}_0$ is negligible. This results in the following relation.

$$\left(I_{n\times n} + \Delta G(x_0)\, G_n^{-1}(x_0)\right)\dot{x} = \left(I_{n\times n} + \Delta G(x_0)\, G_n^{-1}(x_0)\right) v \tag{3.27}$$

Eq.(3.27) leads to the control law $\dot{x} = v$, which is same as the one where uncertainties are not considered and was first analyzed by Simplício et al. [78]. Therefore, uncertainties in the control effectiveness matrix does not affect the performance of INDI controller, as long as the sampling frequency of the system is very high.

3.3. State-of-the-Art Review on Incremental Control

One of the first well-known references of INDI control was provided by [84], where they developed a simple and robust approach based on NDI control. It was applied for the longitudinal control of a high performance aircraft. Their formulations required the feedback of pitch acceleration and it was assumed that the required vehicle-response bandwidth is much lower than that required by the sensors. These relationships were assumed to be unity and it resulted in an simplified expression for the commanded pitch acceleration, which did not require a mathematical model for the baseline aircraft. A random number generator was used in [84] to introduce noise in the lateral rotational acceleration, but it neither affected the tracking results nor the stability of the system. Besides the robustness to parameter variations, the formulated controller is also robust to actuator saturation. However, the range of variation of the system parameters was not investigated by them. It was also observed that the system performance degraded by the introduction of a second order lag, which is used for filtering the noise. [85] demonstrates the implementation of the above mentioned controller on an VAAC Harrier aircraft, in which the system showed oscillatory responses at lower speeds. Following them in [10], the concept of incremental control based on NDI was tested using NASA's simulation framework ATLAS. The controlled system remained stable, as long as the bias uncertainties in the center of gravity (CG) remained within the safety bounds, but it relied heavily on failure detection and isolation (FDI) of the rate gyros. Moreover, uncertainties in the gyroscope measurements resulted in a low phase margin of the system.

3.3.1. Applications of INDI

In the recent years, INDI control is becoming very predominant because of its reduced dependency on the actual system dynamics. Delft University of Technology in the Netherlands is one of the leading pioneers in this field with numerous research on INDI control. [77] is one of the first well-documented paper on INDI control published by TU Delft. In this paper, INDI control was simulated on an UAV and it showed satisfactory performance in the presence of mismatches in model, inertia and center of gravity. This insensitivity to uncertainty was proved mathematically using a closed-loop transfer function from the reference angular velocity to the actual angular velocity. Its robustness was compared with a conventional NDI controller.

In [28], a flight envelope protection was developed by designing a constraint flight control law and virtual control-limiting techniques, based on INDI control. It was compared with others techniques such as PID and Model predictive controller (MPC) in the presence of parameter uncertainties, wind gusts, time-delays and turbulence. INDI based control of a spacecraft was done in [1], where the authors clearly demonstrated the attitude-tracking capability of a rigid aircraft in the presence of external disturbances. It was concluded in this paper that INDI performs better than a conventional NDI and PI-based control, provided the actuator and sensor measurements are accurate and also synchronised. INDI control was also implemented for the position tracking of aircraft [53] and it showed better performance than model-based control techniques, in the presence of uncertainties.

Helicopter dynamics is very complicated and nonlinear. It is often difficult and also costly to obtain its accurate and high-fidelity model. Therefore, INDI control for such applications can be advantageous for adapting to such issues. In [78], INDI control was implemented for a single main-rotor and tail-rotor helicopter, to achieve two maneuvers of ADS-33 standard. A three-loop controller was developed which sequentially involves a navigation controller, attitude controller and a attitude-rate controller in the end. The simulation results clearly demonstrate that the designed controller takes into account the involved non-linearities in the model, and is robust to uncertainties such as malfunctioning of tail-rotor and aerodynamic uncertainties. Similar to [77], in [78] a second-order closed-loop transfer function from the commanded to the actual attitude angle was derived and it was shown that by proper selection of the constants, a desired damping and natural frequency can be imposed. INDI control is also successfully tested on a passenger aircraft [34], where the authors took into account the various delays and also the actuator saturation, while designing the controller. This paper concluded that INDI is robust to a certain amount of discrepancy in synchronisation between the state derivative and the control input. Apart from fixed-wing aircraft, INDI control was implemented and tested on quadrotor MAVs ([81],[82], [83]), which is becoming a very popular platform for research in aerial robotics. It clearly validates the disturbance rejection property of INDI, when the MAV flies a through a windy environment. This is possible because the obtained angular accelerations are a measure of the complex aerodynamic uncertainties, which is difficult to be modelled accurately. Bias estimation of the acceleration sensors can thus greatly improve the performance of an INDI controller.

INDI control has got equivalence with time-delay control (TDC), as was established in [2]. TDC assumes that the aircraft model matrix at the current and the previous sampling instant are same, whereas INDI assumes that the aircraft states at the current and previous instant are equal. It was proven mathematically in [2], that by subtracting the components of PI controller at two consecutive instants, an incremental form is achieved which is similar to INDI and TDC controller. INDI control can have enormous applications in the aircraft and MAV industry, as discussed previously in this section. Besides these applications, INDI is also implemented for the accurate tracking-control of motion simulators, driven by hydraulic actuators ([40], [41]). Similar to a acceleration feedback in the previously mentioned formulations, hydraulic application requires the feedback of pressure difference derivatives, which can be obtained from sensors. Motion simulators can be considered as a highly complex closed-chain parallel robot, and implementing INDI controller for such a system reduces the dependency on accurate models. It has been shown in [40], through extensive simulation studies that INDI controller performs better, when compared with a model-based cascaded ΔP controller (Cdp).

3.3.2. Issues in INDI controller

Even though an INDI controller shows robustness to a number of practical issues, its performance degrades if the following cases are not taken care of. Firstly, INDI control law for an UAV ([77]) requires the feedback of angular acceleration. These state-derivative measurement received by the sensors might get altered by noise. In INDI control, the feedback of state-variables contains many valuable information, such as any model mismatches and uncertainties. Therefore, erroneous sensor readings can reduce the efficiency of controlled system. The second issue of INDI control is the time-synchronisation of various sensor feedbacks. The control command generated by an INDI controller in the current step relies on the previous control command and also on the previous sensor readings. Therefore an INDI controller is highly sensitive to even small mismatches in time-delay, like 1 millisecond. Thirdly, an INDI controller does not take into account the actuator saturation which is very crucial, especially in the field of aerospace applications, such as control of an UAV or a fixed-wing aircraft. Neglecting the actuator saturation can lead to reduced efficiency of the controller or even instability of the system.

3.3.3. Improvements and further research

In order to tackle some of the issues of INDI control as discussed above, various remedies have been proposed. For instance in [77], a predictive incremental nonlinear dynamic inversion (PINDI) was proposed to calculate angular acceleration using a linear prediction filter, which is more accurate and also less prone to noise, than performing numerical differentiation. The coefficients of this filter are calculated using least squares estimation. In some literature ([81],[82],[53],[40], [34]), a second-order Butterworth filter was implemented to provide the filtered acceleration signals. These filtered information gets delayed due to the dynamics of a lag-filter and is very crucial in reducing any oscillations of the system. The same filter was also used for obtaining the input signals, in order to synchronise the sensor-measurements with the input signals. It was also proven mathematically ([81],[40]) that by considering the same filter dynamics for both the feedback loops, the expression of the closed-loop controlled system is simplified and consists only of an actuator dynamics. Thus, a stable actuator dynamics is sufficient for attaining a stable closed-loop system. An angular acceleration sensor can also be used for obtaining feedback, instead of differentiating the angular velocities [16], thus preventing any additional delay due to the sensors. Time synchronisation is also very vital for the effective performance of INDI control. To ensure it, the time delay of the sensor feedback is made equal to the update frequency of the control system, for instance 100 Hz in [77].

Actuator saturation can be a serious problem in some scenarios, such as the control surfaces of a aircraft. In order to tackle such issues, the technique of pseudo control hedging (PCH) is usually combined with INDI controller ([78], [34], [16]). If the commanded reference signal cannot be achieved by an actuator, then PCH will generate a signal opposite to the commanded direction. A first-order reference model (RM) based on time-scale separation is utilized in PCH, which gives rise to feasible reference commands that can be achievable by an actuator. The other useful property of PCH is the output of a feed-forward component for the virtual control law. The parameters of INDI are often tuned using Multi-Objective-Parameter-Optimization (MPOS) tool, whereas multi-modal approach is used for achieving robustness in parameter variations [34]. Even though INDI control reduces the dependency on the accurate model of the system dynamics, the control effectiveness matrices must be known and the angular acceleration measurements should also be available. Adaptive INDI [81] was implemented on-board a MAV to approximate the control effectiveness matrix by using a Least Mean Sqaure (LMS) filter. Its adaptation constants will dictate the stability and the rate of convergence of the unknown parameters.

3.4. Conclusions and Recommendations

INDI is a convenient control technique for highly nonlinear systems, where a complete and accurate model of the plant is difficult to obtain. INDI has been tried and tested multiple times, mostly in the field of aerospace controls. One of the primary reasons for its increased demand is the ease of implementation. The formulation of INDI is relatively simpler as compared with the other nonlinear control techniques, such as model predictive control (MPC), artificial neural networks (ANN), etc. INDI being less dependent on the plant model, is thus more robust and when compared with a model-based controller, INDI gives better results in handling increased nonlinearities and parameter variations in the system. Model-based controllers such as NDI relies on full state-feedback, which is not feasible for a number of physical systems. This chapter presented some of the available literature, which validates the improvement in the performance of INDI controller over model-based and linear controllers.

Although INDI controller have shown a number of significant improvements over the conventional model-based controllers, certain factors must be taken into consideration while designing it. INDI control is not robust to variation in time-delays and requires accurate time-synchronisation of different feedback signals in the system. For the case of a pneumatic system, it should be ensured that the feedback of pressure-derivatives and the control input should have the same time-delay. The unmodelled dynamics in the INDI controller are taken care of by the feedback of state-derivatives, and therefore it should not be erroneous, or else the system performance degrades. For pneumatic systems, appropriate filters might be necessary for obtaining these noise-free measurements of the state-derivatives. Another important factor while designing INDI controller is the saturation of actuator. As already pointed out from some of the available literature, actuator saturation can pose a serious problem by reducing the performance of the designed controller. For pneumatic systems, appropriate measure will be needed for handling the saturation of the pneumatic valves.

4

Preliminary Study on Controller Design for a Pneumatic Actuator

The selection of model parameter is discussed first in section 4.1, as it will be required for the controller design process. The formulation of an INDI controller for a pneumatic actuator is then explained, following which the design of PID controller will be shown. The INDI controller is initially designed with only position feedback and then, with both position and pressure feedback. This chapters also deals with some of the augmentations of INDI such as filter design, PCH and actuator dynamics, as discussed briefly in section 3.3.3.

4.1. Selection of Model Parameters

This research proposal plans to specifically design INDI controller for pneumatic cylinder, which is capable of generating long-stroke of up to 1m. The major objective of this proposal as already mentioned in section 1.4.2, is to design controllers for pneumatic cylinders which can be used for actuating a flight simulator. Therefore, such a pneumatic cylinder should be capable of generating enough force to lift an external weight of roughly 10000 N. This research proposal will specifically try to design pneumatic controller for the SIMONA flight simulator [87]. The total mass of the SIMONA cabin including all the on-board systems and two crews members is below the the margin of 4,500 kg [27]. It's maximum speed of operation can go up to 0.95 m/s. Currently it uses 6 hydraulic actuators, which are capable of generating massive amount of torque for propelling the flight simulator with such a high speed. The primary goal of SIMONA Research Simulator (SRS) is to conduct research projects related to human machine interactions [87]. There are a number of subsystems of the SRS, such as its computer architecture, visual display system, motion base, cabin and other cues for increasing the fidelity of simulation. In this research proposal, only the motion base has been considered in order to design appropriate controllers for it. The motion-base has 6 degrees-of-freedom and currently runs on hydraulic actuation. A Gough-Stewart platform is obtained by connecting six of those hydraulic cylinders in pairs, at three different points. The cylinders are driven by an electro-hydraulic servo-valve, which is linked to the cylinder by a series of connecting tubes.

The main objective of this research project is investigate the viability of pneumatic actuation for operating the SRS. The dimensions and the parameters of the required pneumatic cylinder are initially calculated, based on the total weight of the SRS and the desired speed of operation. Next, a number of pneumatic cylinders are searched from the available models of SMC [24] and Festo [23], which can provide nearly the same specifications calculated in the first step. Following are the requirements for a single cylinder to be used in SIMONA simulator:

- Payload: The total payload is around 4500 kg. By equally distributing it among the six cylinders, a load of 750 kg is obtained for each of them. Now considering the fact that the legs are not perpendicular to the base and also after including some safety margin, a load of 1000 kg is considered for each cylinder.
- Maximum Stroke Length: 1.25 m
- Maximum piston velocity: 0.9 m/s

The external load of 4500 kg is kept perpendicular to the ground and is thus under the influence of gravity. So this external load will generate roughly 45000 N of force. The area of the cylinder is first calculated, which will be needed to generate sufficient thrust. The required thrust will be around 10000 N for a single cylinder after considering the safety margin, which is discussed previously. The atmospheric pressure is conventionally taken as 101325 Pa (1 bar), the temperature is taken as 293.15 K, the specific-heat ratio is taken as 1.4 and the gas constant is considered as 287.

The maximum supply pressure is 10 bar but it is assumed that only 70 % of maximum pressure is applied, which is around 7 bar. So the driving pressure for the piston will be 6 bar. The efficiency of the cylinder is considered to be 90 % in our computation. So the bore area of a single cylinder is calculated as follows.

$$\text{Bore Area} = \frac{\text{Thrust Needed}}{\text{Pressure} \times \text{Efficiency}} = \frac{10000}{600000 \times 0.9} = 0.0185 m^2 \tag{4.1}$$

The area calculated in Eq.(4.1) corresponds to a bore diameter of around 15.4 cm. In our simulations, we considered the next available bore size, which is 16 cm. The total air consumption by the cylinder is then calculated, which is required for a stroke length of 0.5 m to be completed in 1 second. The total volume of air consumed by the system is 9.3 litres every second, which was found by multiplying the area of the chamber with the stroke length. Next utilizing Boyle's law [98], the following relation is obtained.

$$P_1 V_1 = P_2 V_2 \tag{4.2}$$

In the above equation, P_1 equals 8 bar, V_1 equals 9.3 L and P_2 equals 1 bar. Thus the air consumed from the environment is 74.4 L, for a stroke of 0.5 m to be completed in 1 second. In terms of minutes, the air consumption rate is found to be 4464 l/min. The valve suitable for our applications should be capable of generating such a consumption-rate. Some valve manufacturers specify Cv rating which also depends on available pressure drop (Δp), which in our case is around 3 bars, due to the maximum supply pressure of 10 bar.

$$C_v = \frac{Q}{400 \times \sqrt{p^2 + 1.033 \times \Delta p}} = 0.5016 \tag{4.3}$$

Usually the C_v calculated above is split between the connecting tube and the valve by the use of following relation.

$$\frac{1}{C_v^2} = \frac{1}{C_{vv}^2} + \frac{1}{C_{vt}^2} \tag{4.4}$$

In Eq.(4.4), C_{vv} and C_{vt} denotes the C_v rating for the valve and connecting tube respectively. So the C_v rating of valve comes to be around 0.3522.

Parameter	Small pneumatic system	Big pneumatic system
Piston Length	0.5 m	1.2 m
Piston Ineffective Length	0.05 m	0.1 m
Chamber Diameter	0.025 m	0.125 m
Piston Diameter	0.01 m	0.027 m
External load mass	2.5 kg	200-1000 kg
Piston Rod Mass	0.30615 kg	2 kg
Maximum Displacement of spool	0.002 m	0.004 m
Maximum Orifice opening	2.2062e-05 m^2	2.2062e-03 m^2
Supply Pressure	6 bar	10 bar

Table 4.1: Dimensions of a small and big pneumatic cylinder

The dimensions of a small and big cylinder are summarized in Table.4.1, and their comparison result is shown in Fig.4.1. To compare their speed of controller response and to avoid any overshoot, the integral component was ignored due to which some steady-state error can be observed. The bigger cylinder takes more time to converge to the specified reference piston position. The effects of time-delay for a big and small cylinder are plotted in Fig.4.2. For the case of small cylinder, the oscillations introduced due to the time-delays gets damped and results in a steady-state value with some error. For the case of large cylinder, the oscillatory response does not cease and is thus necessary to be compensated in the controller. It can also

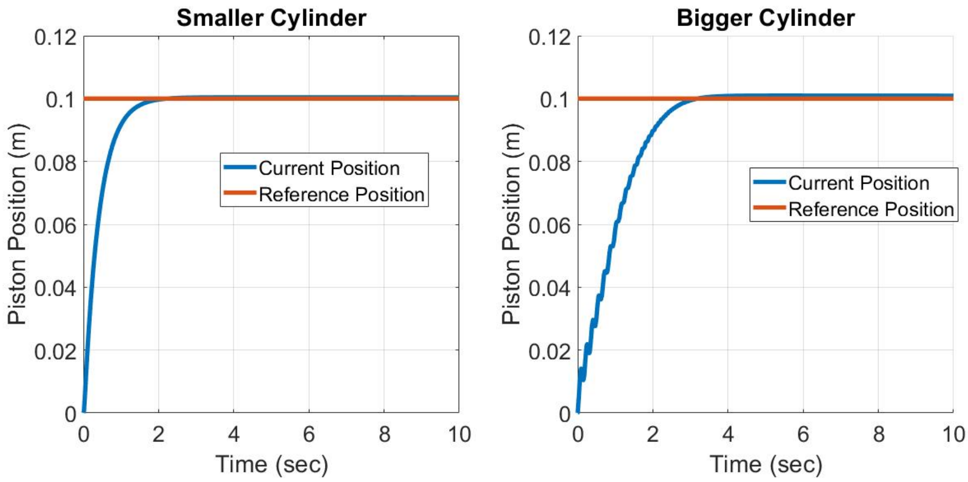

Figure 4.1: Response of smaller and bigger cylinder

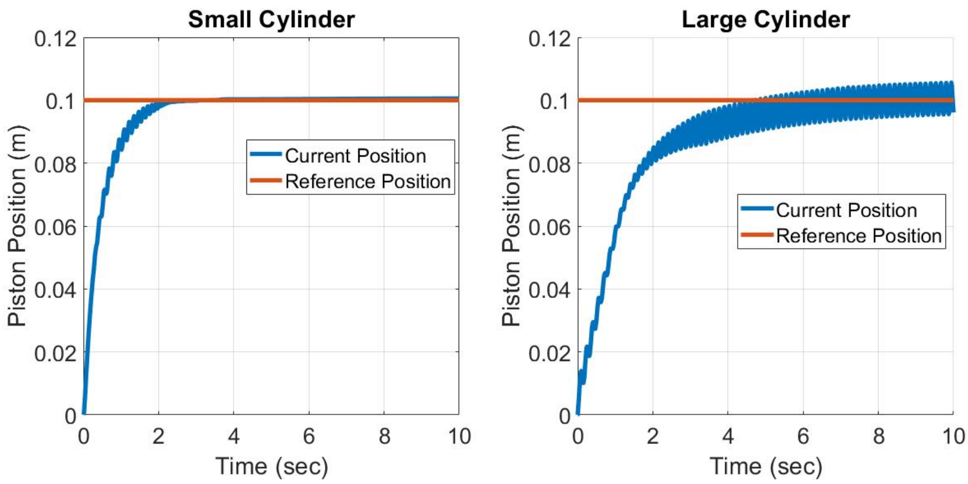

Figure 4.2: Effect of time-delays in connecting tubes

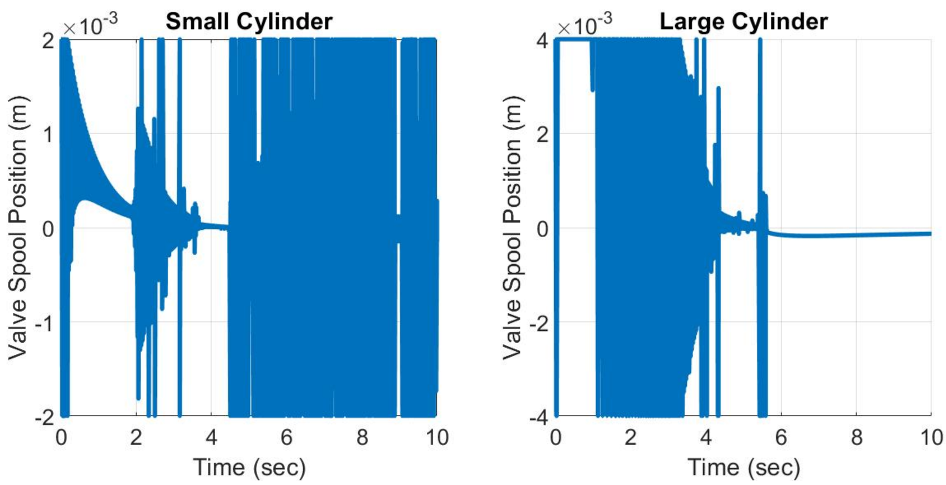

Figure 4.3: Valve-spool displacement for Fig.4.1

be observed from Fig.4.3 that the valve-spool in the small cylinder oscillates between the two saturation-limits, like a bang-bang controller. This is one of the explanations for the attainment of steady-state value in a small cylinder, which is due to this constant switching of the control command. For the case of the bigger cylinder, the the controller output settles down to a steady-state value, once the response starts oscillating after 4 seconds of simulation time (Figs.4.2 and 4.3).

4.2. INDI Controller

The design of INDI controller is described in this section. First a single-loop INDI controller will be framed in section 4.2.1, by using only position feedback. Following this, three-loop and two-loop controllers will be designed in section 4.2.3 and 4.2.4 respectively.

4.2.1. INDI controler with position feedback

First, an NDI formulation will be shown, following which an INDI controller is designed. The simplified equation of motion for a piston-rod assembly is given as follows.

$$\ddot{x} = \frac{1}{(M_p + M_L)}\left(P_A A_A - P_B A_B - P_a A_r - F_f - F_L\right) \tag{4.5}$$

Differentiating it once, the following expression is obtained.

$$\dddot{x} = \frac{1}{(M_p + M_L)}\left(\dot{P}_A A_A - \dot{P}_B A_B\right) \tag{4.6}$$

In Eq.(4.5), the actual control input is the valve current i_c which changes the valve spool position x_s. This valve spool position x_s will dictate the total effective orifice area A_v. However in this formulation, we have considered A_v as the control input, instead of i_c. Now using the dynamical equations for the variation of pressure (Eq.(2.13)) and mass-flow rate (Eq.(2.16)) in Eq.(4.6), the control input A_v is obtained as a function for the virtual control v and some other parameters.

$$u = A_v = f(v, \text{Other Parameters}) \tag{4.7}$$

The other parameters in Eq.(4.7) includes the chamber pressures P_A and P_B, supply pressure P_s, ambient pressure P_a, area of the chambers A_A and A_B, area of piston A_p, temperature T, specific heat ratio k, discharge constant C_f, friction F_f, load force F_l, piston displacement x and its velocity $\dot{x}$, load of mass M_l and mass of piston M_p. The mass flow-rate through a pneumatic value is expressed using the flapper-nozzle equation [73]. Depending on whether the flow is choked or under-choked, a total of 16 conditions are obtained for evaluating A_v. The virtual control v is defined as follows.

$$\dddot{x} = v \tag{4.8}$$

In order to track the reference piston-position, a third-order error dynamics is used as follows.

$$v = \dddot{x}_d + K_{d1}(\ddot{x}_d - \ddot{x}) + K_{d2}(\dot{x}_d - \dot{x}) + K_p(x_d - x) \tag{4.9}$$

In Eq.(4.9), x_d denotes the desired piston-position and x is the actual piston-position. K_p, K_{d1} and K_{d2} are the tuning parameters of the controller. The philosophy behind the selection of these controller coefficients is discussed below in section 4.3.1. The performance of NDI controller can be increased by using an accurate version of the dynamical model. The performance of NDI will degrade once the actual system dynamics starts deviating from the nominal model.

For the formulation of INDI, a complete knowledge of plant dynamics is not required but rather only an information of control effectiveness, as explained in section 2.4. In the following sections, a one-loop and then a two-loop INDI controller will be derived. First, the following relation (Eq.(4.10)) is obtained similar to Eq.(4.7) of NDI formulation.

$$\dddot{x} = f(A_v, \text{Other Parameters}) \tag{4.10}$$

In order to find the control effectiveness matrix G, Eq.(4.10) is partially differentiated with respect to A_v. Once the G matrix is calculated, then the INDI control law is obtained as follows.

$$\dddot{x} = \dddot{x}_0 + G(A_v - A_{v0}) \tag{4.11}$$

$$\dddot{x} = v \tag{4.12}$$

Now, substituting the linear control law of Eq.(4.12) in Eq.(4.11), the INDI controller for the inner-loop is obtained as follows.

$$A_v = A_{v0} + G^{-1}(v - \dddot{x}_0) \tag{4.13}$$

In Eq.(4.13), A_{v0} and $\dddot{x}_0$ denotes the orifice area and the third-derivative of the piston-position respectively, both in the previous sampling instants. The above formulation of INDI considers the control input to be orifice area A_v. The controller coefficients for both the NDI and INDI controller are summarized below in Table.4.2.

Position-based NDI	K_p	K_{d1}	K_{d2}	K_{i1}
	10000	10000	0	0
Position-based INDI	K_p	K_{d1}	K_{d2}	K_{i1}
	1300	900	300	0.025

Table 4.2: Coefficients of position-based NDI and INDI controller

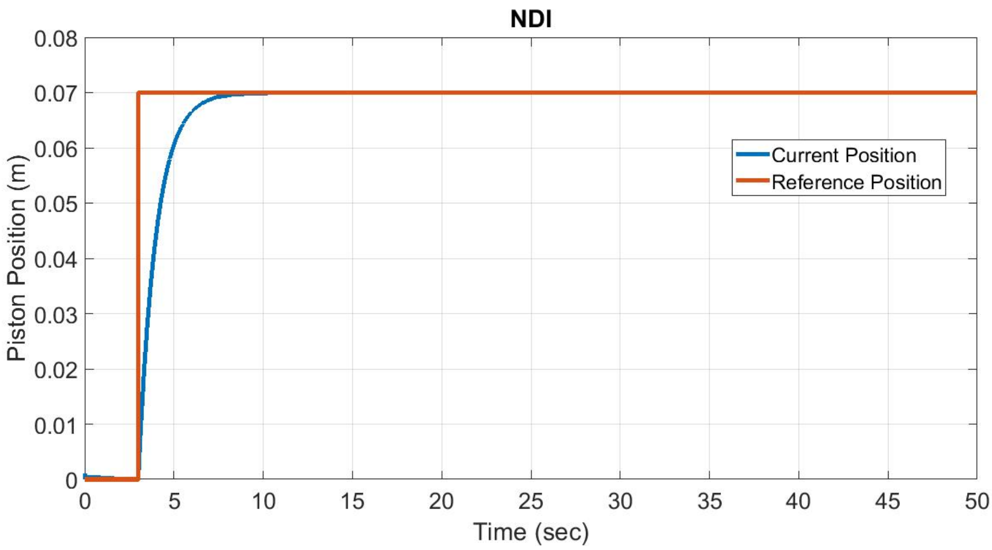

Figure 4.4: Tracking results of NDI control with only position feedback

The results of position-tracking using NDI controller is shown in Fig.4.4. The model used for designing the NDI controller does not contain any uncertainty and thus the performance of the model-based controller is satisfactory, with zero steady-state error. The final response can be further tuned to meet a given time-domain specification. Note that in Fig.4.4, the effect of time-delays in the connecting tubes is not taken into consideration.

The response of INDI controller without integral action and with integral action are shown in Fig.4.5 and Fig.4.6 respectively. We can observe that there is a there is slight bump in the initial section of the graph when the reference position is zero. The reason for this unusual behaviour is that even though the load force, the friction force and the force due to the ambient pressure are active in the system but while deriving the control effectiveness matrix, these terms gets cancelled, as can be observed from Eqs.(4.5) and (4.6). Therefore these three forces are acting in the system, but there is not compensating term for these forces, in the designed INDI controller. For the case of NDI controller, the above mentioned three forces are present in the controller formulation and thus the unusual deviation at the start of the tracking response is absent. This necessitates a force-control loop, as will be explained in the following sections. The other observation which can be made from Fig.4.6 is that the overshoot starting from 5 seconds is due to the integral part, which can be further tuned to obtain a desired time-domain specification. By removing the integral part, this overshoot vanishes, as can be seen in Fig.4.5.

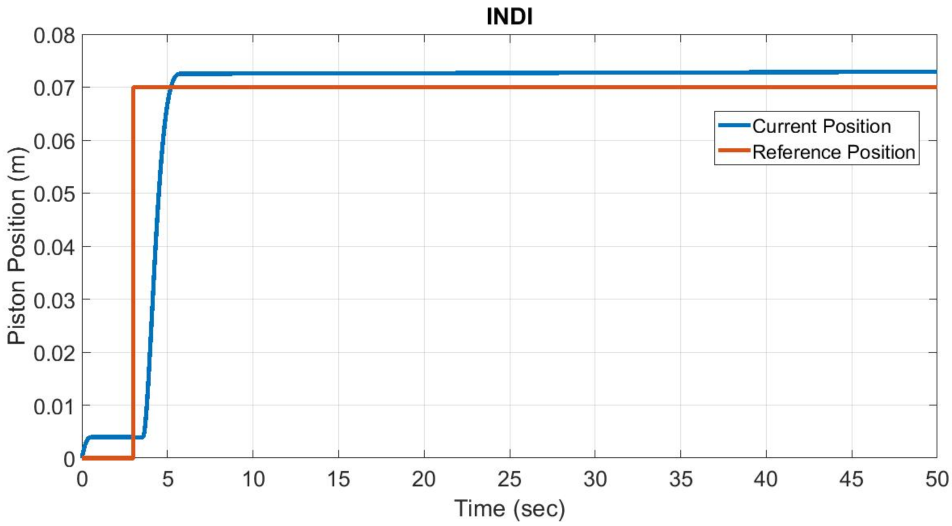

Figure 4.5: Output of position-based INDI controller without integral action

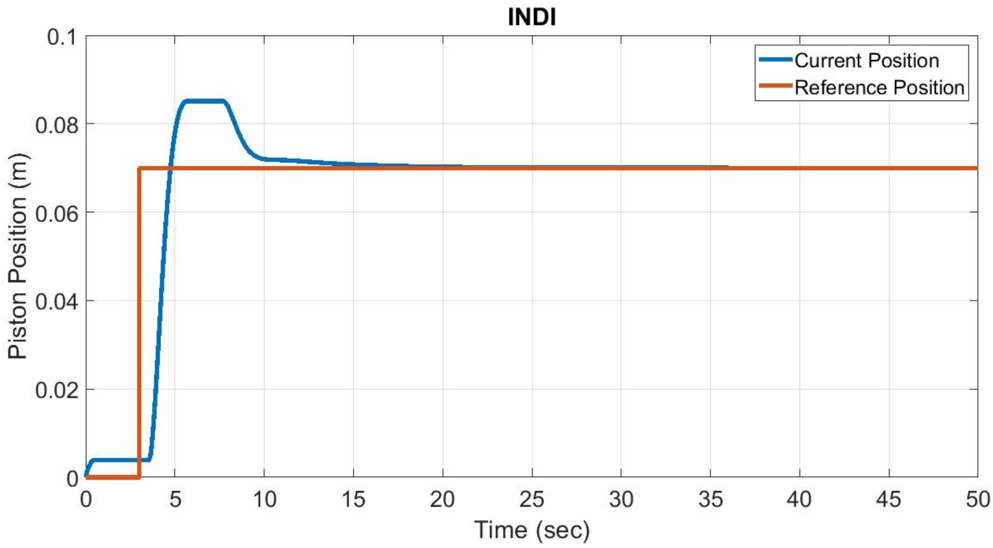

Figure 4.6: Tracking results of INDI control with only position feedback

4.2.2. Position-based INDI with additional feedback of coil-current

Next, a two-loop controller is designed. The outer-loop controller delivers the desired valve-spool displacement x_{s_d}, and the inner-loop controller has to track the desired orifice area by controlling the current in the valve solenoid. In Eq.(4.10), the area A_v is replaced with Eq.(4.14) and partially differentiated with respect to x_s in order to obtain the control effectiveness matrix $\tilde{G}$.

$$A_v = \frac{x_s}{|x_s|}\pi x_s^2 \tag{4.14}$$

We can observe from Eq.(4.14) that depending on the sign of x_s, the area of orifice-opening can be either positive or even negative. Positive area occurs when the displacement x_s is positive, which physically means that it pumps air into cylinder chamber B and simultaneously pumps air out of chamber A. Negative area physically signifies that the valve is pumping air into chamber A and simultaneously out of chamber B (Fig.2.1). Using these relations, an INDI law is framed which outputs the desired spool displacement x_{s_d} to the outer-loop controller.

$$x_{s_d} = x_{s0} + \tilde{G}^{-1}(\nu_1 - \dddot{x}_0) \tag{4.15}$$

Next, an inner-loop controller is derived. The dynamics of a pneumatic valve can be described by using a first-order assumption as follows.

$$c_s \dot{x}_s + k_s x_s = K_f i_c \tag{4.16}$$

c_s is the viscous friction coefficient, k_s is the spring constant and K_f is the coil force coefficient. The coil-current i_c controls the valve-spool displacement x_s, which further changes the orifice area of the valve. Once the desired spool displacement x_{s_d} is obtained, Eq.(4.16) is used to frame the inner-loop NDI control law. The linearized control law is defined as $\dot{x}_s = v_2$, where v_2 is expressed as follows.

$$v_2 = K_p \left(x_{s_d} - x_s\right) - K_d \dot{x}_s + +K_i \sum \left(x_{s_d} - x_s\right) \tag{4.17}$$

Finally the solenoid current in the valve is calculated using Eq.(4.16), as given below.

$$i_c = \frac{c_s}{k_f} v_2 + \frac{k_s}{K_f} x_s \tag{4.18}$$

The controller coefficients are summarized below in Table.4.3.

Position-based INDI with additional feedback of current	K_p	K_{d1}	K_{d2}	K_{i1}	K_p	K_d	K_i
	800	970	10	0.01	800	0.75	40

Table 4.3: Coefficients of position-based INDI controller with additional current feedback

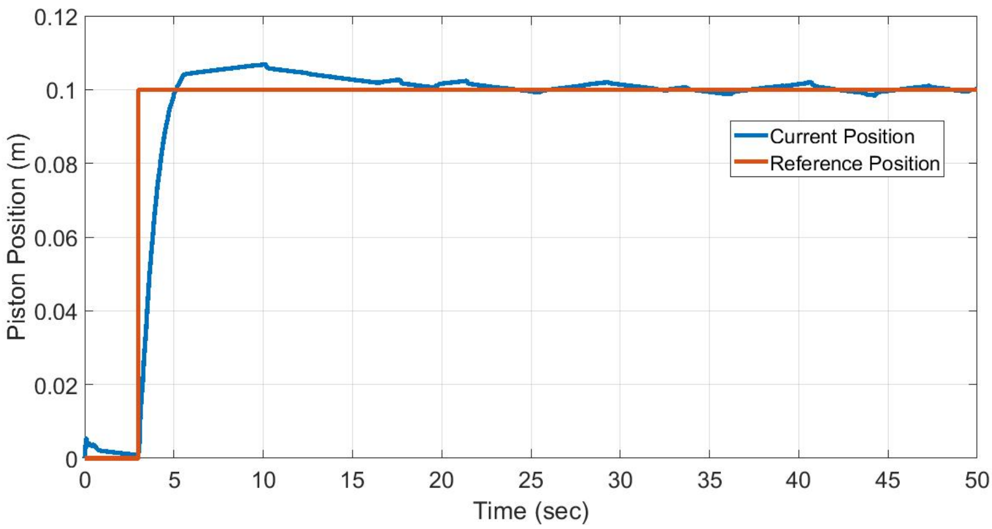

Figure 4.7: Tracking Results of position-based INDI with additional feedback of coil current

The tracking result of the INDI controller with coil-current as the control input, is plotted in Fig.4.7. It can be observed that the controlled trajectory tends to be very oscillatory, when compared with the previous results in Fig.4.4-4.5. The explanation for such an observation is the control command, which in this case is the coil current of solenoid. A number of spikes are observed in the coil current (Fig.4.8), which can either be handled by putting saturation bounds on the coil-current or by tuning the controller efficiently.

4.2.3. Three-loop controller

The designed controller consists of three loops, as depicted in Fig.4.9. The outer-most loop is for position control, the intermediate loop is for force control and the inner-most loop controls the current flowing through the solenoid in the valve. The outer-most position control loop is based on NDI, intermediate force loop is INDI-based and the inner-most current loop is based on NDI. The position control loop outputs the desired differential pressure P_{L_d}. The linearizing control law for the position loop is $\ddot{x} = v_1$.

$$P_{L_d} = \frac{\left(M_p + M_L\right) v_1 + P_a A_p - A_p P_B + F_f + F_l}{A_a} \tag{4.19}$$

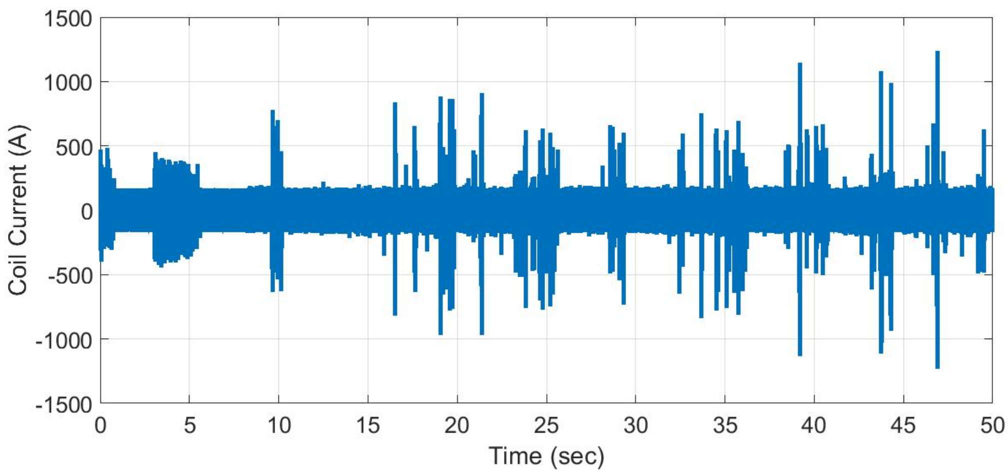

Figure 4.8: Coil current in the valve solenoid

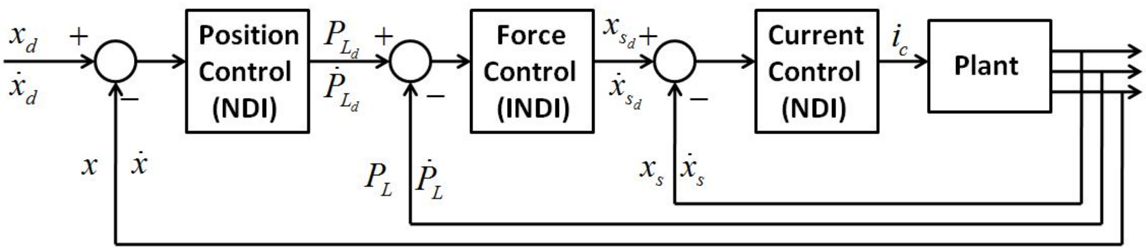

Figure 4.9: Block diagram of three-loop controller

$$v_1 = K_{p_1}(x_d - x) - K_{d_1}(\dot{x}_d - \dot{x}) + K_{i_1}\sum(x_d - x) \tag{4.20}$$

K_{p_1}, K_{d_1} and K_{i_1} are the tuning parameters of the controller. The intermediate force control loop consists of an INDI law, which is summarized below. It outputs the desired valve spool displacement x_{s_d} as follows.

$$x_{s_d} = x_{s_0} + G^{-1}\left(v_2 - \dot{P}_L\right) \tag{4.21}$$

$$v_2 = \dot{P}_{L_d} + K_{p_2}\left(P_{L_d} - P_L\right) + K_{i_2}\sum\left(P_{L_d} - P_L\right) \tag{4.22}$$

In the above equation, the control effectiveness G is calculated by partially differentiating the differential pressure-derivatives with respect to valve-spool displacement, i.e. $G = \frac{\partial(\dot{P}_A - \dot{P}_B)}{\partial x_s}$. Finally the actual control-input which is the valve current, is calculated as follows.

$$i_c = \left(\frac{C_d}{C_v}\right)v_3 + \left(\frac{K_s}{C_v}\right)x_s \tag{4.23}$$

The linear control law v_3 is calculated as given in Eq.(4.24). K_{p3}, K_{d3} and K_{i3} are the tuning parameters.

$$v_3 = K_{p_3}\left(x_{s_d} - x_s\right)) - K_{d_3}\dot{x}_s + K_{i_3}\sum\left(x_{s_d} - x_s\right) \tag{4.24}$$

The controller coefficients are summarized below in Table.4.7.

Three-loop controller	K_1	K_{d1}	K_{i1}	K_{p2}	K_{i2}	K_{p3}	K_{d3}	K_{i3}
	400	100	0.2	12	0	800	0.75	40

Table 4.4: Coefficients of three-loop controller

The tracking performance of the controller increases on the introduction of the inner force-control loop, which is based on INDI (Fig.4.10). The frequency of the reference sine-waves were considered as 0.2 Hz and

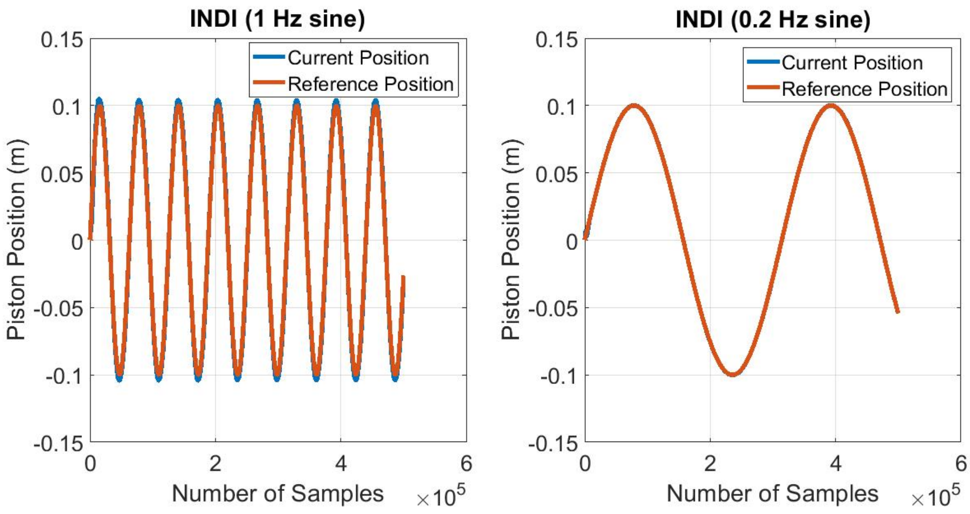

Figure 4.10: Tracking results of three-loop controller for two different reference signals

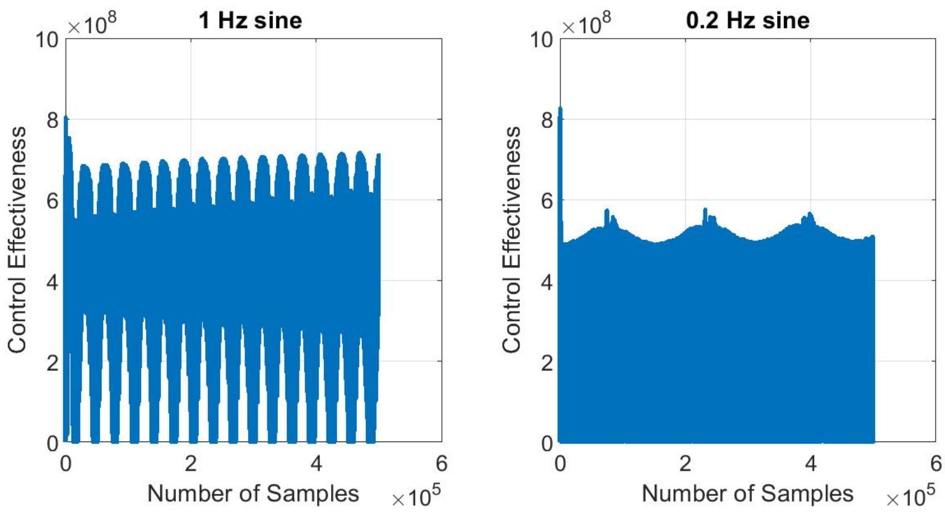

Figure 4.11: Variation of control effectiveness for the two responses in Fig.4.10

1 Hz. For the 1 Hz sine wave, some tracking error is visible at the peaks points. The control effectiveness keeps switching very rigorously to ensure that the control-input supplied to the actuator can track the reference sine wave (Fig.4.11). The time-synchronisation of different signals reaching the INDI controller is very crucial, as its basic principle involves calculating the increments of control input, which is then added to the actual control input supplied in the previous sampling instant. Increasing the length of the connecting-tube consequently increases attenuation and time-delay in the acoustic signal. This leads to degradation in the performance of INDI controller. Fig.4.12 shows that deterioration of controller output is related to the length of the tube. In our formulation, the pneumatic actuator is run by a flapper-nozzle valve [11], as described previously in section 2.1.3. Fig.4.13 shows the variation of choked and unchoked conditions for the flapper-nozzle formulation of the valve. It is also to be noted that the Figs.4.10-4.13 are plotted with its X-axis denoting the number of samples, rather than time. The total number of samples is equal to the total time considered for simulation, multiplied with the sampling time

4.2.4. Two-loop controller

Most of the commercially available pneumatic valves have a built-in current control loop. It can autonomously control its current supply, in order to bring the desired orifice-opening of the valve. Therefore the previously designed current-control loop was removed and it resulted in a simplified two-loop structure (Fig. 4.14). The

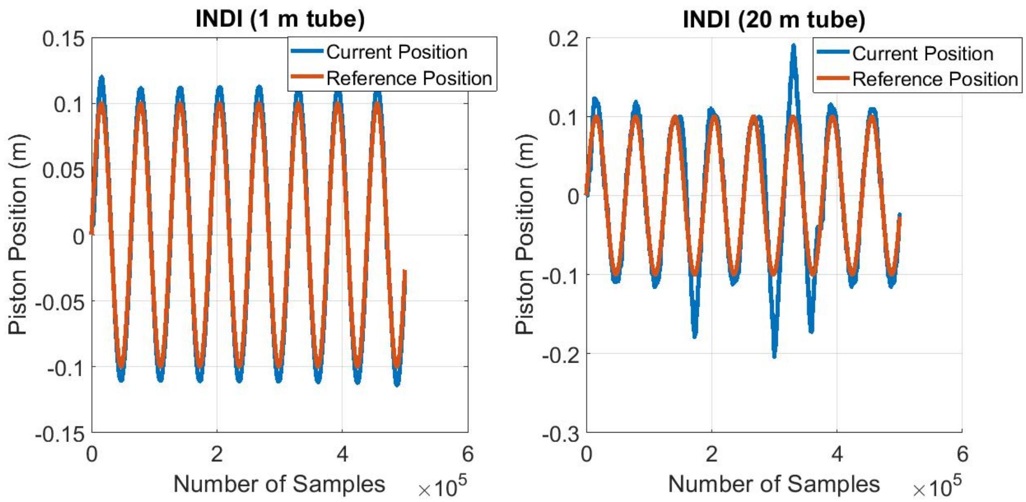

Figure 4.12: Effect of varying length of connecting tube

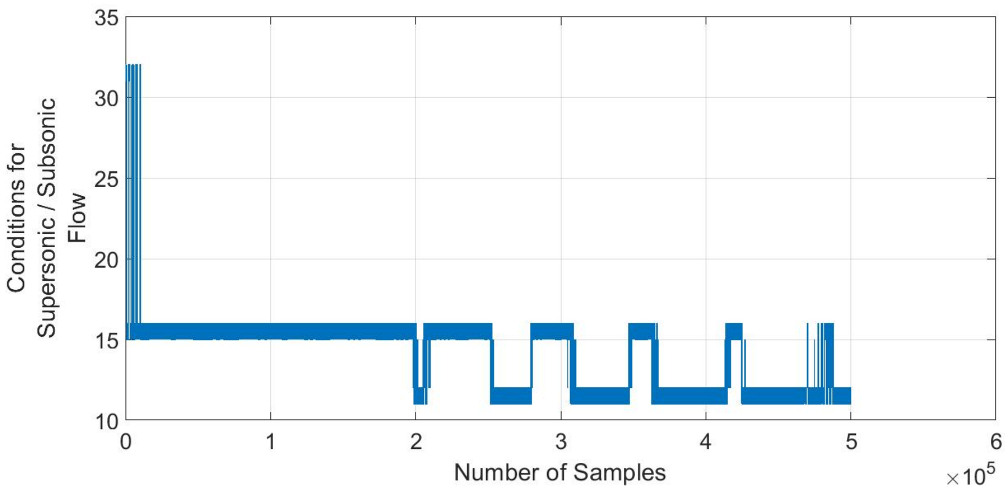

Figure 4.13: Variation of choked and unchoked conditions out of a possible 32

designed controller consists of two loops. The outer-loop is for position control and the inner-loop is for force control. The outer-loop is based on NDI and the inner-loop is based on INDI. The position control loop

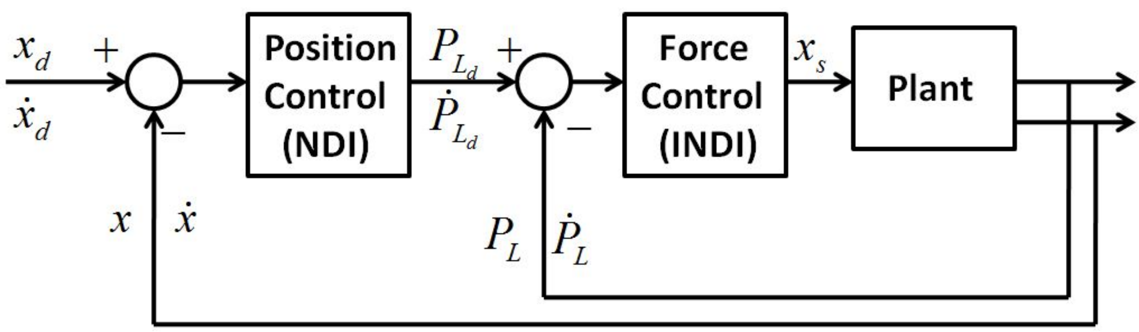

Figure 4.14: Schematic diagram of Two-loop Controller

outputs the desired differential pressure P_{L_d}. The linearizing control law for the position loop is $\ddot{x} = v_1$.

$$P_{L_d} = \frac{\left(M_p + M_L\right) v_1 + P_a A_p - A_p P_B + F_f + F_l}{A_a} \tag{4.25}$$

$$v_1 = K_{p_1} \left(x_d - x\right) - K_{d_1} \left(\dot{x}_d - \dot{x}\right) + K_{i_1} \sum \left(x_d - x\right) \tag{4.26}$$

The inner force-loop controller consists of an INDI law, which is summarized below. It outputs the desired valve-spool displacement x_s as follows.

$$x_s = x_{s_0} + G^{-1} \left(v_2 - \dot{P}_{L0}\right) \tag{4.27}$$

$$v_2 = \dot{P}_{L_d} + K_{p_2} \left(P_{L_d} - P_L\right) + K_{i_2} \sum \left(P_{L_d} - P_L\right) \tag{4.28}$$

The controller coefficients are summarized in Table.4.7. In Eq.(4.27), the control effectiveness G is calculated

Two-loop controller	K_1	K_{d1}	K_{i1}	K_{p2}	K_{i2}
	400	100	0.2	10	0

Table 4.5: Coefficients of two-loop controller

by partially differentiating the differential pressure-derivatives with respect to valve-spool displacement, i.e. $G = \frac{\partial(\dot{P}_A - \dot{P}_B)}{\partial x_s}$. It is assumed that the commanded valve-spool position x_s is achieved instantaneously due to the fast voltage supply of solenoid and is therefore directly used as feedback to the controller.

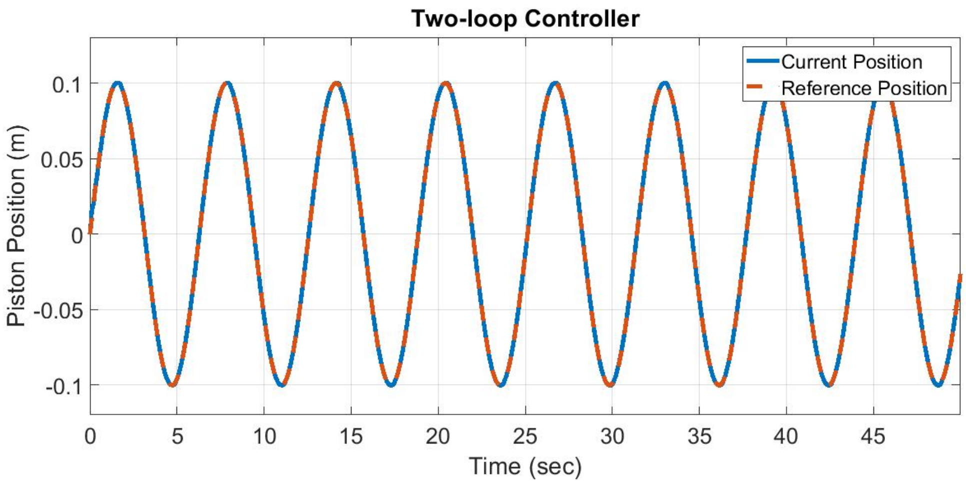

Figure 4.15: Output of two-loop controller with inner-loop based on INDI and the outer-loop based on NDI

Most of the commercially available pneumatic proportional-valves have an inbuilt controller to track the reference valve-spool position, as mentioned previously in this chapter. Thus the inner-most current control loop of the previous formulation was removed and results of the two-loop controller are plotted in Fig.4.15. The tracking improves significantly and one of its main reason is that the whole system now involves the enforcement of two different dynamics which are the position and force, rather than three with an additional dynamics of coil-current. The tracking errors for the outer-loop and the inner-loop controller are shown separately in Fig.4.16. The magnitude of error in the inner-loop is significantly higher than that of the outer-loop controller, but such error-margins are acceptable in a cascaded controller, as long as the error in tracking the reference piston-position is satisfactory. The displacement of the valve-spool does not get saturated in the two-loop controller, which was a major issue in the three-loop controller. Fig.4.18 shows the impact on the controller performance due to the time-delays in the connecting tubes. The other impact of time-delays is the saturation of valve spool displacement (Fig.4.19).

4.3. PID Controller

A single-loop PID controller is initially designed, following which a multi-loop PID controller is constructed. Different reference signals were used for analyzing the controller, such as a constant, stair-case and sinusoidal reference signal.

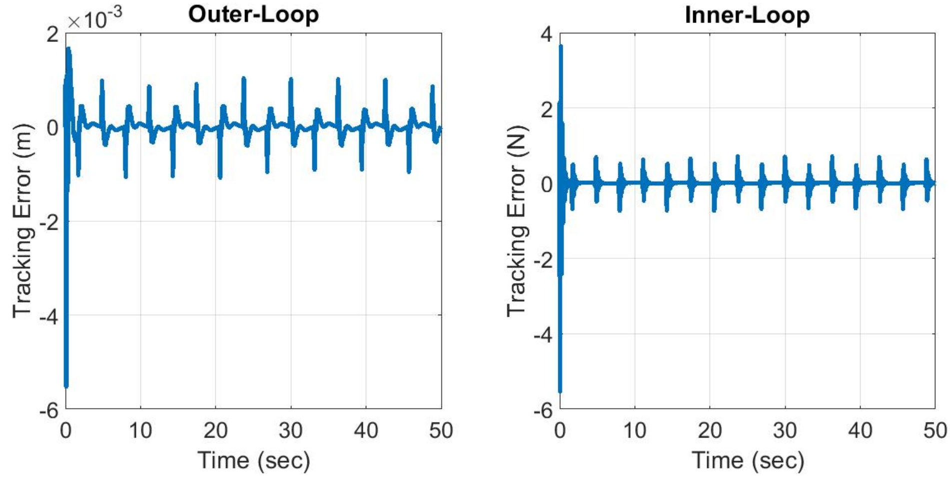

Figure 4.16: Tracking errors for the inner and outer loops in Fig.4.15

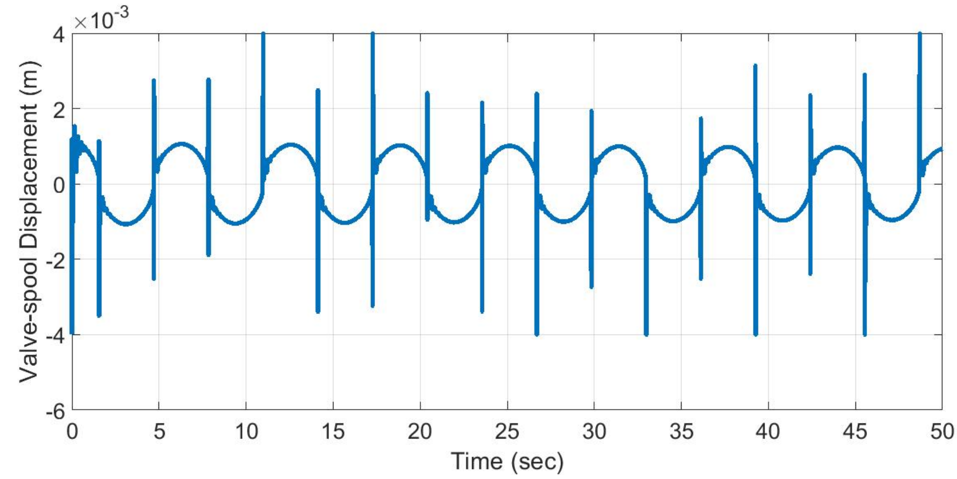

Figure 4.17: Displacement of valve spool for Fig.4.15

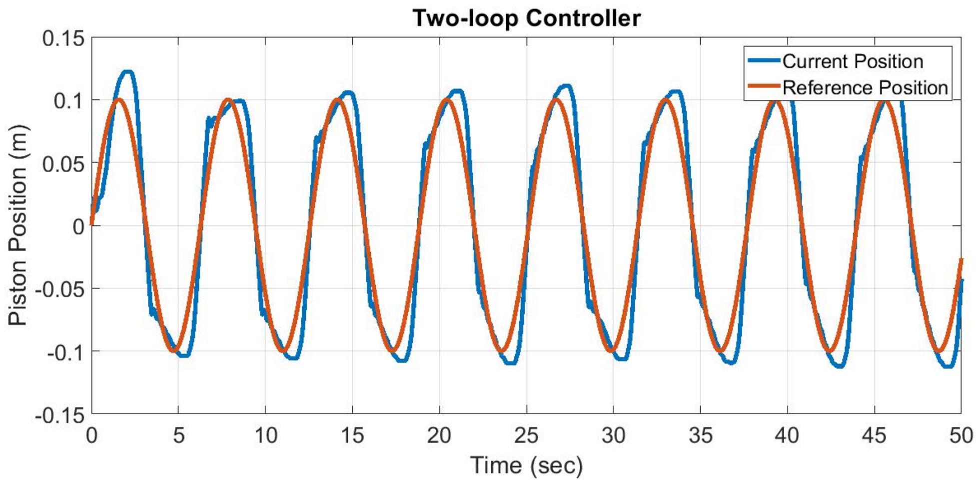

Figure 4.18: Effect of time-delays in the connecting tubes

4.3.1. PID controller with position-feedback

The control input considered in this formulation is the valve orifice area A_v, and only the position and velocity feedback is utilized. The single-loop PID formulation is as follows.

$$i_c = K_p(x_d - x) - K_d \dot{x} + K_i \sum (x_d - x) \tag{4.29}$$

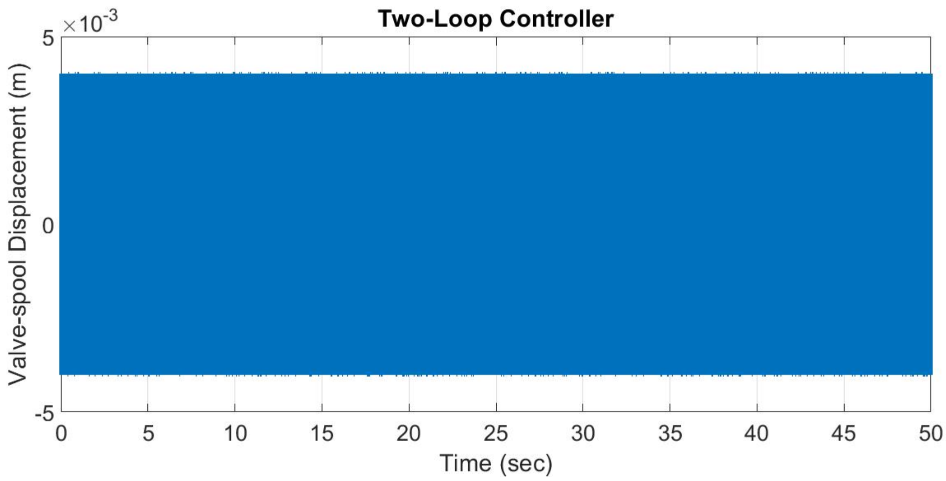

Figure 4.19: Saturation of valve-spool displacement

In Eq.(4.29), x and $\dot{x}$ are the position and velocity of the piston. x_d and $\dot{x}_d$ are the desired position and the desired velocities of the piston to be tracked. K_p, K_d and K_i are the design parameters which can be tuned in order to obtain the desired closed loop system characteristics. The formulation of a two-loop PID controller is given below in Eqs.4.30 and 4.31. The outer-loop controller consists of calculating the desired velocity of the piston while the inner-loop controller tries to enforce this piston velocity.

$$\dot{x}_d = K_{p2}(x_d - x) - K_{d2}\dot{x} + K_{i2}\sum(x_d - x) \tag{4.30}$$

$$i_c = K_{p1}(\dot{x}_d - \dot{x}) - K_{d1}\ddot{x} + K_{i1}\sum(\dot{x}_d - \dot{x}) \tag{4.31}$$

Eq.(4.30) provides us the desired velocity of the piston to be tracked, which is $\dot{x}_d$. Once the outer loop controller outputs $\dot{x}_d$, the desired valve current can be calculated using the inner loop controller given in Eq.(4.31). In Eqs.(4.30) and (4.31), K_{p1}, K_{p2}, K_{d1}, K_{d2}, K_{i1} and K_{i2} are the design parameters which can be tuned to result in a given system response. The proportional constants K_{p1} and K_{p2} are first chosen, following which the derivative components K_{d1} and K_{d2} are decided. Finally the integral parameters K_{i1} and K_{i2} are chosen, if the steady-state error is still not eliminated. For our simulations, the proportional and derivative constants were both initialized with unity. Then the proportional gain is increased is steps of either 10 or 100. This process is repeated until the system response gets over-damped, with a few visible peaks above the steady-state value. After that, the derivative component is increased until all the peaks gets damped. In some cases, increasing the derivative component beyond a certain threshold can make the controlled system unstable. So care must be taken while tuning the derivative component. It should also be noted that increasing the proportional constant can lead to small rise-time, but it will result in a higher overshoot. Similarly, reducing the proportional gain directly decreases the overshoot, but the time taken for such a response to settle increases. Therefore, there is a trade-off involved while choosing these controller coefficients. The integral coefficients are defined to be zero, as the steady-state error in Fig.4.20 and 4.21 is very minimal, with errors of 0.0013 m and 0.00011 m respectively. Care should also taken to ensure that the outer-loop control commands are achievable by the inner-loop, or else it will lead to oscillations and steady-state error in the controller response.

Thus the outer-loop consists of calculating the desired velocities, and the inner-loop controller tries to enforce this velocity. For the analysis of PID controller, a staircase reference of step-size 0.03 m was used. The sampling time for the simulation is taken as 0.0001 sec. The results of position-tracking using a single-loop and two-loop PID controller are shown in Fig.4.20 and 4.21 respectively. We can observe that the output of the single-loop PID controller tends to be oscillatory when the reference changes from one step to the other, and thus giving poor performance compared to a two-loop PID controller. The controller coefficients of one-loop and two-loop controller are summarized below in Table.4.6.

For the case of single-loop PID controller, the variation of pressure across the two chambers is given in Fig.4.22 and the variation of mass flow-rate is given in Fig.4.23. The pressure across both the chambers A and B keeps on changing continuously, but the pressure in chamber B is always more than chamber A, which pushes the piston to execute the specified reference position. The effect of time-delays due to the connecting

Two-Loop PID	K_{p1}	K_{d1}	K_{i1}	K_{p2}	K_{d2}	K_{i2}
	100	10	0	100	80	0
One-Loop PID	K_p	K_d	K_i			
	200	5	0			

Table 4.6: Coefficients of PID controller

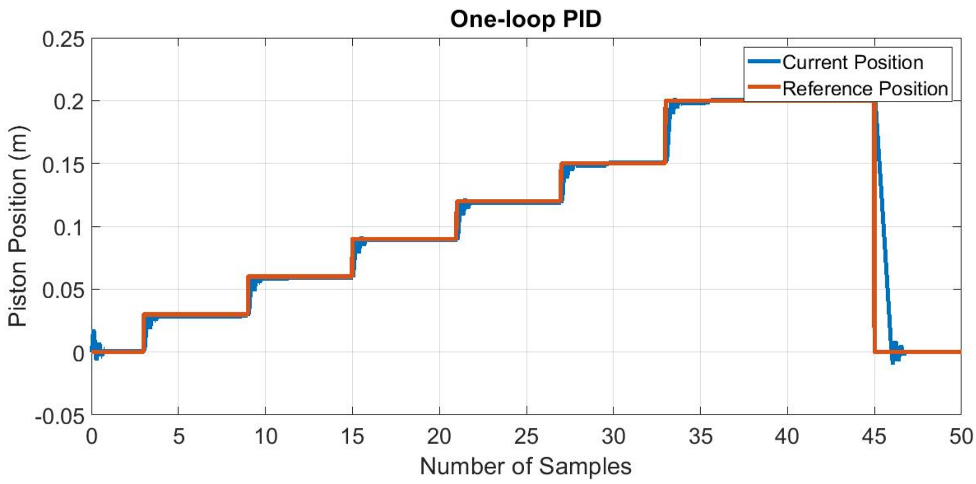

Figure 4.20: Tracking Results of single-loop PID controller

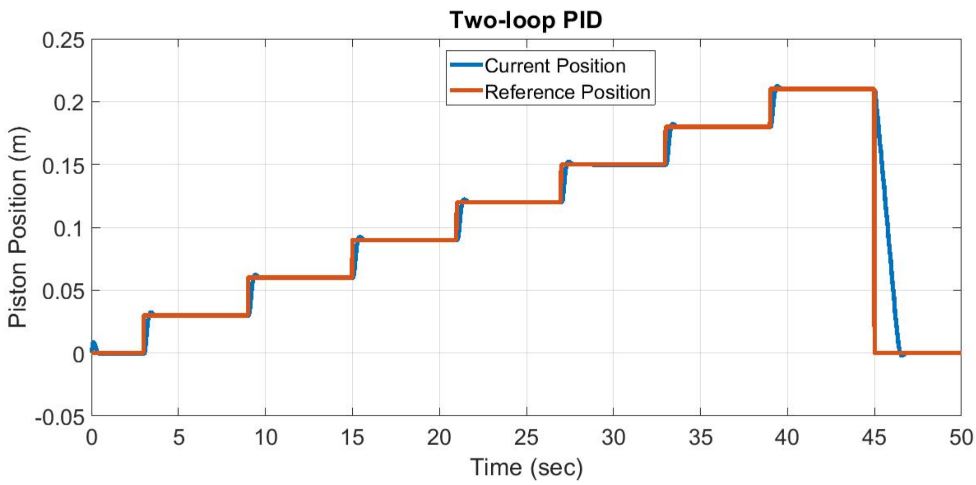

Figure 4.21: Tracking Results of two-loop PID controller

tubes can be clearly observed in Fig.4.24. The time taken to converge for a single-loop PID controller increases manifold in the presence of these time-delays.

4.3.2. PID controller with pressure-feedback

In this section, a two-loop PID controller is framed, where the outer-loop controller calculates the desired pressure variation using the following relation.

$$P_{L_{des}} = K_{p_1}(x_d - x) + K_{d_1}(\dot{x}_d - \dot{x}) + K_{i_1}\sum(x_d - x) \tag{4.32}$$

In the above equation, K_{p_1}, K_{d_1} and K_{i_1} are the controller coefficients, x_d and x are the desired and current positions of the cylinder piston. The inner-loop controller outputs the desired valve-spool displacement using the following relation.

$$x_{s_{des}} = K_{d_2}(\dot{P}_{L_d} - \dot{P}_L) + K_{p_2}\left(P_{L_d} - P_L\right) + K_{i_2}\sum\left(P_{L_d} - P_L\right) \tag{4.33}$$

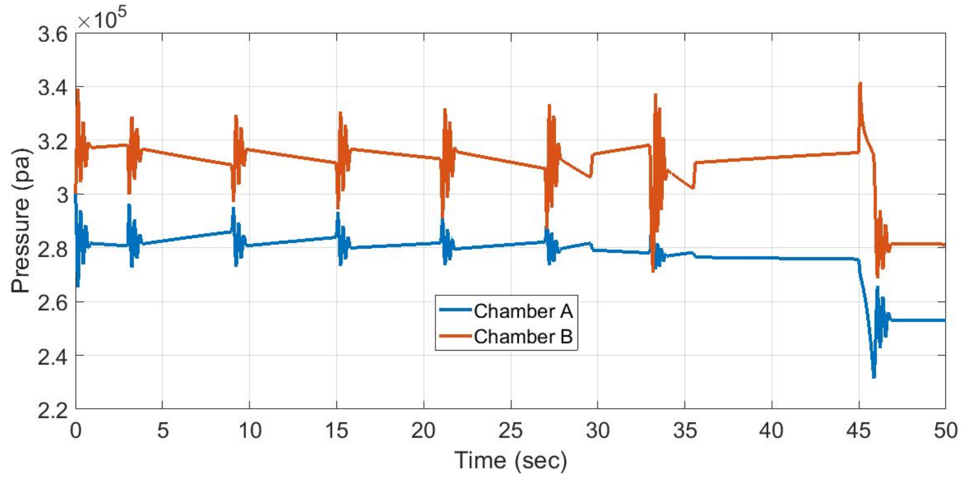

Figure 4.22: Variation of pressure across the two chambers

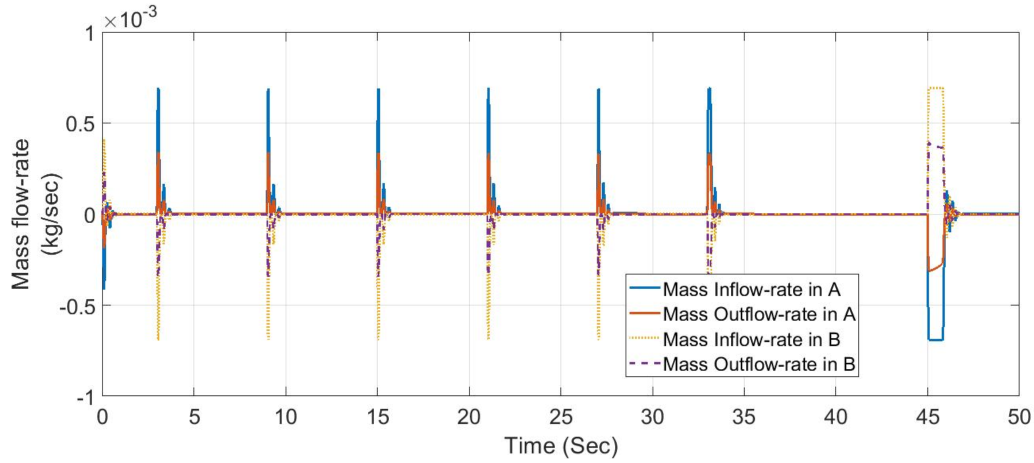

Figure 4.23: Variation of mass-flow rate in and out of the two chambers

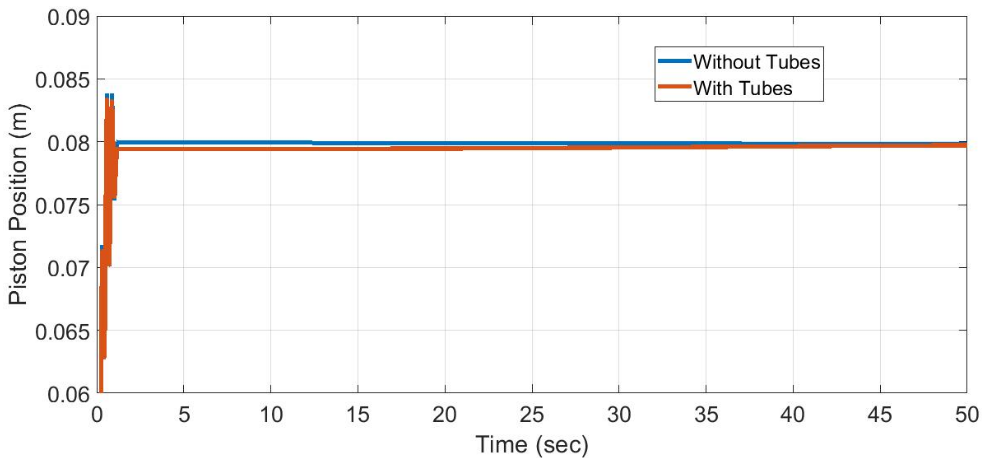

Figure 4.24: Effect of time-delay in the connecting tubes on the performance of a single-loop PID controller

The controller coefficients are summarized in Table.4.7.

The tracking results of PID controller with an additional pressure feedback is plotted in Fig. 4.25. It can

Two-loop controller	K_1	K_{d1}	K_{i1}	K_{p2}	K_{i2}
	400	100	0.2	10	0

Table 4.7: Coefficients of two-loop PID controller

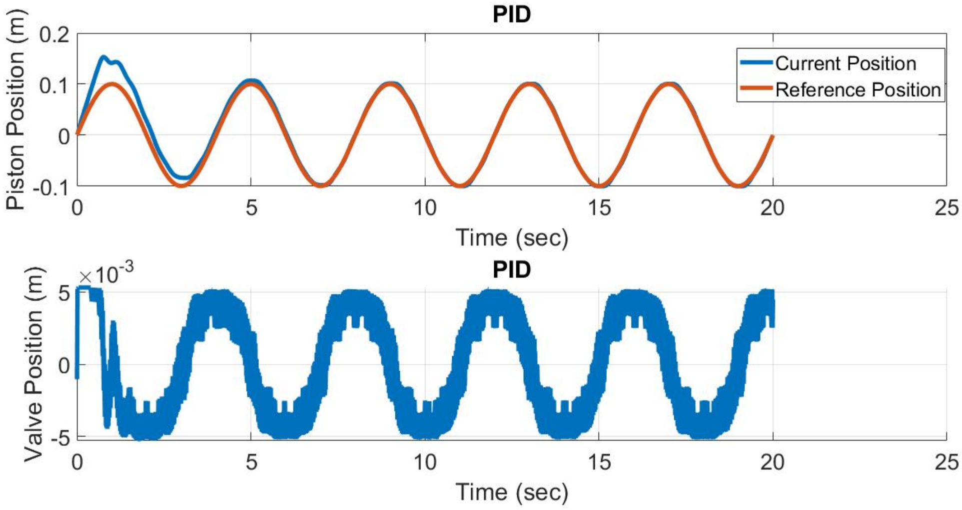

Figure 4.25: Tracking results of two-loop PID controller with pressure feedback, and its corresponding valve displacement

observed that the performance of the PID controller improves with an additional feedback of the differential-pressure across the two chambers.

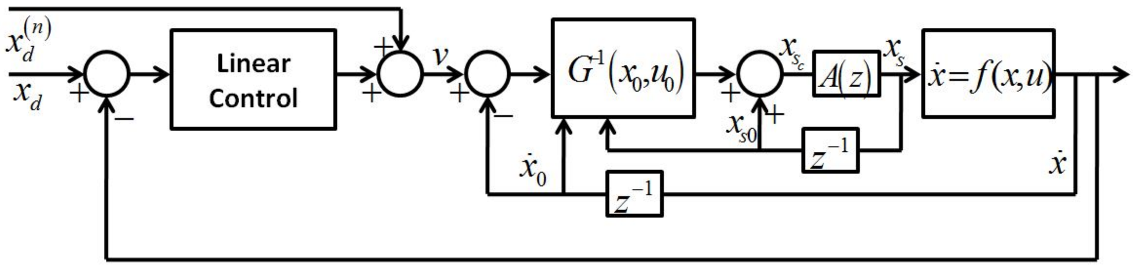

Figure 4.26: INDI controlled system with actuator dynamics

4.4. Pneumatic valve dynamics

The dynamics of a pneumatic valve is represented as follows.

$$c_s \dot{x}_s + k_s x_s = K_f i_c \tag{4.34}$$

In Eq.(4.34), x_s is the valve spool position, c_s is the viscous friction coefficient, k_s is the spool spring constant, K_f is the coil force constant and i_c is the current flowing through the valve solenoid. In Laplace domain, it will be represented as follows.

$$\frac{X_s(s)}{I_c(s)} = \frac{K_f}{c_s s + k_s} \tag{4.35}$$

Eq.(4.35) describes the transfer function with current as the input. However in our final formulations of two-loop controller, current is not considered as the control surface, but rather the valve-spool position. So, the transfer function between the commanded spool position x_{s_c} and the actual spool position x_s can be expressed as follows.

$$\frac{X_s(s)}{X_{s_c}(s)} = \frac{1}{\tau s + 1} \tag{4.36}$$

The equation for the actuator dynamics is similar to a low-pass filter. In Eq.(4.36), τ is the time constant of the valve. Using bilinear transformation, the above equation is converted to discrete Z domain, given by Eq.(4.37) The block diagram of this INDI controlled system is given in Fig.4.26.

$$\frac{X_s(z)}{X_{s_c}(z)} = A(z) = \frac{T(z+1)}{z(2\tau + T) + (T - 2\tau)} \tag{4.37}$$

Next a different control surface is considered, which is the orifice opening of the pneumatic valve. Figs.4.27

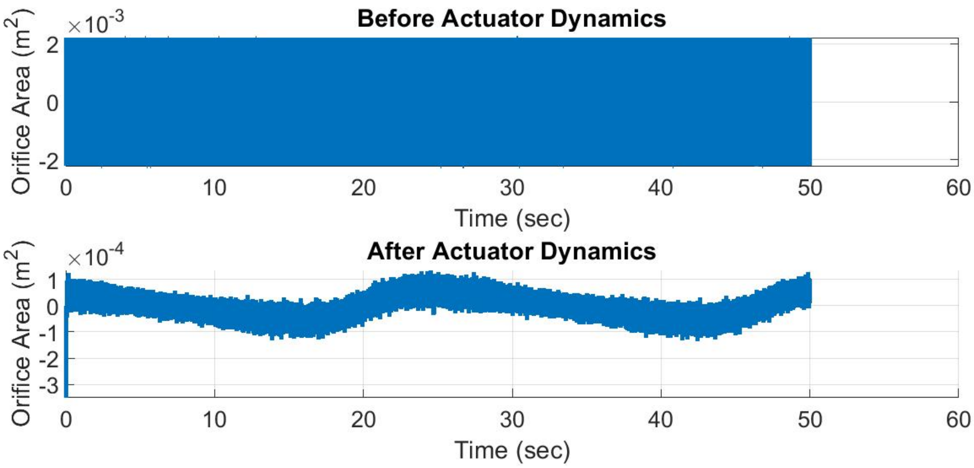

Figure 4.27: INDI controlled system with actuator dynamics (high-bandwidth)

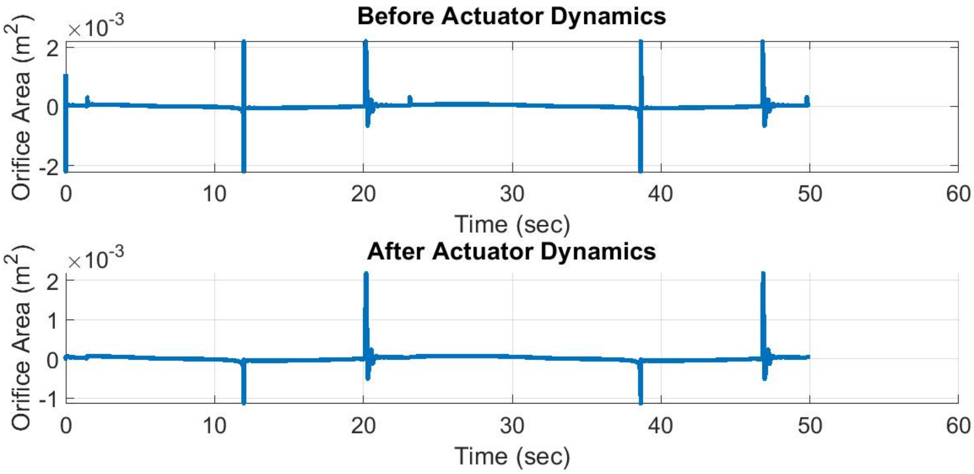

Figure 4.28: INDI controlled system with actuator dynamics (low-bandwidth)

and 4.28 show the orifice opening before and after the filter, which are denoted by A_{v_c} and A_v respectively. The transfer function is similar to Eq.(4.37), as summarized below.

$$\frac{A_v(z)}{A_{v_c}(z)} = \frac{T(z+1)}{z(2\tau + T) + (T - 2\tau)} \tag{4.38}$$

In Fig.4.27, it is observed that the control command directly issued by the controller is oscillatory. These noisy signal is then filtered by the actuator dynamics, due to which high-frequency oscillations reduce. The actuator constant is taken as 10 ms, after analyzing a number of industrially available pneumatic valves. The high-frequency noise in the control command can be completely eliminated by tuning the controller coefficients, as can be seen from Fig.4.28.

4.5. Pseudo-control hedging (PCH)

One of the major reasons for the degradation of INDI performance in pneumatic systems is the actuator saturation. The performance of INDI for tracking a sine wave decreases as we increase the frequency of the reference signal, due to actuator saturation. It can be handled by use of PCH [78], which reduces the reference command to a value, that is achievable by the actuator. The actuator in this specific research proposal refers to a pneumatic valve. In order to implement PCH, the command hedge in the previous instant is calculated as follows.

$$\nu_h = G(u_c - u) \tag{4.39}$$

In the above equation, G is the control effectiveness and $u_c - u$ is the excess control effort, which could not be met by the saturated actuator. For an unsaturated controller, the control hedge is zero. Next, the new reference command for the differential pressure is calculated as follows.

$$PL_{d_{rm}} = \frac{1}{s}(\nu_{rm} - \nu_h) \tag{4.40}$$

In Eq.(4.40), the reference command is found by the integral of the excess command hedge. However in some literature [16], a proportional relation is also used, as given below.

$$PL_{d_{rm}} = \frac{1}{n}(\nu_{rm} - \nu_h) \tag{4.41}$$

In Eq. 4.41, n is a constant and ν_{rm} is obtained from a first-order reference model as follows.

$$\nu_{rm} = K_{rm}\left(PL_{d_c} - PL_{d_{rm}}\right) \tag{4.42}$$

PL_{d_c} is the actual commanded differential pressure, which is obtained from NDI. υ_{rm} can also be used as additional feed-forward term for the linear control law, but however it is not used in our formulations. It has been found in our analysis that the actuator saturation decreases, as we kept increasing the constant K_{rm}. There is also a maximum limit on this proportionality constant K_{rm}, beyond which the valve saturation actually starts increasing.

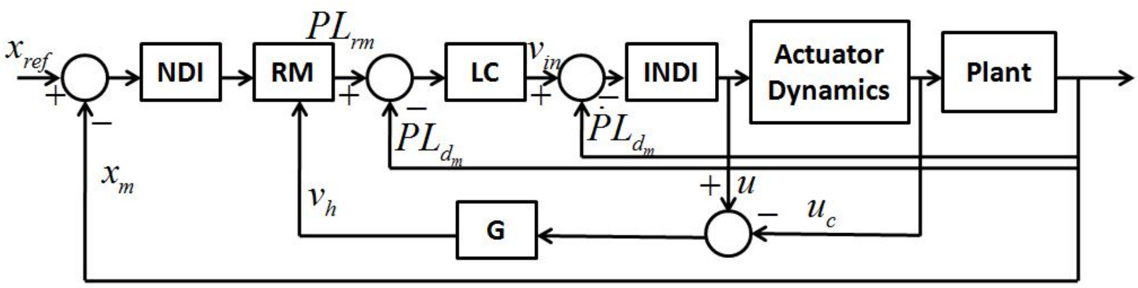

Figure 4.29: Schematic diagram of two-loop controller along with PCH

The concept of PCH is successfully tested on a pneumatic cylinder (Figs.4.30 and 4.31), but however our final simulation results will try to avoid this concept. This is because PCH does not allow the actuator to reach its maximum potential and thus it reduces the maximum tracking speed achievable, by the actuator.

4.6. Open-loop Analysis

Open-loop analysis is very crucial for analysing a given system-dynamics. It gives a better understanding about the working of the system. The dynamic formulation for the plant can also verified by an open-loop analysis, as will be described in this section. Open-loop analysis can also be sometimes used to debug certain issues in the controller output. In this report, it is first described how the given pneumatic system reacts

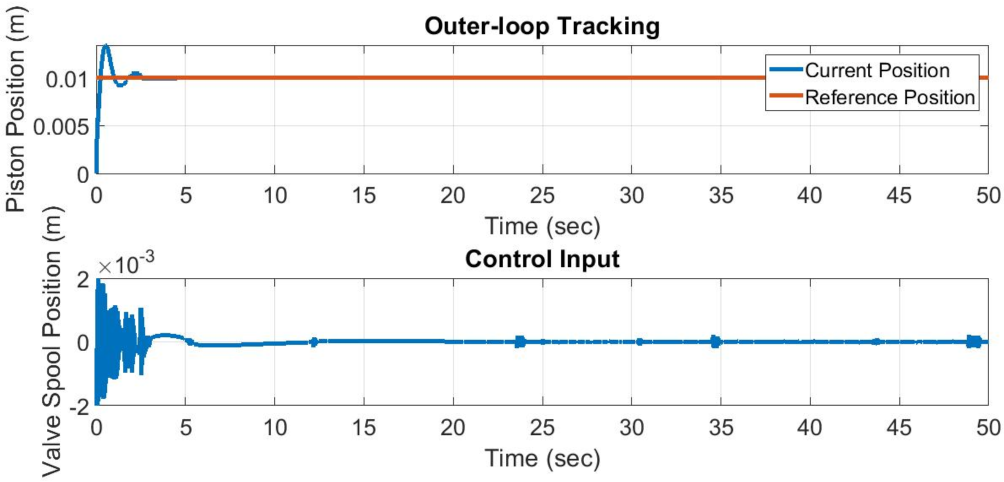

Figure 4.30: Tracking results for small cylinder with PCH

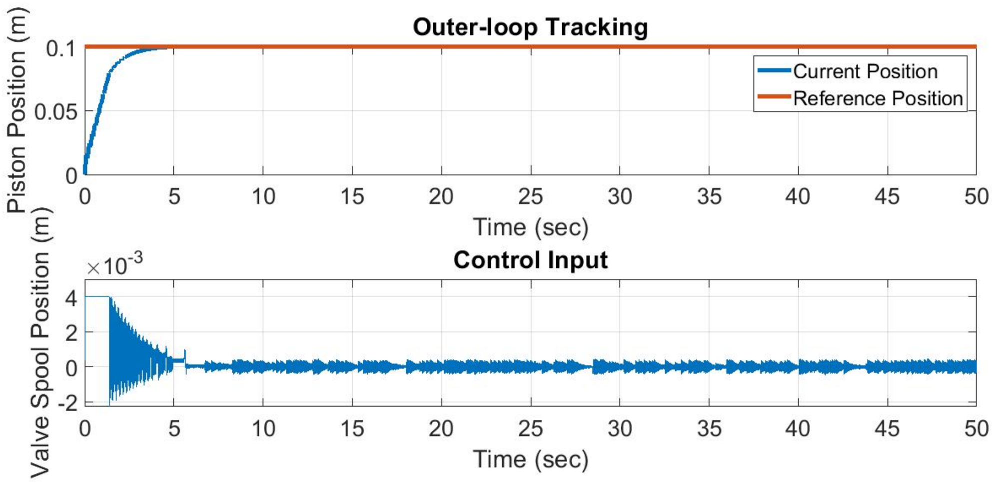

Figure 4.31: Tracking results for big cylinder with PCH

with the valve-orifice being fully closed (Fig.4.32 and 4.33). In Fig.4.32, it is observed that the piston-position initially oscillates, before settling down to 0.008 m. Both the chambers A and B are initially supplied with 5 bar pressure each. The piston is attached on the side containing chamber B and therefore less area is available for generating the force, when compared with the side containing chamber A. Therefore more pressure is required in chamber B than chamber A, in order to balance the external load. From Fig.4.33, it is observed that the pressure in chamber A settles to 4.92 bar, whereas chamber B converges to 5.08 bar.

Next, a orifice opening is issued in the positive direction, such that chamber A is now connected to the supply pressure and chamber B is connected to the exhaust. The air is released from a exhaust directly into the atmosphere. By changing the orifice opening, the amount of pressure in each chamber can be varied and thus the position of piston. Fig.4.34 shows an open-loop response, where the orifice area has a positive opening. For such a configuration of the valve opening, chamber A is connected to supply pressure and chamber B to the atmosphere through the exhaust. As expected, the piston showed positive displacement until 0.6 m, where it reaches the saturation limit. However, we observe in Fig.4.35 that the pressure in chamber B also increases linearly similar to chamber A, due to a compressing effect of the external load. Fig.4.36 then shows an open-loop response with an oscillatory command and it is observed that the piston-position corresponds with the control command. However, there is a phase-lag between the two signals because the pneumatic cylinder is not able to track such a high-frequency command. This phase-lag can be reduced by decreasing the frequency of the reference command.

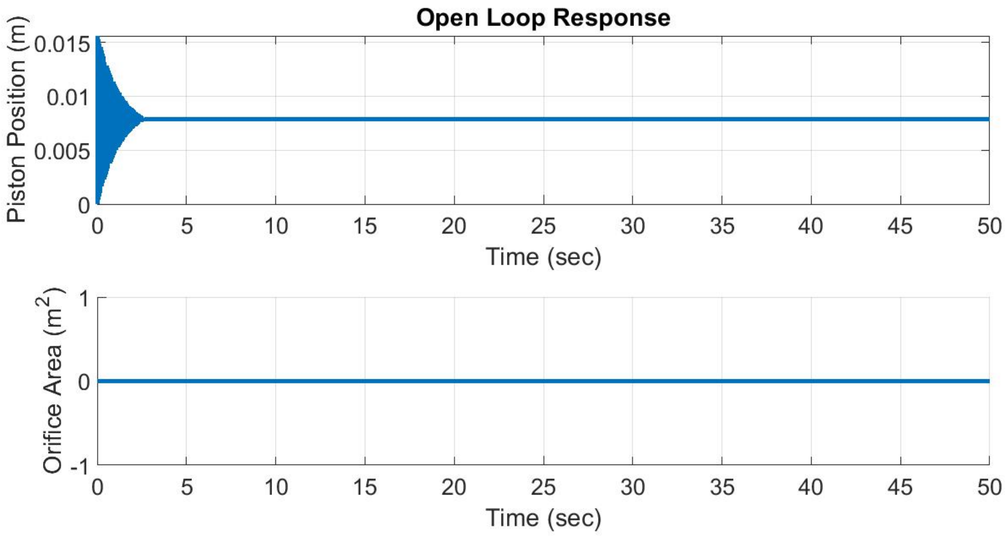

Figure 4.32: Open-loop Response for zero orifice opening

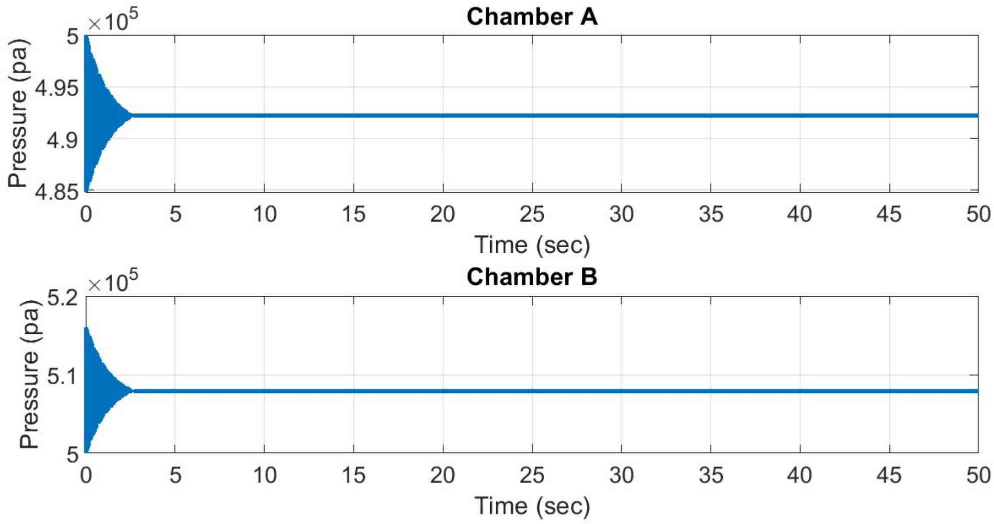

Figure 4.33: Chamber Pressure for the linear open-loop response in Fig.4.32

4.7. Modified NDI and INDI Loop

As discussed previously in Eqs.(4.25) and (4.26), the linear control law in the NDI formulation consists of a friction component. The friction force is simulated using LuGre model ([54]) and it involves the signum function of the piston-velocity, which is a major cause of discontinuity. The signum function starts switching when the piston-velocity is near zero, and this switching causes high-frequency components to be present in friction force. These high-frequency components can also be reflected in other state variables, such as the pressure derivative and piston velocity. Fig.4.38 shows the friction force and the pressure derivatives, while tracking a sinusoidal reference signal.

In order to mitigate this issue, the friction term from the outer-loop NDI law is dropped, as summarized is Eq. (4.43).

$$P_{L_d} = \frac{\left(M_p + M_L\right) v_1 + P_a A_p - A_p P_B + F_l}{A_a} \tag{4.43}$$

The pressure-derivative term of the INDI linear law in Eq.(4.28) is then dropped, as summarized below in Eq.(4.44)

$$v_2 = K_{p_2}\left(P_{L_d} - P_L\right) + K_{i_2} \sum \left(P_{L_d} - P_L\right) \tag{4.44}$$

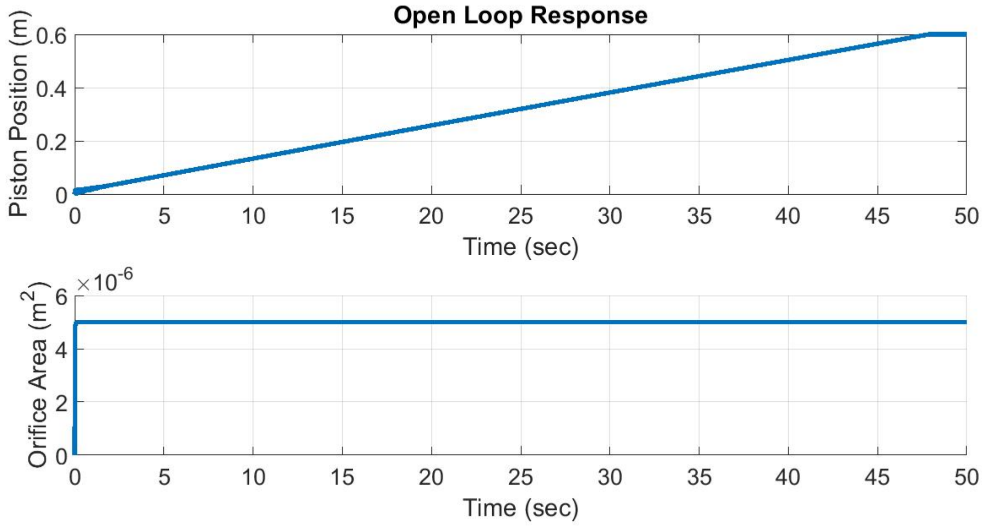

Figure 4.34: Open-loop Response for a linear command

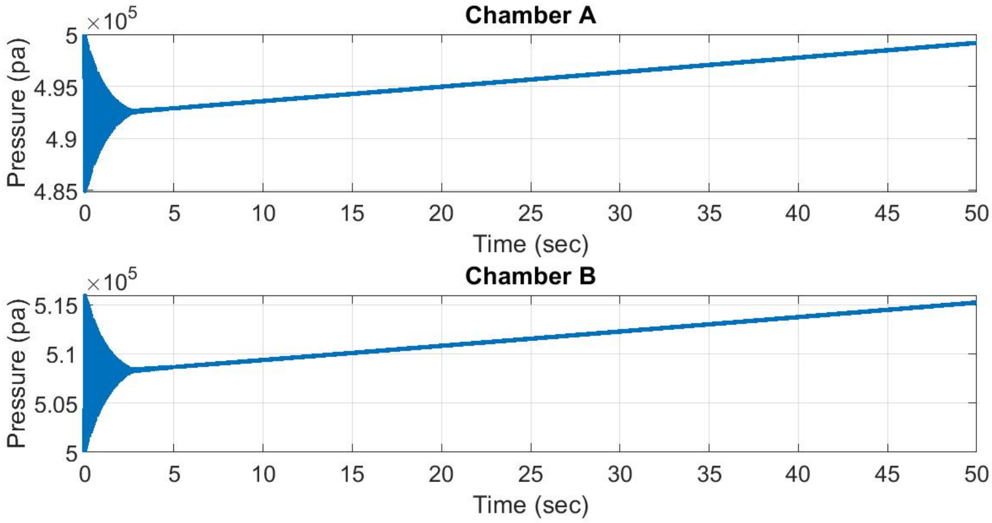

Figure 4.35: Chamber Pressure for the linear open-loop response in Fig.4.34

Fig.4.39 shows the tracking results, where high frequency control components can be clearly observed. The tracking results using the modified NDI and INDI loop are plotted in Fig.4.40. The high-frequency oscillation components have disappeared from the control command. But a few low-frequency oscillation component near the zero crossing of the orifice area are still visible, which can be reduced by further tuning the outer-loop controller coefficients.

4.8. Filter Dynamics

An INDI control law requires the feedback of state-derivatives, as discussed previously. For instance in Eq.(4.27), $\dot{P}_{L0}$ is the differential pressure-derivative at the previous instant. Obtaining this state-derivative directly is difficult due to the limitation of the available sensors. Therefore, in reality it is possible to measure only the differential pressure P_L directly, by the use of sensors. Following this, P_L is then numerically differentiated to obtain $\dot{P}_L$. Numerical differentiation is not preferred, as the sensor signals are prone to a lot of noise. This is usually the case with most physical systems, as they are corrupted with noise and disturbances from the environment. This will be directly discerned by the sensors, and further performing numerical differentiation on them can cause the INDI control inputs to have high-frequency oscillations, which can lead the controlled

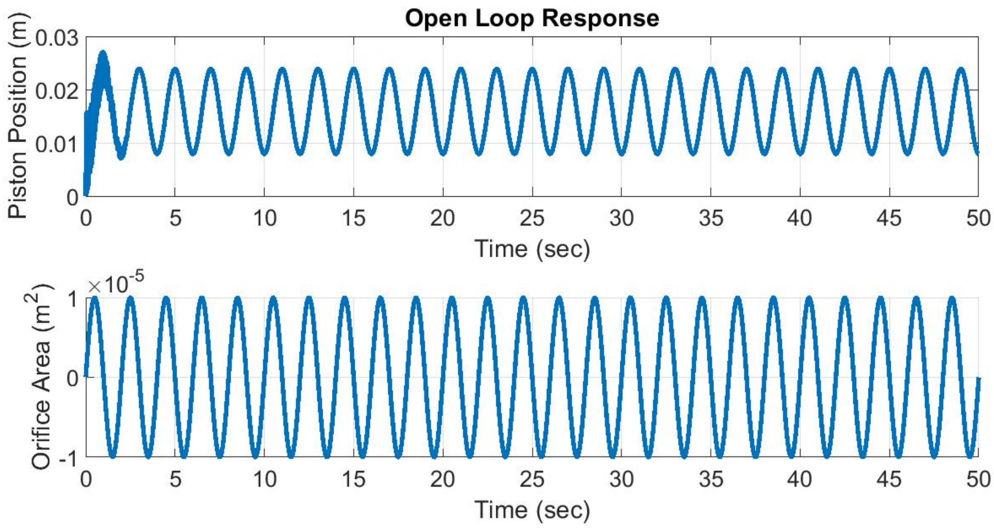

Figure 4.36: Open-loop Response for a oscillatory command

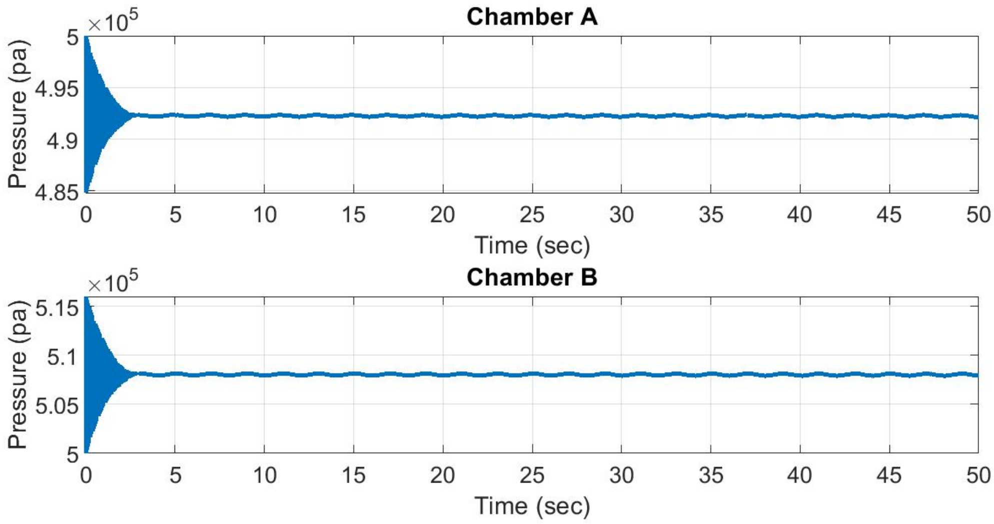

Figure 4.37: Chamber Pressure for the oscillatory open-loop response in Eq. 4.36

system to be on the verge of instability. Therefore in order to tackle this issue, Huang et.al [40] implemented a second-order low-pass filter $H(s)$, as summarized in the Eq. 4.45.

$$H(s) = \frac{\omega_n^2}{s^2 + 2\zeta\omega_n s + \omega_n^2} \tag{4.45}$$

Introducing a filter will cancel-out any high-frequency noise from the feedback signals. However, the filter also introduces some phase-loss, as it is a second-order lag. In order to handle this issue, a second filter of the same dynamics was introduced in the feedback signal of the control input ([81],[40],[40]). Thus on introducing this filter dynamics, a mutual cancellation happens and thus the phase-lag due to the filters no longer exist. The closed-loop transfer function from the linear control law (V) to the state-derivative ($\dot{x}$) now becomes just the actuator dynamics $A(z)$, i.e. $\dot{x}/v = A(z)$. If both the filter dynamics are not same, then an exact cancellation will not happen and the performances of controller starts degrading. It also needs to be ensured this transfer function is stable, by checking its pole location. For our simulations, these poles which also corresponds to the actuator time-constant, are chosen by analyzing a number of commercially available pneumatic valves.

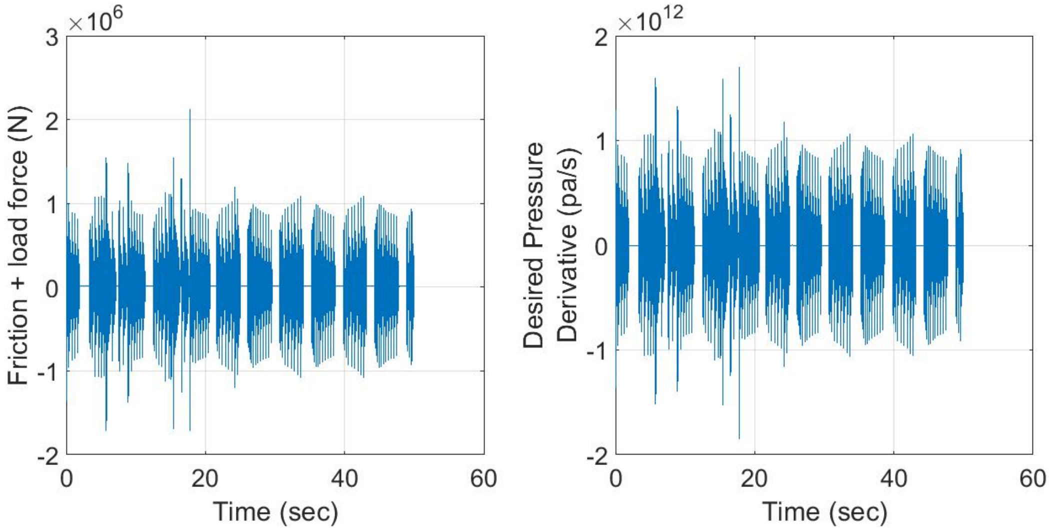

Figure 4.38: High-frequency components in the friction force and the pressure derivatives)

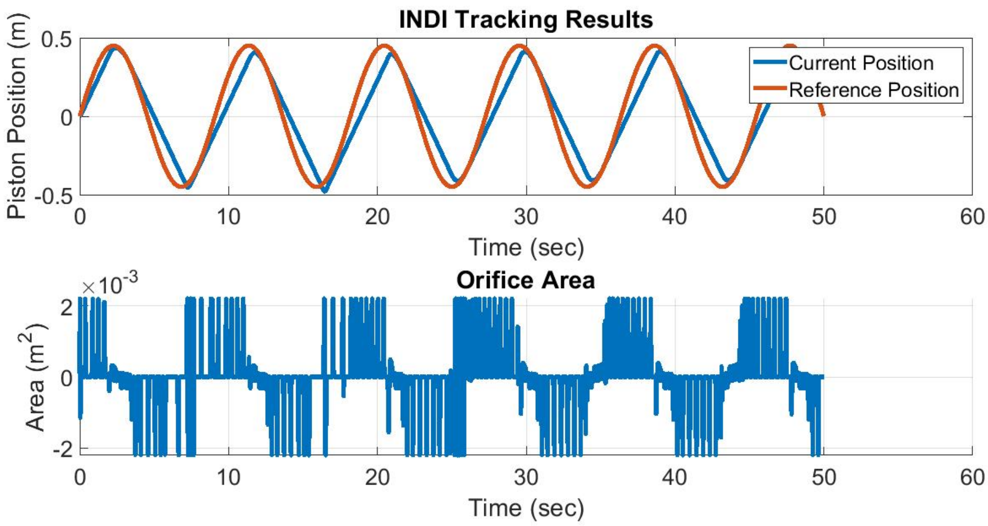

Figure 4.39: Tracking Results and Orifice opening for a higher load of 10000 N

As mentioned previously in section 3.3.3, the time-delays of the two feedback signals should also be the same, in order for the INDI control law to give maximum efficiency. For our simulations, a unit-delay is used in the feedback of the pressure-derivative and the control input. It can be analytically shown that any positive time-delays in either of the feedback loops can induce a right-hand pole in the closed-loop transfer function. This will lead the controlled system to be on the verge of instability. For practical systems, it might be difficult to obtain the actual time-delays accurately. In such cases, one of the time-delays is kept unchanged, and the other time-delay is varied externally until the INDI controller starts giving good performance. For the current simulation framework, all the time-delays were synced and it did not create any issue. A low-pass filter will be implemented and analyzed if needed, after the introduction of sensor noises and external disturbances in the later stages of this research project.

4.9. Trim Conditions

The valve spool position needs to be trimmed with proper initial conditions, depending on the applied external load. The dynamics of the piston and load as discusses before, is summarized again in Eq.(4.46).

$$\left(M_L + M_p\right)\ddot{x} + \beta\dot{x} + F_f + F_L = P_1 A_1 - P_2 A_2 - P_a A_r \tag{4.46}$$

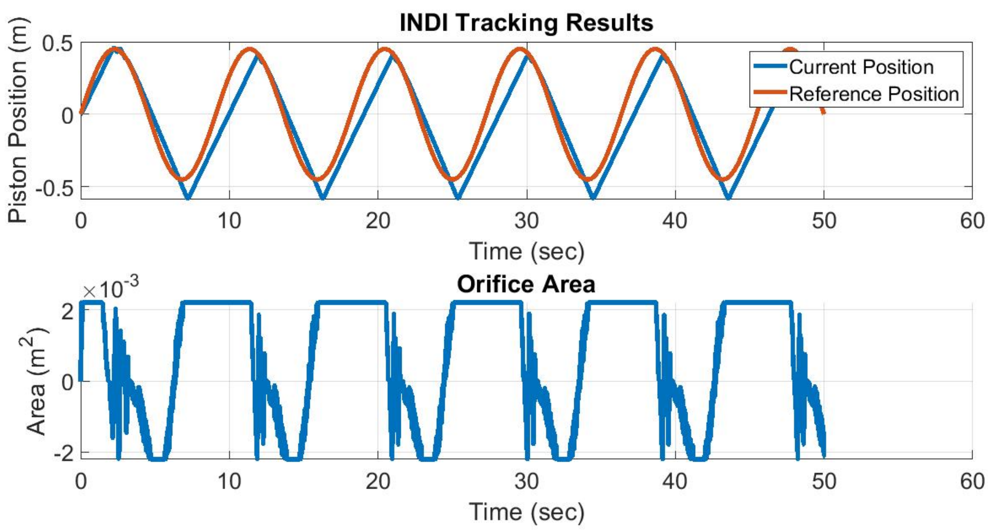

Figure 4.40: Tracking Results and Orifice opening for a higher load of 10000 N, with modified NDI and INDI loop

By equating the acceleration to zero, the expression of the pressure in chamber A can be expressed as Eq.(4.47). The initial sum of pressure, across the two chamber should be equal to the supply pressure (Eq.(4.48)).

$$P_A = \frac{F_f + F_L + P_B A_B + P_a A_r}{A_A} \tag{4.47}$$

$$P_A + P_B = P_s \tag{4.48}$$

Therefore, by solving Eqs.(4.47) and (4.48) the pressures in chamber A and B can be calculated. The obtained pressure will depend on parameters like P_a, F_L and A_r. The friction force F_f is taken to be zero at the start of simulation, when the piston has not moved yet. Fig.4.41 shows the tracking response for a cylinder, both with trimming and without trimming the pneumatic valve.

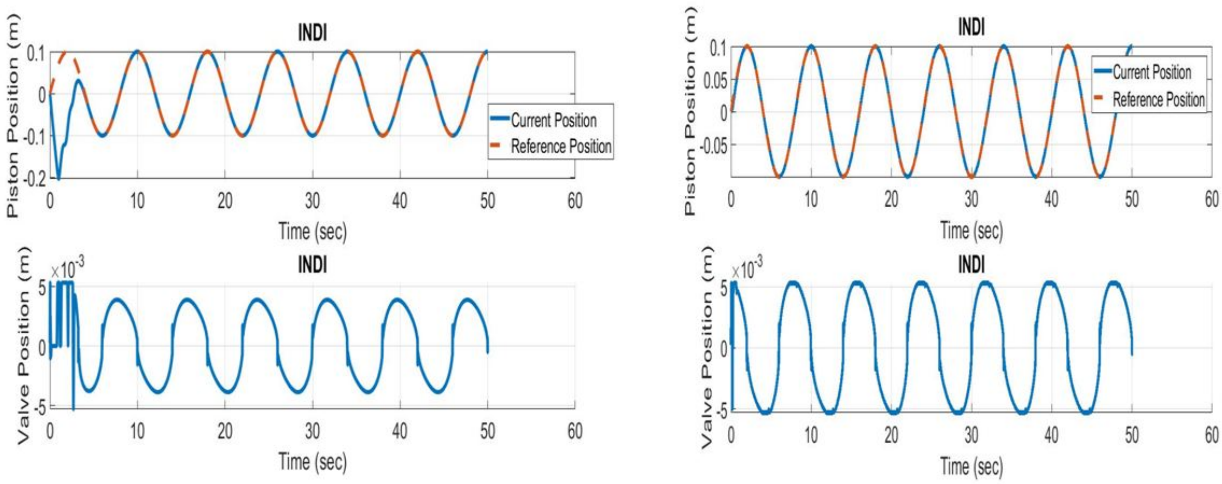

Figure 4.41: Tracking Results for External load of 500 kg (5000 N) and reference sine of amplitude 0.1 m and frequency 0.125 Hz (Left Figure: Without trim , Right Figure: With trim)

III

Wrap-up

5

Conclusion and Recommendations

The simulation study documented in this report demonstrates that INDI controller have the capability to successfully harness the potential of pneumatic actuators, whereas the literature study presented in this report explains the various components and capabilities of a pneumatic system. A number of contributing factors make it advantageous over other conventional actuation such as electric and hydraulic. Some of these advantages are increased force-to-weight ratio, minimal harmful leakage into the environment, less friction and increased durability. These advantages substantiate the use of pneumatic technology for flight simulators. The research objective of this project is to increase the position-tracking accuracy of a pneumatic actuator with respect to a baseline PID controller, by designing a nonlinear controller which relies less on the system dynamics, and is also simple to implement. The system analyzed in this report is a single pneumatic actuator, which will be utilized in the later stages of this research project to construct a fully functional parallel-robot, capable of performing flight simulations. Pneumatic actuators are highly nonlinear in behaviour and is thus difficult to be controlled with precision. The presence of external disturbances, sensor noises and a low critical-frequency of pneumatic actuators makes it even more challenging. This report investigates some of these mentioned issues to improve pneumatic actuator technology for commercial applications.

The controller chosen for this research project is INDI and its primary reason is that INDI relies less on the system dynamics. This makes it robust to both external disturbances and parameter variations in the system. The concept of incremental form and NDI controller amalgamated to generate the approach of INDI control command. It requires time-synchronisation of various sensor feedback, as INDI calculates only the required incremental control which is then added to the previous control command to generate a final control. INDI is a very popular choice of control technique for aircraft applications [34], and it mostly involves multi-loop control design. The outer-loop tends to be slow and the inner-loop controller usually have a higher bandwidth. In this report, different controllers are designed for a single pneumatic actuator, with different conditions on the external load and added sensor noise. Finally, the comparison of the incremental control approach is done with that of a PID controller in the presence of above-mentioned realistic scenarios.

The performed literature survey and simulation study on pneumatic systems is then used to generically answer some of the research sub-questions raised in Section 1.4.2 of this report, as follows:

1. *How to describe the dynamics of a pneumatic system ?*

    (a) *What are the various components of a pneumatic system and what are its working principle ?* A pneumatic system consists of a number of different components, some of which are pneumatic cylinder, valve, connecting-tubes, compressed air supply, transducers for sensing force, pressure and position. The basic principle of operation is that the spool displacement of valve will change the pressure-difference across the two cylinder chambers, which will then generate a force to move the piston in either of the two directions, depending on the spool displacement.

    (b) *How can the dynamics of each of these components be described using mathematical models?* The dynamics of the piston-load combination and the valve are both derived using Newton's second law. The relation between the mass flow-rate and the rate of change of pressure in the cylinder chamber has been derived using ideal gas law, energy equation and the continuity equation. The mass flow-rate equation through the connecting tubes is generated using one-dimensional wave equation. Furthermore, friction forces across the cylinder chambers have been modelled using LuGre friction model.

(c) *How to choose the various parameters in these sets of equations, such that it replicates the actual hardware and also suits our application?* The dimensions of various components such as cylinder diameter, piston mass, etc. are first calculated by considering the total mass of the flight simulator and the required stroke-speed. Following this, data-sheets of different manufacturers are explored to find the most feasible dimension of hardware, that is currently available in the market.

2. How to implement incremental control for a pneumatic system ?

   (a) *What measures are needed in order to implement INDI controller on a long-stroke pneumatic cylinder ?* Framing INDI control law for a pneumatic system involves calculating a linear control law, which depends on the error in the pressure difference across the chambers. The INDI controller also involves the time-derivative of the chamber pressure-difference, measured in the previous time-instant. The control effectiveness of INDI which depends on the ratio of upstream to the downstream pressure in chamber is rather kept fixed in this report, in order to exploit the robustness property of INDI.

   (b) *How does the designed controller take into account the various physical phenomenons associated with an actual hardware ?* Some of the actual phenomenon taken into account while designing INDI controller are the trim condition for valve, time-constant of valve, efficiency of pneumatic cylinder and type of air-flow which can be either choked or unchoked. It has been found in this research that the orifice area of the valve needs to be initialized with a proper condition for every external-load. This will ensure that there is no initial-displacement of the piston due to the force of the external load. The effect of connecting-tube dynamics on the controlled system is also studied, and it has been observed that the performance of INDI gets affected after its introduction.

   (c) *How can a conventional INDI controller be augmented for improving the tracking performance of a pneumatic system ?* The designed two-loop incremental control approach shows satisfactory tracking performance for pneumatic cylinders of large dimensions. The performance starts degrading when the external load is increased so much that the chamber pressure saturates. Perhaps implementing pseudo control hedging can aid this, as discussed in the preliminary report. It has also been found that introducing connecting-tube dynamics in the system can result in oscillations of control command. This can later be tackled by the use of appropriate filters. Besides this, low-pass filters are introduced in the robust-case scenario for filtering the sensor noises, which improved the performance of the designed incremental controller.

3. How the check the robustness and any limitations of the designed controller?

   (a) *How to introduce uncertainty and noise in the system dynamics, while performing the simulations ?* For the current simulation framework, sensor noise are added in the feedback of both position and chamber pressure, by utilizing realistic zero-mean Gaussian noise. Moreover, the external load connected to the system is made variable, besides increasing it by five times from the nominal case.

   (b) *When does the controlled system becomes unstable and starts to degrade its performance ? Can the stability of this controlled system be proved ?* After adding realistic sensor noise in the system, the performance of the controlled system starts degrading, with tracking errors rising by over 99 % higher than the nominal case. Moreover, the pressure in the cylinder chambers start saturating, once the external load is increased by five times. Besides this, the effect of sudden jumps in the pressure-derivatives of the chamber are reflected in the position-tracking, which occurs when the cylinder comes out of saturation. The stability of the designed controlled system has not been analyzed in this report.

   (c) *What are its limitations, in terms of the fidelity of a flight simulator ?* The limitations of the designed controlled system in terms of fidelity of a flight simulator is not analyzed in this report.

4. What measures are needed for comparing the performance of INDI with a baseline PID controller ?

   (a) *How to implement PID controller for a long-stroke pneumatic cylinder ?* A cascaded control approach is designed in this report using PID. The outer-loop tracks the desired position and the inner-loop tracks the desired differential-pressure. Besides this, the derivative components of the inner-loop PID is considered as zero, in order to minimize any high-frequency oscillations due to it.

(b) *Which tasks should the controlled system perform, such that it gives a fair comparison of both the controllers ?* The time-responses of the two controllers are compared by tracking a sinusoidal reference signal of 0.5 m amplitude and a frequency of 0.0375 Hz.

(c) *What metrics are needed for comparing the tracking results of the two controllers ?* The performance of PID is compared with INDI using maximum absolute error, mean absolute error and root mean square error.

Ultimately, the main research question is addressed as follows:

Research Question : *How can an incremental control law (INDI) be designed for controlling a pneumatic actuator with highly nonlinear and uncertain dynamics, such that the position tracking accuracy of such a system increases with respect to a conventional linear controller ?* In this report, an incremental control is successfully designed for the position-tracking tasks of a long-stroke pneumatic cylinder, by utilizing a cascaded control structure where the inner-loop controls the force generated by the system, whereas the outer-loop controls the position of cylinder-piston. The dynamics of the pneumatic system is found to be highly nonlinear due to a number of contributing factors such as the switching law of air-flow through the pneumatic valve, compressibility of air and the Coulomb friction forces. Moreover, sensor noises are introduced in the feedback of both position and pressure sensor in order to create a realistic simulation scenario. The comparative study with a cascaded PID controller is then done using RMSE and absolute error, and it has been found that for a nominal case with a low external load and no added sensor noise, the performance of both the control approaches are similar and satisfactory, with both their maximum absolute tracking errors being less than 5 mm. Both the control approaches are tuned based on some time-domain specifications, prior to controller testing, in order to ensure a "fair" comparison of both the control approaches. For the nominal case, a high initial transient is also observed in the inner-loop tracking response of both control approaches but it did not affect the tracking performance of the rest of the trajectory, as the transient vanishes in a very minimal time of around 10 ms.

Following the nominal case, the performance of both the controllers deteriorated after addition of sensor noise, with errors of both the controllers rising by over 99 % as compared to their nominal case. This observation highlighted one of the downfalls of incremental approach in the presence of unfiltered high-frequency sensor noise, which are then attenuated using two different filtering schemes. The tracking accuracy of both the control approaches improved after the introduction of moderate filtering scheme, with the outer-loop tracking errors reducing by 10 times as compared to the robust case without any added filter, for the incremental control approach. Following it, the introduction of high-filtering scheme reduced the inner-loop tracking errors in incremental approach by around 5 times as compared to their nominal case, whereas the inner-loop tracking errors of PID increased by around 3 times as compared to its moderate-filtering case. Similarly, the position tracking accuracy for the case of both heavy external load and varying load is higher for incremental controller, when compared with PID because the former considers the external load in its controller formulation, which is not the case with PID. It is also to be noted that a fixed-control effectiveness is used throughout our simulations for generating the final control command of the incremental approach, which glorifies its robustness property to both initial transients and uncertainties in the system dynamics. Besides this, the effects of both the chamber pressure saturation and discontinuities in the derivative of chamber pressure-difference are visible in the tracking results of incremental control, both for the case of heavy external load and varying external load, which necessitates further investigation into it. Furthermore, the RMSE of outer-loop tracking using PID is found to be 98.4 % higher than the corresponding error of the incremental control, for the case of varying external load.

This masters thesis emphasizes the fact that INDI control is feasible for highly nonlinear systems like a pneumatic cylinder where it gives better performance when compared to a baseline PID controller, for a few realistic case scenarios. The designed control system in this research project specifically focuses on a long-stroke pneumatic cylinder, which can be combined with a general position controller for a Stewart platform. The preliminary literature review, along with the developed research framework serves as a strong foundation for the next phase of this research project. In particular, the connecting-tube dynamics will be included in the controller design, following which six of these actuators will be used for controlling an actual flight simulator. The successful completion of the next stages of this research project will stress the importance of pneumatic actuation in the commercial flight-simulation industry, which will result in a significant decrease in environmental leakage as well as the maintenance required for a flight simulator, thus reducing its operating costs. Moreover, an incremental law will ensure that the controlled flight simulator will be robust to both a variety of operating conditions and external disturbances.

Bibliography

[1] Paul Acquatella, Wouter Falkena, Erik-Jan van Kampen, and Q Ping Chu. Robust nonlinear spacecraft attitude control using incremental nonlinear dynamic inversion. In *AIAA Guidance, Navigation, and Control Conference*, page 4623, 2012.

[2] Paul Acquatella, Wim van Ekeren, and Qi Ping Chu. Pi (d) tuning for flight control systems via incremental nonlinear dynamic inversion. *IFAC-PapersOnLine*, 50(1):8175–8180, 2017.

[3] Kyoung Kwan Ahn and Huynh Thai Chau Nguyen. Intelligent switching control of a pneumatic muscle robot arm using learning vector quantization neural network. *Mechatronics*, 17(4-5):255–262, 2007.

[4] Abdulrahman Mohammed Al-Ibrahim. *Transient air temperature and pressure measurements during the charging and discharging processes of an actuating pneumatic cylinder*. University of Wisconsin–Madison, 1991.

[5] Pedro Albertos, Alicia Esparza, and Antonio Sala. Iterative identification and control design: Methodology and applications. In *Identification and Control*, pages 247–276. Springer, 2007.

[6] Hazem I Ali, SBBM Noor, SM Bashi, and MH Marhaban. A review of pneumatic actuators (modeling and control). *Australian Journal of Basic and Applied Sciences*, 3(2):440–454, 2009.

[7] Sahar Alinia, Masoud Hemmatian, Wen Fang Xie, and Rui Zeng. Posture control of 3-dof parallel manipulator using feedback linearization and model reference adaptive control. In *2015 IEEE 28th Canadian Conference on Electrical and Computer Engineering (CCECE)*, pages 1145–1150. IEEE, 2015.

[8] Boris Andrievsky, Dmitry V Kazunin, Daria M Kostygova, Nikolay V Kuznetsov, Gennady A Leonov, Pavel Lobanov, and Andrey A Volkov. Control of pneumatically actuated 6-dof stewart platform for driving simulator. In *2014 19th International Conference on Methods and Models in Automation and Robotics (MMAR)*, pages 663–668. IEEE, 2014.

[9] Harald Aschemann, Robert Prabel, and Dominik Schindele. Observer-based backstepping control of an electro-pneumatic clutch. In *2012 American Control Conference (ACC)*, pages 509–514. IEEE, 2012.

[10] Barton J Bacon, Aaron J Ostroff, and Suresh M Joshi. Nonlinear dynamic inversion reconfigurable controller utilizing a fault tolerant accelerometer. In *19th DASC. 19th Digital Avionics Systems Conference. Proceedings (Cat. No. 00CH37126)*, volume 2, pages 6F5–1. IEEE, 2000.

[11] Da Ben-Dov and Septimiu E Salcudean. A force-controlled pneumatic actuator. *IEEE Transactions on Robotics and Automation*, 11(6):906–911, 1995.

[12] James E Bobrow and Faryar Jabbari. Adaptive pneumatic force actuation and position control. In *1989 American Control Conference*, pages 1508–1513. IEEE, 1989.

[13] RF Boian, M Bouzit, GC Burdea, J Lewis, and JE Deutsch. Dual stewart platform mobility simulator. In *9th International Conference on Rehabilitation Robotics, 2005. ICORR 2005.*, pages 550–555. IEEE, 2005.

[14] Ion Boldea and Syed A Nasar. Linear electric actuators and generators. *IEEE Transactions on Energy Conversion*, 14(3):712–717, 1999.

[15] CR Burrows. Use of the root loci in design of pneumatic servomotors. *Control*, 1966.

[16] Can Cakiroglu, Erik-Jan Van Kampen, and Q Ping Chu. Robust incremental nonlinear dynamic inversion control using angular accelerometer feedback. In *2018 AIAA Guidance, Navigation, and Control Conference*, page 1128, 2018.

[17] Ming-Kun Chang. An adaptive self-organizing fuzzy sliding mode controller for a 2-dof rehabilitation robot actuated by pneumatic muscle actuators. *Control Engineering Practice*, 18(1):13–22, 2010.

[18] Cheng Chen, Jian Huang, Dongrui Wu, and Zhikang Song. Ts fuzzy logic control with genetic algorithm optimization for pneumatic muscle actuator. In *2018 10th International Conference on Modelling, Identification and Control (ICMIC)*, pages 1–6. IEEE, 2018.

[19] Syuan-Yi Chen and Sheng-Sian Gong. Speed tracking control of pneumatic motor servo systems using observation-based adaptive dynamic sliding-mode control. *Mechanical Systems and Signal Processing*, 94:111–128, 2017.

[20] Ye Chen, Guoliang Tao, and Fangan Meng. An intelligent adaptive robust controller based on neural network for a pneumatic system. In *IOP Conference Series: Materials Science and Engineering*, volume 575, page 012016. IOP Publishing, 2019.

[21] Yuan-Ming Cheng and Yu-Song Chen. An angle trajectory tracking for a 3-dof pneumatic motion platform by the ni compact rio embedded system. *Journal of Mechanics Engineering and Automation*, 3: 14–21, 2013.

[22] Chia-Jui Chiang and Ying-Chen Chen. Incremental fuzzy sliding mode control of pneumatic muscle actuators. *International Journal of Innovative Computing, Information and Control*, 14(5), 2018.

[23] FESTO Cylinders. Online website for bigger cylinders. https://shop.eriks.nl/nl/pneumatische-componenten-cilinders-zuigerstang-cilinders-standaard-cilinders/normcilinder-dsbg-pr455266037361155/, .

[24] SMC Cylinders. Online website for bigger cylinders. https://www.pneumatiek.nl/pneumatiek/smc-pneumatics/cilinders/cp96-iso-32-t-m-100/cp96-c-iso15552/, .

[25] Hemjyoti Das. Dynamic inversion control of quadrotor with a suspended load. *IFAC-PapersOnLine*, 51 (1):172–177, 2018.

[26] Bhaskar Dasgupta and TS Mruthyunjaya. Closed-form dynamic equations of the general stewart platform through the newton–euler approach. *Mechanism and machine theory*, 33(7):993–1012, 1998.

[27] TU Delft. Flight deck · simona. URL http://cs.lr.tudelft.nl/simona/facility/flight-deck/.

[28] Wouter Falkena, Clark Borst, QP Chu, and JA Mulder. Investigation of practical flight envelope protection systems for small aircraft. *Journal of Guidance, Control, and Dynamics*, 34(4):976–988, 2011.

[29] Hubert Gattringer, Ronald Naderer, and Hartmut Bremer. Modeling and control of a pneumatically driven stewart platform. In *Motion and Vibration Control*, pages 93–102. Springer, 2009.

[30] Zheng Geng and Leonard S Haynes. Six-degree-of-freedom active vibration isolation using a stewart platform mechanism. *Journal of Robotic Systems*, 10(5):725–744, 1993.

[31] Alexis Girin, Franck Plestan, Xavier Brun, and Alain Glumineau. High-order sliding-mode controllers of an electropneumatic actuator: Application to an aeronautic benchmark. *IEEE transactions on control systems technology*, 17(3):633–645, 2009.

[32] M Girone, Grigore Burdea, Mourad Bouzit, V Popescu, and Judith E Deutsch. A stewart platform-based system for ankle telerehabilitation. *Autonomous robots*, 10(2):203–212, 2001.

[33] Karmjit Singh Grewal, Roger Dixon, and John Pearson. Lqg controller design applied to a pneumatic stewart-gough platform. *International Journal of Automation and Computing*, 9(1):45–53, 2012.

[34] Fabian Grondman, Gertjan Looye, Richard O Kuchar, Q Ping Chu, and Erik-Jan Van Kampen. Design and flight testing of incremental nonlinear dynamic inversion-based control laws for a passenger aircraft. In *2018 AIAA Guidance, Navigation, and Control Conference*, page 0385, 2018.

[35] S Hajji, A Ayadi, M Smaoui, T Maatoug, M Farza, and M M'saad. Position control of pneumatic system using high gain and backstepping controllers. *Journal of Dynamic Systems, Measurement, and Control*, 141(8), 2019.

[36] Ted Hesselroth, Kakali Sarkar, P Patrick Van Der Smagt, and Klaus Schulten. Neural network control of a pneumatic robot arm. *IEEE Transactions on Systems, Man, and Cybernetics*, 24(1):28–38, 1994.

[37] Tianyu Huang, Liang Shan, Jun Li, Zhen Yu, and Chenglin Liu. Closed-loop rbf-pid control method for position and attitude control of stewart platform. In *2019 Chinese Control Conference (CCC)*, pages 3096–3101. IEEE, 2019.

[38] Y Huang. *Incremental nonlinear control of hydraulic parallel robots: An application to the SIMONA research simulator*. PhD thesis, Delft University of Technology, 2019.

[39] Yingzhi Huang, Daan M Pool, Olaf Stroosma, Q Ping Chu, and Max Mulder. Modeling and simulation of hydraulic hexapod flight simulator motion systems. In *AIAA modeling and simulation technologies conference*, page 1437, 2016.

[40] Yingzhi Huang, DM Pool, O Stroosma, and QP Chu. Incremental nonlinear dynamic inversion control for hydraulic hexapod flight simulator motion systems. *IFAC-PapersOnLine*, 50(1):4294–4299, 2017.

[41] Yingzhi Huang, DM Pool, O Stroosma, and Qiping Chu. Robust incremental nonlinear dynamic inversion controller of hexapod flight simulator motion system. In *Advances in Aerospace Guidance, Navigation and Control*, pages 87–99. Springer, 2018.

[42] DA Hullender and RL Woods. Modeling of fluid control components. In *Integral methods in science and engineering*, pages 608–619. Taylor & Francis/Hemisphere, 1986.

[43] Xianzhi Jiang, Zenghuai Wang, Chao Zhang, and Liangliang Yang. Fuzzy neural network control of the rehabilitation robotic arm driven by pneumatic muscles. *Industrial Robot: An International Journal*, 42 (1):36–43, 2015.

[44] Cao Junyi, Cao Binggang, Zhang Xining, and Wen Guangrui. Fractional proportional integral control for pneumatic position servo systems. In *2008 IEEE/ASME International Conference on Mechtronic and Embedded Systems and Applications*, pages 347–352. IEEE, 2008.

[45] Somyot Kaitwanidvilai and Manukid Parnichkun. Genetic-algorithm-based fixed-structure robust h loop-shaping control of a pneumatic servosystem. *Journal of robotics and mechatronics*, 16:362–373, 2004.

[46] Seon M Kim and JS Gibson. Digital adaptive control of robotic manipulators with flexible joints. In *1991 American Control Conference*, pages 944–949. IEEE, 1991.

[47] C Kunt and R Singh. A linear time varying model for on-off valve controlled pneumatic actuators. *Journal of dynamic systems, measurement, and control*, 112(4):740–747, 1990.

[48] Amir Salimi Lafmejani, Mehdi Tale Masouleh, and Ahmad Kalhor. Trajectory tracking control of a pneumatically actuated 6-dof gough–stewart parallel robot using backstepping-sliding mode controller and geometry-based quasi forward kinematic method. *Robotics and Computer-Integrated Manufacturing*, 54:96–114, 2018.

[49] Jiing-Yih Lai, Chia-Hsiang Menq, and Rajendra Singh. Accurate position control of a pneumatic actuator. In *1989 American Control Conference*, pages 1497–1502. IEEE, 1989.

[50] B Li, W Dong, and X Wang. Design and simulation of an active vibration isolator based on pneumatic-electromagnetic hybrid driving. *J. Northwestern Polytechnical University*, 31(6):871–877, 2013.

[51] Yihua Liao. Neural networks in hardware: A survey. *Department of Computer Science, University of California*, 2001.

[52] S Liu and JE Bobrow. An analysis of a pneumatic servo system and its application to a computer-controlled robot. *Journal of dynamic systems, measurement, and control*, 110(3):228–235, 1988.

[53] Peng Lu, Erik-Jan van Kampen, Cornelis de Visser, and Qiping Chu. Aircraft fault-tolerant trajectory control using incremental nonlinear dynamic inversion. *Control Engineering Practice*, 57:126–141, 2016.

[54] Melaka Malaysia. Non-linear modeling and cascade control of an industrial pneumatic actuator system. *Australian Journal of Basic and Applied Sciences*, 5(8):465–477, 2011.

[55] JJ Mannetje. Pneumatic servo design method improves system bandwidth twenty-fold. *Control Eng*, 28(6):79–83, 1981.

[56] Mahmood Mazare, Mostafa Taghizadeh, and Mohammad Ghasem Kazemi. Optimal hybrid scheme of dynamic neural network and pid controller based on harmony search algorithm to control a pwm-driven pneumatic actuator position. *Journal of Vibration and Control*, 24(16):3538–3554, 2018.

[57] Anirban Mazumdar, Jiann-Cherng Su, Steven J Spencer, and Stephen P Buerger. Autonomous control of pneumatically-powered percussive drilling through highly layered formations. In *2019 American Control Conference (ACC)*, pages 5215–5221. IEEE, 2019.

[58] BW McDonell and JE Bobrow. Adaptive tracking control of an air powered robot actuator. *Journal of dynamic systems, measurement, and control*, 115(3):427–433, 1993.

[59] Deyuan Meng, Guoliang Tao, and Xiaocong Zhu. Integrated direct/indirect adaptive robust motion trajectory tracking control of pneumatic cylinders. *International journal of control*, 86(9):1620–1633, 2013.

[60] Kenta Nomura, Teru Yonezawa, Takeki Ogitsu, Hiroshi Mizoguchi, and Hiroshi Takemura. Development of stewart platform type ankle-foot device for trip prevention support. In *2015 37th Annual International Conference of the IEEE Engineering in Medicine and Biology Society (EMBC)*, pages 4808–4811. IEEE, 2015.

[61] Takayuki Onodera, Eiji Suzuki, Ming Ding, Hiroshi Takemura, and Hiroshi Mizoguchi. Force, stiffness and viscous damping control of a stewart-platform-type ankle-foot rehabilitation assist device with pneumatic actuator. *Journal of Robotics and Mechatronics*, 25(6):897–905, 2013.

[62] Shunmugham R Pandian, Yasuhiro Hayakawa, Y Kamoyama, and S Kawamura. Practical design of adaptive model-based sliding mode control of pneumatic actuators. In *Proceedings of IEEE/ASME International Conference on Advanced Intelligent Mechatronics*, page 140. IEEE, 1997.

[63] MG Papoutsidakis, G Chamilothoris, and A Pipe. Auto-selective three term control of position and compliance of a pneumatic actuator. In *Proceedings of World Academy of Science, Engineering and Technology*, volume 20, pages 284–288, 2007.

[64] Arun K Paul, JE Mishra, and MG Radke. Reduced order sliding mode control for pneumatic actuator. *IEEE Transactions on Control Systems Technology*, 2(3):271–276, 1994.

[65] George H Pfreundschuh, Vijay Kumar, and Thomas G Sugar. Design and control of a 3-dof in-parallel actuated manipulator. In *Proceedings. 1991 IEEE International Conference on Robotics and Automation*, pages 1659–1664. IEEE, 1991.

[66] Justin Pradipta, Mario Klünder, Martin Weickgenannt, and Oliver Sawodny. Development of a pneumatically driven flight simulator stewart platform using motion and force control. In *2013 IEEE/ASME International Conference on Advanced Intelligent Mechatronics*, pages 158–163. IEEE, 2013.

[67] Dragan Pršić, Novak Nedić, and Vladimir Stojanović. A nature inspired optimal control of pneumatic-driven parallel robot platform. *Proceedings of the Institution of Mechanical Engineers, Part C: Journal of Mechanical Engineering Science*, 231(1):59–71, 2017.

[68] LA Quinchia, MA Delgado, C Valencia, JM Franco, and C Gallegos. Viscosity modification of different vegetable oils with eva copolymer for lubricant applications. *Industrial Crops and Products*, 32(3):607–612, 2010.

[69] Zhihong Rao and Gary M Bone. Modeling and control of a miniature servo pneumatic actuator. In *Proceedings 2006 IEEE International Conference on Robotics and Automation, 2006. ICRA 2006.*, pages 1806–1811. IEEE, 2006.

[70] Hai-Peng Ren and Chao Huang. Adaptive backstepping control of pneumatic servo system. In *2013 IEEE International Symposium on Industrial Electronics*, pages 1–6. IEEE, 2013.

[71] Hai-Peng Ren, Xuan Wang, Jun-Tao Fan, and Okyay Kaynak. Fractional order sliding mode control of a pneumatic position servo system. *Journal of the Franklin Institute*, 2019.

[72] E Richard and S Scavarda. Comparison between linear and nonlinear control of an electropneumatic servodrive. 1996.

[73] Edmond Richer and Yildirim Hurmuzlu. A high performance pneumatic force actuator system: Part i—nonlinear mathematical model. *J. dyn. sys., meas., control*, 122(3):416–425, 1999.

[74] A Saleem, Chi-Biu Wong, Junsheng Pu, and Philip R Moore. Mixed-reality environment for frictional parameters identification in servo-pneumatic system. *Simulation Modelling Practice and Theory*, 17 (10):1575–1586, 2009.

[75] SNS Salim, MF Rahmat, L Abdullah, SA Shamsudin, M Zainon, and AFM Amin. Enhanced self-regulation nonlinear pid for industrial pneumatic actuator. *International Journal of Electrical and Computer Engineering (IJECE)*, 9(4):3015–3024, 2019.

[76] JL Shearer. Study of pneumatic processes in the continuous control of motion with compressed air. part i and ii. *Trans. ASME*, 78(1):233–249, 1956.

[77] S Sieberling, QP Chu, and JA Mulder. Robust flight control using incremental nonlinear dynamic inversion and angular acceleration prediction. *Journal of guidance, control, and dynamics*, 33(6):1732–1742, 2010.

[78] P Simplício, MD Pavel, E Van Kampen, and QP Chu. An acceleration measurements-based approach for helicopter nonlinear flight control using incremental nonlinear dynamic inversion. *Control Engineering Practice*, 21(8):1065–1077, 2013.

[79] Jean-Jacques E Slotine, Weiping Li, et al. *Applied nonlinear control*, volume 199. Prentice hall Englewood Cliffs, NJ, 1991.

[80] Mohamed Smaoui, Xavier Brun, and Daniel Thomasset. A study on tracking position control of an electropneumatic system using backstepping design. *Control Engineering Practice*, 14(8):923–933, 2006.

[81] Ewoud JJ Smeur, Qiping Chu, and Guido CHE de Croon. Adaptive incremental nonlinear dynamic inversion for attitude control of micro air vehicles. *Journal of Guidance, Control, and Dynamics*, 38(12): 450–461, 2015.

[82] Ewoud JJ Smeur, Guido CHE de Croon, and Qiping Chu. Gust disturbance alleviation with incremental nonlinear dynamic inversion. In *2016 IEEE/RSJ International Conference on Intelligent Robots and Systems (IROS)*, pages 5626–5631. IEEE, 2016.

[83] Ewoud JJ Smeur, Guido CHE de Croon, and Qiping Chu. Cascaded incremental nonlinear dynamic inversion for mav disturbance rejection. *Control Engineering Practice*, 73:79–90, 2018.

[84] P Smith. A simplified approach to nonlinear dynamic inversion based flight control. In *23rd Atmospheric Flight Mechanics Conference*, page 4461, 1998.

[85] Phill Smith and Andrew Berry. Flight test experience of a non-linear dynamic inversion control law on the vaac harrier. In *Atmospheric Flight Mechanics Conference*, page 3914, 2000.

[86] Qiang Song, Fang Liu, and Raymond D Findlay. Improved fuzzy neural network control for a pneumatic system based on extended kalman filter. In *2006 International Conference on Computational Inteligence for Modelling Control and Automation and International Conference on Intelligent Agents Web Technologies and International Commerce (CIMCA'06)*, pages 76–76. IEEE, 2006.

[87] Olaf Stroosma, MM Van Paassen, and Max Mulder. Using the simona research simulator for human-machine interaction research. In *AIAA modeling and simulation technologies conference and exhibit*, page 5525, 2003.

[88] Ning Sun, Dingkun Liang, Yiming Wu, Yiheng Chen, Yanding Qin, and Yongchun Fang. Adaptive control for pneumatic artificial muscle systems with parametric uncertainties and unidirectional input constraints. *IEEE Transactions on Industrial Informatics*, 2019.

[89] BW Surgenor and ND Vaughan. Continuous sliding mode control of a pneumatic actuator. *Journal of dynamic systems, measurement, and control*, 119(3):578–581, 1997.

[90] Mostafa Taghizadeh, Farid Najafi, and Ali Ghaffari. Multimodel pd-control of a pneumatic actuator under variable loads. *The International Journal of Advanced Manufacturing Technology*, 48(5-8):655–662, 2010.

[91] Hiroshi Takemura, Takayuki Onodera, Ding Ming, and Hiroshi Mizoguchi. Design and control of a wearable stewart platform-type ankle-foot assistive device. *International Journal of Advanced Robotic Systems*, 9(5):202, 2012.

[92] Jakub Emanuel Takosoglu, Ryszard Filip Dindorf, and Pawel Andrzej Laski. Rapid prototyping of fuzzy controller pneumatic servo-system. *The International Journal of Advanced Manufacturing Technology*, 40(3-4):349–361, 2009.

[93] Kanya Tanaka, Yuuji Yamada, Masaru Sakamoto, and S Uchilado. Model reference adaptive control with neural network for electro-pneumatic servo system. In *Proceedings of the 1998 IEEE International Conference on Control Applications (Cat. No. 98CH36104)*, volume 2, pages 1130–1134. IEEE, 1998.

[94] TU Diep Cong Thanh and Kyoung Kwan Ahn. Nonlinear pid control to improve the control performance of 2 axes pneumatic artificial muscle manipulator using neural network. *Mechatronics*, 16(9): 577–587, 2006.

[95] Patrick Van der Smagt and Klaus Schulten. Control of pneumatic robot arm dynamics by a neural network. In *Proc. of the 1993 World Congress on Neural Networks*, volume 3, pages 180–183. Lawrence Erlbaum Associates, Inc. Cambridge, Massachusetts, 1993.

[96] J Wang, JD Wang, N Daw, and QH Wu. Identification of pneumatic cylinder friction parameters using genetic algorithms. *IEEE/ASME transactions on mechatronics*, 9(1):100–107, 2004.

[97] Jihong Wang, Junsheng Pu, and Philip Moore. A practical control strategy for servo-pneumatic actuator systems. *Control Engineering Practice*, 7(12):1483–1488, 1999.

[98] John B West. The original presentation of boyle's law. *Journal of applied physiology*, 87(4):1543–1545, 1999.

[99] Michael Zeller, Rajeev Sharma, and Klaus Schulten. Motion planning of a pneumatic robot using a neural network. *IEEE Control Systems Magazine*, 17(3):89–98, 1997.

[100] Xiong Zhang and Jiwei Hu. Model-free adaptive iterative learning control for a pneumatic muscle-driven robot. In *2019 IEEE 3rd Information Technology, Networking, Electronic and Automation Control Conference (ITNEC)*, pages 2246–2249. IEEE, 2019.

[101] Xiaocong Zhu, Guoliang Tao, Bin Yao, and Jian Cao. Adaptive robust posture control of a parallel manipulator driven by pneumatic muscles. *Automatica*, 44(9):2248–2257, 2008.